UNIVERSITY OF KWAZULU-NATAL
INYUVESI YAKWAZULU-NATALI

Synthesis and characterization of new gold and silver complexes based on P/N and P/S ligands; P/S ligand-stabilized gold nanoparticles

by

Vashen Moodley

Dissertation submitted in fulfillment of the academic requirements for the degree of

Master of Science

School of Chemistry and Physics, University of KwaZulu-Natal, Durban

As the candidate's supervisor I have approved this dissertation for submission.

Dr WE van Zyl	_____	_____
Name	Signature	Date

June 2013

DECLARATION I: PLAGIARISM

I, Vashen Moodley, declare that the experimental work described in this dissertation was carried out at the School of Chemistry and Physics, University of KwaZulu-Natal, Westville campus, between March 2011 and June 2012, under the supervision of Dr. W. E. van Zyl, and that:

1. The research reported in this thesis, except where otherwise indicated, and is my original research.
2. This thesis has not been submitted for any degree or examination at any other university.
3. This thesis does not contain other persons' data, pictures, graphs or other information, unless specifically acknowledged as being sourced from other persons.
4. This thesis does not contain other persons' writing, unless specifically acknowledged as being sourced from other researchers. Where other written sources have been quoted, then:
    a. Their words have been re-written but the general information attributed to them has been referenced
    b. Where their exact words have been used, then their writing has been placed in italics and inside quotation marks, and referenced.
5. This thesis does not contain text, graphics or tables copied and pasted from the Internet, unless specifically acknowledged, and the source being detailed in the thesis and in the References sections.

Signed

_____

Vashen Moodley

DECLARATION II: PUBLICATION

Details of publication:

1.1.3 Moodley, V.; Van Zyl, W. E. *Acta Crystallog. Sect. E* 2012, ***68***, o3477.

From the above publication entitled ***2-[(4-Bromobenzylidene)amino]ethanol*** , my role included carrying out all the experimental work and contributing to the writing of the publication along with my supervisor.

Signed

_____

Vashen Moodley

ABSTRACT

This dissertation comprises three distinct studies, two of which concerns molecular inorganic chemistry, and one concerns inorganic materials science.

Firstly, the synthesis and characterization of new dithiophosphonate ligands of the type $(NH_4)[S_2P(4\text{-}C_6H_4OMe)(OCH_2C_6H_5)]$ and $(NH_4)[S_2P(4\text{-}C_6H_4OMe)(OCH_2CH_2CH_2CH_3)]$ followed by their reaction with [AuCl(tht)] (tht = tetrahydrothiophene) and $[Ag(NO_3)]$ (molar ratio 1:1). This yielded two new dinuclear gold(I) complexes, $[Au\{S_2P(4\text{-}C_6H_4OMe)(OCH_2C_6H_5\})]_2$, **1** and $[Au\{S_2P(4\text{-}C_6H_4OMe)(OCH_2CH_2CH_2CH_3\})]_2$, **2**, and one new silver complex $[Ag\{S_2P(4\text{-}C_6H_4OMe)(OCH_2CH_2CH_2CH_3\})]_2$, **3**. Complex **1** and **2** displayed intramolecular Au···Au interactions of 3.0923(5) and 3.0613(7) Å, respectively, and revealed no intermolecular Au···Au interactions. Complex **1** additionally showed intermolecular hydrogen bonding interactions between the sulfur atom and an aromatic hydrogen atom with a contact distance of *ca.* 2.895 Å. The reaction of **1** with bis(diphenylphosphino)methane (dppm) (molar ratio 1:1) yielded a metallacyclic mixed-ligand complex tentatively assigned as $[Au_2(dppm)_2\{S_2P(4\text{-}C_6H_4OMe)(OCH_2C_6H_5)\}_2]$ **4**, (based on partial X-ray refinement) which is nevertheless a complex type derived from bis-phosphine reactions that has never been observed. Complex **3** followed the same predictable ^{1}H, ^{13}C, ^{31}P and IR patterns as with **1** and **2.**

Secondly, the synthesis and characterization of a phosphinamide ligand, $[(C_6H_5)_2PO(NH\text{-}t\text{-}C_4H_9)]$, **5**, has been described. The ligand showed solid state structures with a remarkable number of structural features which include hydrogen bond interactions as well as unique packing properties. Compound **5** contains two molecules in a single asymmetric unit linked *via* hydrogen bonds with a contact measuring *ca.* 2.03 Å. The dimeric asymmetric units in turn are held together by a network of weak hydrogen interactions measuring *ca.* 2.28 Å. The phosphinamide ligand, **5**, was further reacted with silver triflate which led to the formation of a novel dinuclear silver(I) complex

$[Ag(CF_3SO_3)(OPPh_2N(H)CMe_3)_2\}\{Ag(OPPh_2N(H)CMe_3)_2\}]SO_3CF_3$, **6**, that adopts two unique geometries around the silver nuclei, namely a trigonal planar and linear geometry. The two silver atoms show a strong intramolecular argentophillic interaction of 2.8979(3) Å.

From the above complexes, **1, 2, 5** and **6** were fully characterized by single crystal X-ray crystallography, ^{1}H, ^{13}C and ^{31}P solution NMR, elemental analysis, and IR. Complex **3** and **4** were characterized using ^{1}H, ^{13}C and ^{31}P solution NMR, elemental analysis, and IR.

The final study comprised the synthesis and characterization of gold nanoparticle/silica or AuNP/SiO_2-composites. The nanocomposites were prepared by the *in-situ* thermal reduction of tetrachloroauric acid, $H[AuCl_4].3H_2O$. Two variable parameters were considered namely temperature (50 °C, 100 °C, 200 °C and 300 °C) and concentration of the gold acid (0.01 M, 0.5 M and 1.25 M). The gold solution was pipetted onto the silica and allowed to soak for 2 hours and was then reduced in a furnace for one hour. The AuNP/SiO_2 composites were characterized by four methods, namely Brunauer Emmet and Teller (BET) surface area analysis, Scanning Electron Microscopy (SEM), Transmission Electron Microscopy (TEM) and X-Ray Diffraction (XRD). SEM revealed the gold particles was deposited on the surface of the silica. TEM results showed the AuNPs were formed with the smallest diameter around 3.6 nm and the largest 54 nm. Not surprisingly, the distribution of AuNPs increased with increase in concentration of gold solution. BET surface area results showed that surface area decreases with increase in concentration of gold solution. In addition to the synthesis of the composites, it was also used in the preparation of self-assembled monolayers (SAMs). SEM results showed post work-up images and analyses of P and S elements derived from a dithiophosphonate-cholesterol compound on the gold surface.

To My Family

“All truths are easy to understand once they are discovered; the point is to discover them.”

(Galileo Galilei)

ACKNOWLEDGEMENTS

- My parents and family for their love and support, and always pushed me to be a better person and for this I will always be indebted to you.
- Dr. Werner E.van Zyl for giving me an opportunity to work and develop in the field of chemistry. Thank you for your inspiration, guidance and support.
- Dr. R. J. Staples, Michigan State University, for data collection and refinement of some of the crystal structures presented in this study.
- Dr. B. O. Owaga and Sizwe Zamisa, UKZN, School of Chemistry and Physics, Westville campus, for some of the data collection and refinement of the crystal structures presented in this study.
- My colleagues in the lab for making research fun, interesting and worthwhile.
- My friends Fezile Potwana, Drushan Padayachee, Kaalin Gopaul, Kavashan Naidoo, Kyle Gaffar, Michael Pillay, Mohammed Fadlalla, Samashan Pillay, Sicelo Sithole , Shirveen Sewerpersad and especially Hegandrie Pillay. Thanks for the unconditional support and love.
- The Technical Staff at UKZN, School of Chemistry, Westville campus. With special mention to Mr. Dilip Jagjivan and Mr. Raj Somaru
- The Electron Microscopy Unit at UKZN, Westville campus.
- The honours class of 2010, UKZN, School of Chemistry, Westville campus.
- The National Research Foundation/Department of Science and Technology (NRF/DST) for financial support through an Innovative Grant.
- Rand Refinery for a generous gift of gold salt.

ABBREVIATIONS AND SYMBOLS

1°	Primary
2°	Secondary
3°	Tertiary
μ	Absorption coefficient
Å	Angstrom
^{o}C	Degrees Celsius
ρ	Density
AuNP	Gold nanoparticle
BET	Brunauer, Emmet and Teller surface area
BPMO	Bis-phosphine mono-oxide
cm^{-1}	Wavenumber
DCM	Dichloromethane (CH_2Cl_2)
DoM	Directed ortho metalation
Et_2O	Diethyl ether
EtOH	Ethanol
EDX	Energy dispersive X-ray spectroscopy
FTIR	Fourier Transform Infrared
GoF on F^2	Goodness of Fit on F^2
HSAB	Hard and Soft acid-base
IR	Infrared
• s	strong
• m	medium
• w	weak
IUPAC	International Union of Pure and Applied Chemistry
Ln	Lanthanum
LC	Liquid crystals
LMCT	Ligand to Metal Charge Transfer
LR	Lawesson's reagent
mol equiv.	Mole equivalent
NH_3	Ammonia

NMR	Nuclear Magnetic Resonance
• ^{1}H	Proton Nuclei
• ^{13}C	Carbon-13 Nuclei
• ^{31}P	Phosphorus-31 Nuclei
• s	singlet
• d	doublet
• t	triplet
• quart	quartet
• dd	doublet of doublets
• d quart	doublet of quartets
• m	multiplet
ORTEP	Oak Ridge thermal ellipsoid plot
P_4S_{10}	Phosphorous pentasulfide
PIN	Preferred IUPAC name
SAMs	Self assembled monolayers
SEM	Scanning electron microscopy
SHAB	Soft hard acid base theory
SiO_2	Silica gel
SPO	Secondary phosphine oxide
SPR	Surface plasmon resonance
TEM	Transmission electron microscopy
THF	Tetrahydrofuran
UV	Ultraviolet
V	Volume

TABLE OF CONTENTS

LIST OF FIGURES

LIST OF SCHEMES

LIST OF TABLES

CHAPTER 1

Introduction

1.1 Phosphor-1,1-dithiolato ligands

This class of compounds can be broadly defined as dithiophos***pha***tes, dithiophos***phi***nates, and dithiophos***pho***nates (**Figure 1.1**). Dithiophosphonates are a hybrid of the former two. The dithiophosphates are well established when compared to the other two groups, presumably due to the relative ease of ligand preparation, and complexes of the main- and transition-metals are prevalent in literature.[1] The advantage gained from the use of dithiophosphonates over the other two groups is the asymmetric nature of the ligand. This allows for the formation of complex isomers, not possible for the symmetric molecules of **A** and **B**.

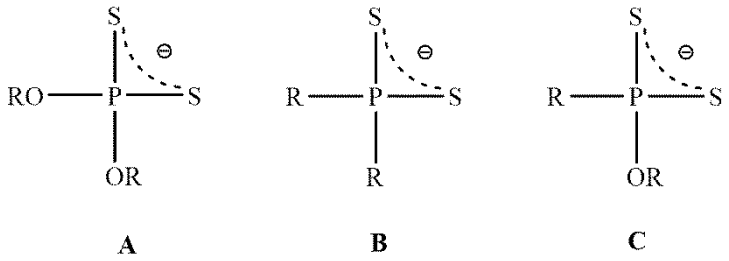

Figure 1.1 Phosphor-1, 1-dithiolates comprise of ligands derived from dithiophosphoric acid (A), dithiophosphinic acid (B), and the hybrid dithiophosphonic acid (C)

It has been shown that 2,4-diaryl-1,3-dithiadiphosphetane disulfide dimers react with two stoichiometric equivalents of alcohol to form corresponding dithiophosphonic acids.[2] A detailed description on the reaction follows in **Chapter 2** (**Section 2.1.1**).

Commercial application of these compounds include insecticides,[3] antioxidant additives in motor oil,[4] and the selective extraction of metals.[5] Furthermore, the transition metal complexes have shown biological importance in aspects pertaining to the modeling of metal-sulfur interactions present in natural systems.[6] The aforementioned applications are mainly due to the capacity of the ligand to form stable chelates.

1.1.1 S-P-S coordination modes and related complexes

The research possibilities of the S-P-S moiety have been exploited due to the variation and flexibility in the coordination patterns observed. This can be attributed to the resonance structures of the monoanionic acids (**R_1**, **R_2**, **Figure 1.2**). In mononuclear systems various coordination patterns have been observed, the most common are shown below:[1b]

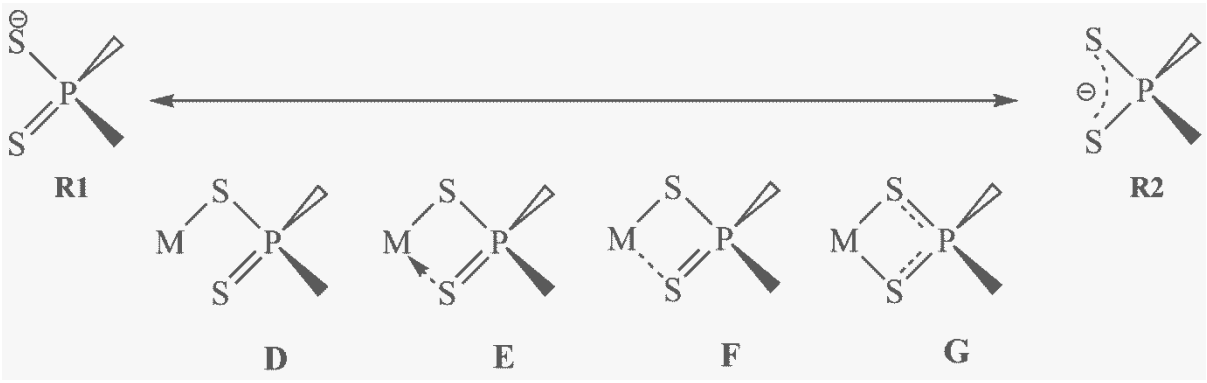

Figure 1.2 Resonance structures of dithiophosphonic acids

D. Monodentate with the non-coordinating P=S bond.
E. Bidentacity increasing through P=S bond with dative coordination.
F. Anisobidentate increasing the sulfur interaction.
G. Isobidentate with equal sulfur interactions.

Generally, soft metals tend to form monodentate coordination patterns in which primary covalent metal-sulfur bonds are formed, **D**. Hard metals tend to prefer resonance form **R_2** forming bonds with greater ionic character and delocalization of the negative charge over the S-P-S moiety **G**.[1b] The predominant factor which facilitates variable coordination patterns is the hypervalency of the phosphorus and sulfur atoms.[7] The S-P-S moiety facilitates μ_1 and μ_2 binding modes, bridging two metal centres. (**Figure 1.3**)

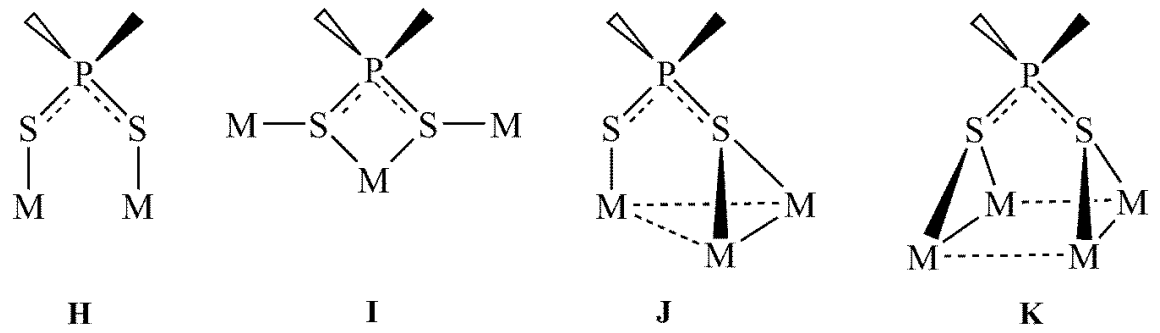

Figure 1.3 Multi-nuclear coordination patterns derived from P/S type ligands

1.1.2 Dithiophosphonate ligands and related metal complexes

Bimetallic biconnective systems, (**H**, **Figure 1.3**) are prevalent in the synthesis of dinuclear gold(I) dithiophosphonates. The ligand provides an effective framework for the study of aurophilic interactions due to relativistic effects closely related with gold chemistry.[8] Comprehensive studies on the reactivity and luminescent characteristics of dinuclear gold(I) dithiophosphonates have been reported, [9] and the present study reports the adaption of such complexes and the formation of a novel dinuclear unit. (**Chapter 2**)

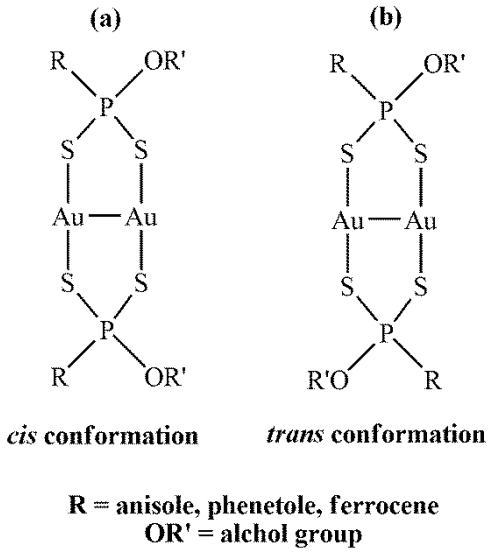

Figure 1.4 Common 8-membered gold(I) metallacycles form two possible isomers (a) cis or syn and (b) trans or anti[10]

The reactivity of gold(I) dithiophosphonate complexes towards bis(phosphines) has been reported by Maspero *et al.*[11] **Scheme 1.1** shows the reaction of gold(I) dithiophosphonate complexes with one molar equivalent of dppm results in the formation of an open ended complex. In the same study reactions of dithiophosphonates with several other bis(phosphines) yielded an analogues result. Solvent dependent products (one yellow and one white) were isolated with only a change in the solvent system. The stoichiometric dependence is also established, and the addition of 2 equivalents of the bis(phosphine) formed an adduct.[11]

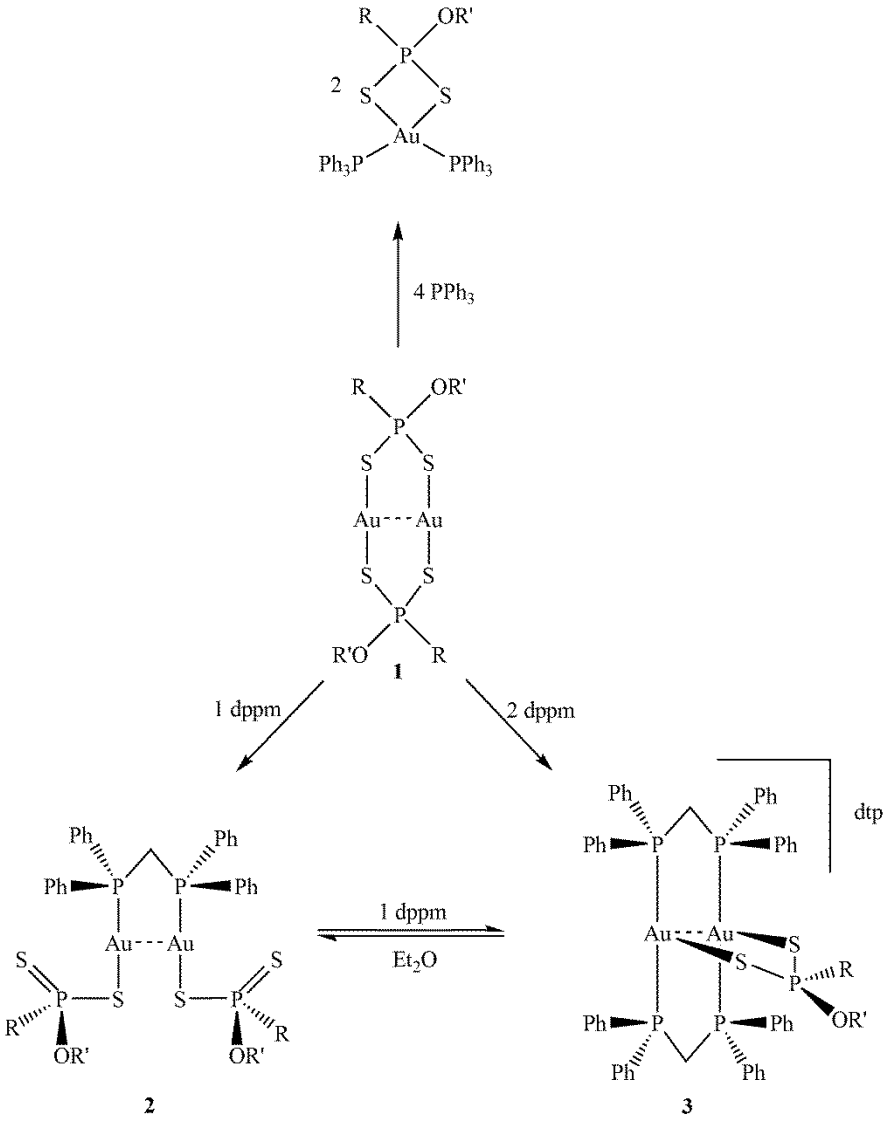

Scheme 1.1 Reaction scheme for reactivity studies of gold(I) dithiophosphonate complexes.[11] In certain cases, alternate results were obtained in the present study

1.1.3 Gold and Silver

Silver(I)[12] and gold(I)[13] complexes have attracted amplified interest recently due to their structural features and their potential applications. Silver(I) complexes with oxo- and thio ligands have proved to be valuable candidates for catalysis[14] and material science.[15] Gold(I) complexes containing ligands with N, P or S donor atoms have already proved to be valuable candidates in medicine,[16] catalysis[17] and material science.[18]

1.2 The ligand classes of phosphinamide and phosphine oxide

Phosphine oxides are a broad field and are differentiated as secondary, tertiary, scalemic P-chiral phosphine oxides.

1.2.1 Secondary Phosphine oxides

Most phosphines are sensitive to air oxidation and moisture, and possess a foul odour,[19] which in turn makes them difficult to handle. To overcome this, research into using air and moisture stable secondary phosphine oxides (SPOs) as ligands has lead to numerous advantageous breakthroughs. The first noted synthesis of SPOs was reported by Williams and Hamilton in 1952.[20] The research involved the preparation of di-*n*-hexyl-, *n*-octyl- and *n*-octadecylphosphine oxides via reaction of an appropriate Grignard reagent with diethylphosphite.[21] During the same time period, Kosolapoff and Watson reported on the oxidation of phosphinate to its corresponding phosphinic acid by reaction with H_2O_2 without isolating di-alkyl phosphine oxides.[22] Mislow and co-workers disclosed a study of $LiAlH_4$ induced stereo mutation of phenyl-α-phenyl ethyl phosphine oxide in 1970.[23] The first occurrence of phosphinous acid-phosphinito complexes of Pt(II) were reported by Roundhill *et al*.[24] Later in 2001, the preparation of air-stable secondary phosphine oxides ligated metal complexes were observed.[25]

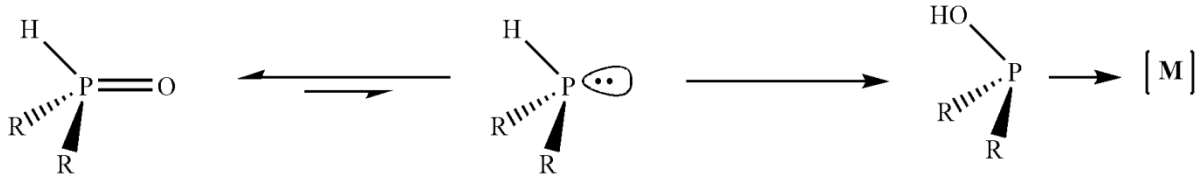

Scheme 1.2 Path to formation of stable phosphinous coordinated metal complex

Scheme 1.2 shows a probable reaction path leading to the formation of stable phosphinous acids coordinated to metal complexes. Secondary phosphine oxides (SPOs) (**A**) are weak acids and could exist in equilibrium in solution with species (**B**) under ambient conditions.[26] Coordination to the metal center through the phosphorus atom affords (**C**), which are air-stable and resistant to moisture and high temperature.[27] Transition metal complexes (**C**) might function as active catalysts in various reactions.[19]

1.2.2 Tertiary phosphine oxides

Tertiary phosphine oxides are a class of compounds of extreme stability. Strong bases can cause the carbon-phosphorus bond to break, eliminating the most electronegative group of the molecule.[28] This reaction should be considered somewhat exceptional, since heating to the compounds melting point and addition of a strong oxidizing agent in most cases, does not affect the carbon-phosphorus linkage.[28]

Tertiary phosphine oxides posses a phosphorus atom bound to three carbon atoms and to an oxygen atom. **Figure 1.5** illustrates this with $\mathbf{R^1}$, $\mathbf{R^2}$, and $\mathbf{R^3}$ representing the carbon-phosphorus linkages.[28]

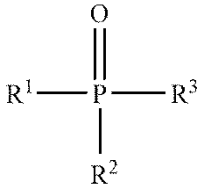

Figure 1.5 Structure of a tertiary phosphine oxide with a P(V) atom

The preparation of tertiary phosphine oxides via the reaction of Grignard reagents with halides and/or esters of phosphorus acids was demonstrated in 1950.[29] Dialkyl chlorophosphates are used as starting materials in the synthesis of phosphonic acids[30] and can serve as reagents in the preparation of tertiary phosphine oxides.[31]

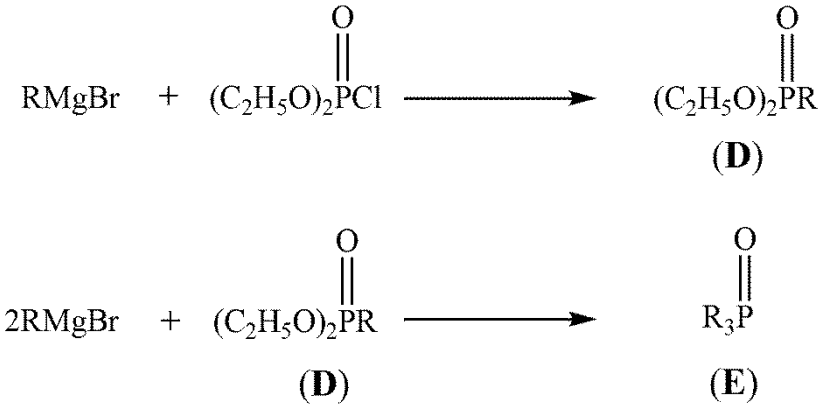

Scheme 1.3 Use of Grignard reagent in the formation of tertiary phosphine oxide

The general reaction (**Scheme 1.3**) is given in the equation in which diethyl chlorophosphate was used. With *ortho*-substituted aryl Grignard reagents it was possible to obtain the substituted phosphonate **D**. It was suggested that a steric effect created by the *ortho* group

hindered further reaction of compound **D** with the Grignard reagent. Tertiary phosphine oxides **E** were prepared by the use of Grignard reagents which were not substituted in the *ortho* position.[31]

In contrast to the method in which tertiary phosphine oxides are obtained directly from oxygen-containing intermediates, **Scheme 1.4** illustrates a viable route; however the tertiary phosphines required here must be synthesized and then allowed to undergo oxidation.[28] Selection of suitable oxidizing agents can be troublesome, as readily oxidizable alkyl groups on the phosphorus atom and on the side chains of aromatic substituents may be involved in the reaction.[32] A key point related to the study is that phosphines are frequently converted to the phosphine oxides upon standing in air or in the presence of oxygen.[33]

Reduction of tertiary phosphine oxides to the corresponding tertiary phosphines is possible with lithium aluminium hydride or calcium aluminium hydride, however the yields of phosphines are higher with the use of lithium aluminium hydride rather than with the calcium counterpart.[28]

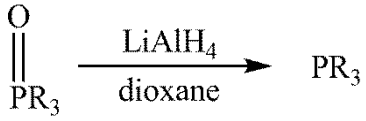

Scheme 1.4 Reduction a general tertiary phosphine oxide with the use of $LiAlH_4$

Tertiary phosphine oxides undergo condensation with alkali metals to form dark-coloured addition compounds which are sensitive to air and moisture. The colour depends somewhat on the metal content of the complexes[28] with zinc chloride showing stable complexes with tertiary phosphine oxides.[29,34] Apart from these complexes trimethylphosphine oxide also acts as an acceptor for electron-deficient groups such as BF_3, SO_3, and SO_2.[35]

1.2.3 Scalemic P-chiral phosphines

Scalemic P-chiral phosphines are compounds in which the central phosphorus atom is connected with three carbons or at least two carbons and one hydrogen atom (*e.g.*, **F** in **Figure 1.6)** and of those of their higher oxidation level derivatives in which this distinction is held (*e.g.*, **G-I** in **Figure 1.6).**

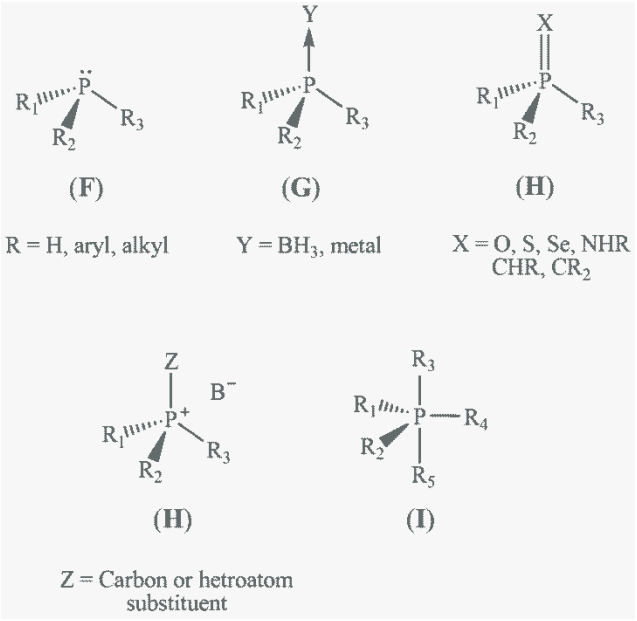

Figure 1.6 Categories of scalemic P-chiral phosphines

In principle, to mount three different carbon substituents on phosphorus one needs to start from simple PX_3 or $O{=}PX_3$ (X = C1, Br, OR, etc.) molecules and to carry out selective step by step displacement of the X groups at the P atom.

One early developed route in which symmetrical phosphine is first quaternized and then one of the two alike substituents in the resulting phosphonium salt is hydrolytically removed to yield non-symmetrical phosphine oxide is demonstrated in **Scheme 1.5**.[36]

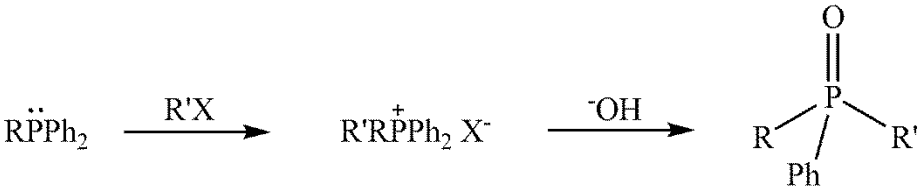

Scheme 1.5 Synthesis of non-symmetrical phosphine oxide

The first known optically active organophosphorus compound, ethylmethylphenylphosphine oxide (**J** in **Figure 1.7**)**,** was obtained by direct resolution of the racemate using (+)-bromocamphorsulfonic acid for the formation of separable diastereomeric salts.[37]

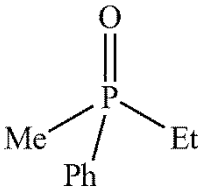

(J)

Figure 1.7 The first known optically active organophosphorus compound, ethylmethylphenyl-phosphine oxide **(J)**

1.2.4 Phosphinamides

Phosphinamides and phoshine oxides (**Figure 1.8**) are, with few exceptions, crystalline substances. They are odourless, resistant to hydrolysis, and of low acute toxicity, but are not easily biologically degradable[38] making this class of ligands important functional groups in organic synthesis.

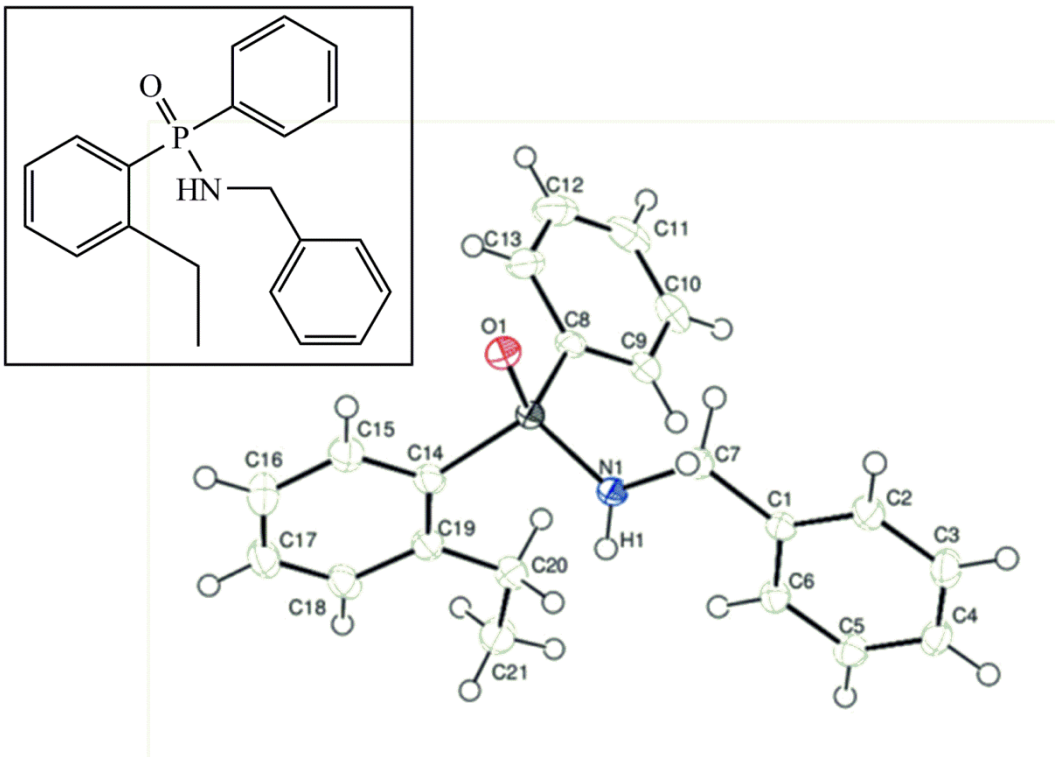

Figure 1.8 N-Benzyl-P-(2-ethylphenyl)-P-phenylphosphinic amide, a typical example of a phosphinamide[39]

In comparison phosphinamides show different reactivities to their carbon counterparts as seen in **Figure 1.9**. Diphenylphosphinamide (**K**) which results in hydrolysis shown to be 10^5 times faster than its carbon analogue, benzamide (**L**), under acidic conditions.[40]

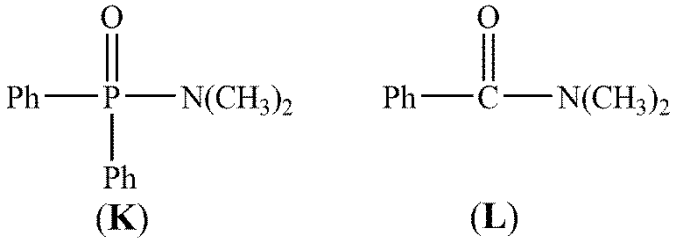

(**K**) (**L**)

Figure 1.9 Illustration of diphenylphosphinamide (K), benzamide (L)

Another noteworthy feature of phosphinamides is the acidifying effect of the substitution of the H atom with a P=O group on RNH_2 which increases the RN-**H** acidity significantly.[41] Also the known stability of both primary and secondary amides of P(V) acids in alkaline medium provide for easy introduction of various alkyl substituent to nitrogen.

The stability of P(III)–N bonds in phosphinamides depends to a large extent on the phosphorus and nitrogen substituents.[42] The P(III)–N bonds are stable to attack by lithium and Grignard reagents[43] and can survive a variety of nucleophilic substitution reactions at the phosphorus centers.[42] However, P(III)–N bonds can undergo hydrolytic cleavage in the presence of trace amounts of acid/base impurities.[44] The cleavage of P(III)–N bonds has also been demonstrated during complexation reactions with transition metals.[45]

1.2.5 The multi-array of uses of phosphinamides and phosphine oxide

The field of research in terms of their uses are quite extraordinary, as they have been employed as amine protecting groups and as substrates for imine activation[46] and are also used as catalysts for enantioselective reduction of ketones as building blocks for the synthesis of peptidomimetics *via* phosphinamide-directed benzylic lithiation[47] and as chiral ligands[48].

1.2.5.1 The Direct-*ortho* Metalation (DoM)

Recently a major application of phosphinamides is in Direct-*ortho* Metalation (DoM) which has become one of the most employed strategies in organic synthesis for derivatizing arenes.[48] A large number of heteroatom-directed metalation groups (DMGs) can be used for promoting DoM reactions, while a few are based on the directing effect of tetra-coordinated phosphorus containing functional groups. The synthetic utility of these DoM reactions generally suffer limitations such as ineffective directing ability, reduced scope due to the use of triaryl derivatives, and competing side reactions, with the nucleophilic attack at the phosphorus being the most important.[49] This is overcome by the use of bulky *tert*-butyl substituents linked to the phosphorus atom to avoid P-attack.

1.2.5.2 Luminescent Ln complexes of phosphine oxides

Luminescent lanthanum complexes are being used in numerous analytical applications, ranging from water proton relaxation agents for NMR imaging[50] to luminescent probes in time-resolved fluoroimmunoassays.[51]

A Ln (Lanthanum) complex (**Figure 1.10**) engineered from a ligand consisting of a single P=O fragment and two methylene linked bipyridine subunits, forms a complex that possess a long lifetime, pronounced absorption in the near UV, and tuneable emission depending in the presence of anions.[52] Charbonnière *et al.* demonstrated that the P=O bond will provide relatively stable complexes because of the strong coordination ability of the P=O for lanthanides and that the bipyridine fragments will coordinate to the Ln.[52]

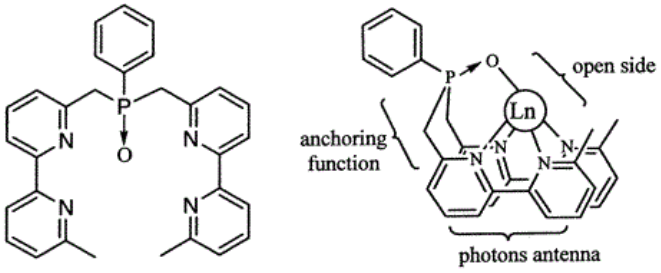

Figure 1.10 The ligand and coordination pocket provided by Ln complexation[52]

The present study reports the formation of a polymorphic phosphinamide precursor and its novel silver complex (Chapter 3)

1.3 Materials: The new old science

Materials science is an interdisciplinary field applying the properties of matter to various areas of science and engineering. This scientific field investigates the relationship between the structure of materials at atomic or molecular scales and their macroscopic properties. Herein we look at gold nanoparticles and their role in the formation of self assembled monolayers.

1.3.1 Gold and gold nanoparticles

Gold is a chemical element with the symbol Au and an atomic number of 79.[53] The physical properties of gold include its ductility, its crystal structure which is cubic close packed (**Figure 1.11**), its melting point (1064 °C), its density (19.32 mg.m^{-3}) and its conduction of heat and electricity.[13]

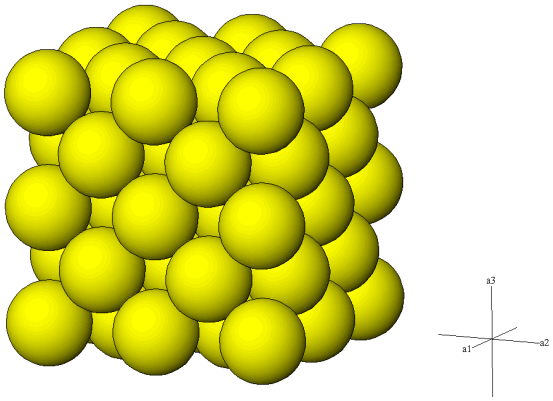

Figure 1.11 Crystal structure of metallic gold[54]

It has been a highly sought-after precious metal for coinage, jewelry, and other arts since the beginning of recorded history.[53] It is thought to be the most noble of all elements remaining untarnished for centuries, when exposed to the atmosphere. Apart from the many properties of gold it has great monetary value, and is linked closely to the world's economy. In the past gold chemistry has been an undeveloped field due to the relative inertness of bulk gold, but now, after the use of nanoscale gold as an active catalyst, this has all changed.[53] Gold nanoparticles (AuNPs), also called gold colloids, are amongst the most stable metal nanoparticles, because of this stability, gold is the most used element in nanoscale science.[55]

1.3.2 Properties of gold nanoparticles

AuNPs have many properties that differ from the bulk form of gold. Among these properties is the surface plasmon resonance (SPR) observed when a metal absorbs light of a resonant wavelength. This causes the electron cloud to vibrate, dissipating the energy. This process usually occurs at the surface of a material (as metals are not usually transparent to light) and is therefore called surface plasmon resonance. Plasmons are the name for the oscillations of the electron cloud and this means that there are certain wavelengths for metals where photons are not reflected, but instead are absorbed and converted into surface plasmon resonance (electron cloud vibrations). For metals, such as gold, these wavelengths occur in the infrared portion of the spectrum, but nanoparticles can experience surface plasmon resonance in the visible portion of the spectrum which means that a certain portion of visible wavelengths will be absorbed, while another portion will be reflected which gives the irradiated region of the material a certain color. Small nanoparticles absorb light in the blue-green portion of the spectrum (~400-500 nm) while red light (~700 nm) is reflected, yielding a deep red color (**Figure 1.12**). As nanoparticles size increases, the wavelength of surface plasmon resonance related absorption shifts to longer, more red wavelengths.[56]

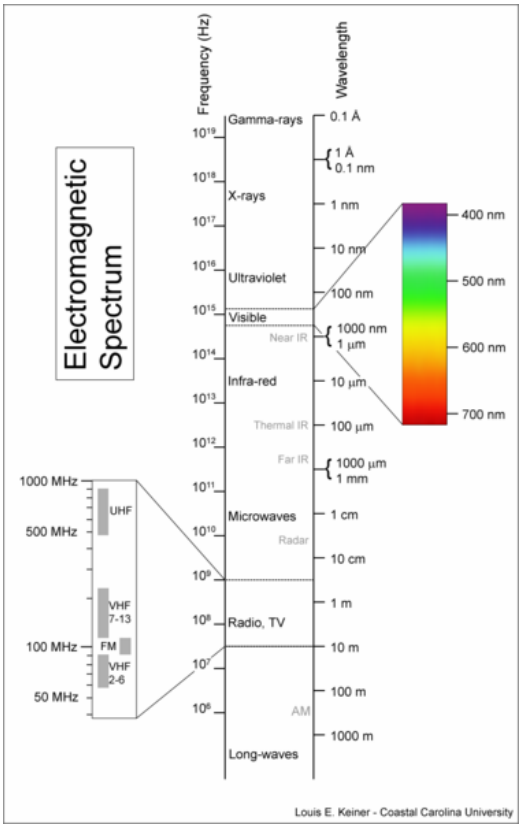

Figure 1.12 Electromagnetic Spectrum[56]

Fluorescence studies of AuNPs have been carried out under various conditions, including femto-second emission and steady-state investigations of the interaction between thiolate ligands and the gold core.[57] The resonant energy transfer was observed in fluorescent ligand-capped AuNPs, this phenomenon is of great interest to the fields of biophotonics and materials science.[58]

Magneto-electrochemistry of AuNPs quantized capacitance charging showed the influence of a magnetic field on the electrochemistry of AuNPs, and in particular the effect of electron parity upon their charging states.[59]

1.3.3 The widespread applications of gold nanoparticles

There is a rapid growth in the potential applications of gold nanoparticles, with current applications including electronics, photonics, biosensors, and catalysis.[60]

1.3.3.1 Biosensors

Tests that take advantage of surface plasmon resonance changes include DNA detection and how specific DNA looks for certain bases. In this test, nanoparticles start out as large aggregates that are blue coloured. If the complementary DNA base is present, the nanoparticles will bind to that base selectively and the aggregates will dissolve producing a deep red color (**Figure 1.13**). This can be followed using a spectrophotometer that measures light absorption at different wavelengths.[56]

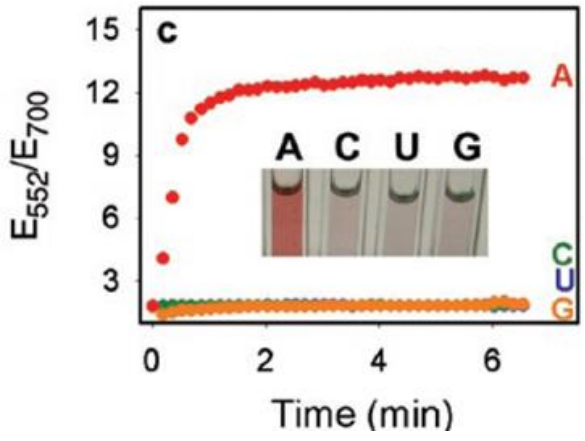

Figure 1.13 Gold nanoparticles for DNA detection[56]

1.3.3.2 Catalysis

Gold is well known to be chemically inert. It is indeed one of the most stable metals in the group 8 elements, and it is resistant to oxidation. Gold nanoparticles exhibit high catalytic activity and efficiency[61], gold catalysts are also comparatively lower in cost than other precious metal catalysts such as Pt or Rh.[62]

Nanoparticulate gold catalysts are unique in their activity under mild conditions. When gold nanoparticles less than ~5 nm in size are supported on base metal oxides or carbon, very active catalysts are produced, showing that AuNPs becomes catalytically active on the nanoscale level.[63] The catalytic applications that these AuNP catalysts are used for, range from pollution and emission control and safety systems,[64] to hydrogen economy/fuel cell systems[65] and specialty/bulk chemical synthesis (**Figure 1.14**).[66]

The controlled size and shape of nanoparticles is one of the key requirements for achieving many nanotechnological goals, since these are the main parameters determining the material properties such as electronic and optical properties.[67]

With regard to AuNP catalysis it is seen that on a large scale, there are industrial processes at ambient temperatures that are established,[62] however the prevalent problem as to why it is not used regularly is aggregation of gold nanoparticles.

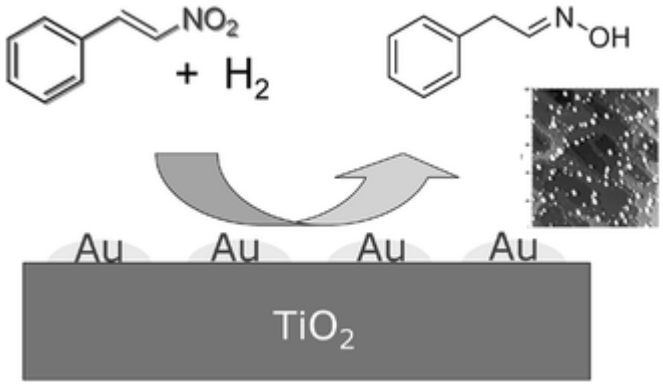

Figure 1.14 Gold catalysts to promote additions to multiple C–C bonds, benzannulations and alcohol oxidation by oxygen[68]

1.3.4 Self-assembled monolayers (SAMs)

SAMs are ordered molecular assemblies formed by the adsorption of an active surfactant on a solid surface (**Figure 1.15**). This simple process makes SAMs intrinsically manufacturable and thus technologically attractive for building super lattices and for surface engineering. The order in these two-dimensional systems is produced by a spontaneous chemical synthesis at the interface, as the system approaches equilibrium. Although the area is not limited to longchain molecules,[18a] SAMs of functionalized long-chain hydrocarbons are most frequently used as building blocks of supramolecular structures.[18a]

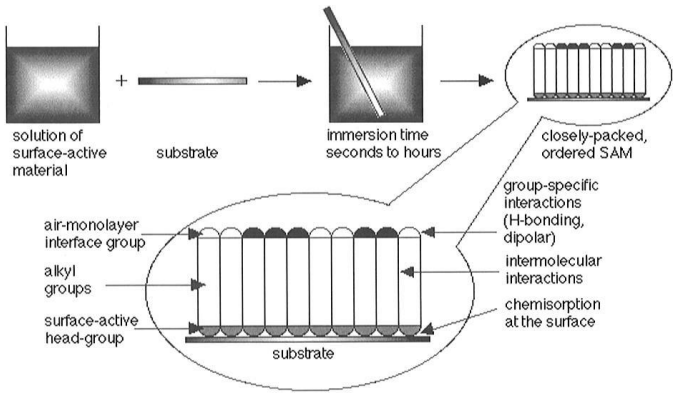

Figure 1.15 Self-assembled monolayers are formed by simply immersing a substrate into a solution of the surface-active material[18a]

The field of self-assembled monolayers has seen tremendous growth in synthetic advancement and in-depth characterization over the past two decades. The field really began much earlier than is now recognized. The first published preparation of a monomolecular layer by adsorption (self-assembly) of a surfactant onto a clean metal surface was seen in 1946.[69] However, at that time, the potential of self-assembly was not recognized, and this preparation initiated only a limited level of interest. The interest later boomed in 1983 with the research of Ralph G. Nuzzo when SAMs of alkanethiolates on gold were prepared by adsorption of di-*n*-alkyl disulfides from dilute solutions.[70] Getting away from the moisture-sensitive alkyl trichlorosilanes, as well as working with crystalline gold surfaces, were two important reasons for the success of these SAMs. Many self-assembly systems have since been investigated, but monolayers of alkanethiolates on gold are probably the most studied SAMs to date.[18a]

1.3.5 The use of different surfactant molecules

Spontaneous adsorption of long-chain *n*-alkanoic acids ($C_nH2_{n+1}COOH$) has been studied in the past few years.[71] This is an acid-base reaction, and the driving force is the formation of a surface salt between the carboxylate anion and a surface metal cation (**Figure 1.16**).

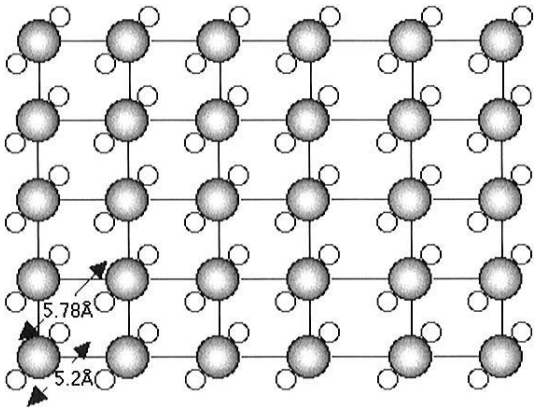

Figure 1.16 The p(2x2) adsorption scheme of fatty acids on AgO. The filled circles are the carboxylate carbon atoms, while the small, hollow circles are carboxylate oxygen atoms[18a]

SAMs of alkylchlorosilanes[72], alkylalkoxysilanes[73], and alkylaminosilanes[74] require hydroxylated surfaces as substrates for their formation. The driving force for this self-assembly is the in situ formation of polysiloxane, which is connected to surface silanol groups (-SiOH) via Si-O-Si bonds.

Sulfur and selenium compounds have a strong affinity to transition metal surfaces.[75] This is probably because of the possibility to form multiple bonds with surface metal clusters.[76] The number of reported surface active organo-sulfur compounds that form monolayers on gold has increased in recent years (**Figure 1.17**). These include, among others, di-*n*-alkyl sulfide[77], di-*n*-alkyl disulfides[70], thiophenols[78], mercaptopyridines[79], mercaptoanilines[80], thiophenes[81], cysteines[82], xanthates[83], thiocarbaminates[84], thiocarbamates[85], thioureas[86], and alkaneselenols.[87] However, the most studied, and probably the best understood SAM is that of alkanethiolates on Au(111) surfaces.

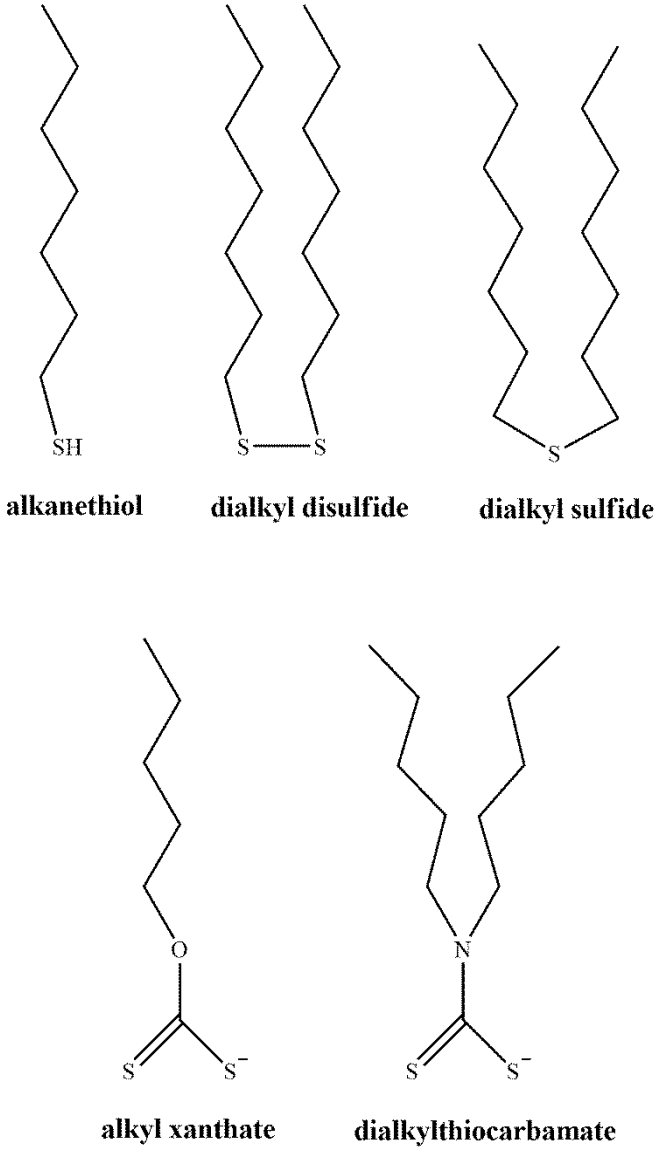

Figure 1.17 Surface-active organo-sulfur compounds that form monolayers on gold

In a recent study the binding and alkyl chain organization in new self-assembled monolayers of dialkyl dithiophosphinic acids (dialkyl-DTPAs)[88] was designed which lead to the use of dithiophosphonates in SAMs used in the current study.

As adsorbates, these molecules (dialkyl dithiophosphinic acids) have two potential binding modes to gold surfaces: (**a**) In the monodentate structure, the dialkyl-DTPA molecule is anchored by a single Au-S interaction, whereas (**b**) in the bidentate structure, a second Au-S interaction anchors the molecule at two points (**Figure 1.18**).

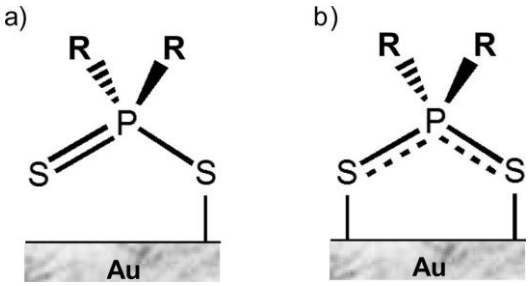

Figure 1.18 Dialkyl dithiophosphinic acid bound to a Gold Surface: (a) Monodentate and (b) Bidentate Binding

1.4 Objectives

The primary objective of the project was to develop novel ligand systems capable of creating complex systems of multinuclearity, with coordination-driven interactions. The synthetic routes to dithiophosphonates and phosphinamides have been exploited previously; however, systems containing multiple binding sites as well as containing unique and application driven functional groups are still in early stages of development. The goals of the first two studies can be summarized as follows:

- Design new ligands and develop materials with unique properties from modified synthetic routes.
- Synthesize and characterize such ligands and complexes with an eye to create large molecular assemblies.
- Prepare multinuclear complexes possessing unique chemical and physical properties.

For the third study the aim was to synthesize gold nanoparticle/silica composites, by an *in situ* thermal approach. The goal was to determine the optimum experimental conditions to form gold nanoparticles of a controlled size and shape within a silica matrix. It was hoped this method would provide an easy protocol to form gold nanoparticles as a homogeneous distribution within a silica matrix. Apart from these aims a sub-study into the formation of self-assembled monolayers was undertaken which have many potential applications from acquiring an understanding of surface chemistry through to finding methods of aiding in drug delivery.

1.5 Overview

Due to the diverse nature of this study, and the unique ligands, complexes and composites formed, the content of this dissertation has been separated into three chapters, each containing its own introduction, results, discussion and experimental sections, respectively.

Chapter 2 outlines the synthetic route to dithiophosphonates used in this study and an overview of aurophilic interactions which dominate gold(I) chemistry. Two dinuclear gold(I) complexes and one silver(I) complex of great interest are reported as well as a reactivity study of one of the complexes.

Chapter 3 introduces the concept of phosphinamide ligand formation, which is discussed fully. Two new crystal structures are reported herein; one phosphinamide ligand that is a polymorph of a previously synthesized molecule which is structurally different, and a dinuclear silver phosphinamide complex in which the silver nuclei two distinct geometries.

Chapter 4 shows that the synthesis of AuNP/SiO_2composites is possible by the use of an *in-situ* thermal approach. The possibility of tailoring size and the number of particles can be done by adjusting the condition parameters. In addition, the possibility of using dithiophosphonates in the formation self-assembled monolayers is also illustrated proving crucial to the understanding of surface chemistry as well essentially stabilizing the nanoparticles in the process.

Chapter 5 gives the summary of findings and the applicability to future research.

1.6 References

(1) (a) Haiduc, I.; Sowerby, D. B. *Polyhedron* **1996**, *15*, 2469(b) Haiduc, I.; Sowerby, D. B.; Lu, S.-F. *Polyhedron* **1995**, *14*, 3389.
(2) van Zyl, W.; Fackler, J. P. *Phosphorous, Sulfur and Silicon* **2000**, *167*, 117.
(3) Edmundson, R. S. *Dictionary of Organophosphorus Compounds*; Chapman and Hall: New York, 1988.
(4) Colclough, T. *Ind. Eng. Chem. Res.* **1987**, *26*, 1888.
(5) Alimarin, I. P.; Tat'yana, V. R.; Vadim, M. I. *Russ. Chem.* **1989**, *58*, 863.
(6) Wiebelhaus, N. J.; Cranswick, M. A.; Klein, E. L.; Lockett, L. T.; Lichtenberger, D. L.; Enemark, J. H. *Inorg. Chem.* **2011**, *50*, 11021.
(7) Reed, A. E.; Schleyer, P. v. R. *J. Am. Chem. Soc.* **1990**, *112*, 1434.
(8) Schmidbaur, H.; Schier, A. *Chem. Society. Rev.* **2012**.
(9) (a) van Zyl, W. E.; Staples, R. J.; Fackler, J. J. P. *Inorg. Chem. Comm.* **1998**, *1*, 51(b) van Zyl, W. E.; López-de-Luzuriaga, J. M.; Mohamed, A. A.; Staples, R. J.; Fackler, J. P. *Inorg. Chem.* **2002**, *41*, 4579.
(10) van Zyl, W. E.; Woollins, J. D. *Coord. Chem. Rev.* **2013**, *257*, 718.
(11) Maspero, A.; Kani, I.; Mohamed, A. A.; Omary, M. A.; Staples, R. J.; Fackler, J. P. *Inorg. Chem.* **2003**, *42*, 5311.
(12) (a) Krebs, B.; Henkel, G. *Angew. Chem. Int. Ed.* **1991**, *30*, 769(b) Housecroft, C. E. *Coord. Chem. Rev.* **1992**, *115*, 141.
(13) Schmidbaur, H. *Interdisciplinary science reviews* **1992**, *17*.
(14) Colombo, F.; Annunziata, R.; Benaglia, M. *Tetrahedron Lett.* **2007**, *48*, 2687.
(15) Ozawa, K.; Iso, F.; Nakao, Y.; Cheng, Z.; Fujii, H.; Hase, M.; Yamaguchi, H. *J. Eur. Ceram. Soc.* **2007**, *27*, 2665.
(16) López-De-Luzuriaga, J. M.; Schier, A.; Schmidbaur, H. *Chem. Ber.* **1997**, *130*, 647.
(17) Zhang, Z.; Widenhoefer, R. A. *Angew. Chem. Int. Ed.* **2007**, *46*, 283.
(18) (a) Ulman, A. *Chem. Rev.* **1996**, *96*, 1533(b) Jørgensen, J. M.; Erlacher, K.; Pedersen, J. S.; Gothelf, K. V. *Langmuir* **2005**, *21*, 10320.
(19) Shaikh, T. M.; Weng, C.-M.; Hong, F.-E. *Coord. Chem. Rev.* **2012**, *256*, 771.
(20) Williams, R. H.; Hamilton, L. A. *J. Am. Chem. Soc.* **1952**, *74*, 5418.
(21) Williams, R. H.; Hamilton, L. A. *J. Am. Chem. Soc.* **1955**, *77*, 3411.
(22) Kosolapoff, G. M.; Watson, R. M. *J. Am. Chem. Soc.* **1951**, *73*, 4101.
(23) Farnham, W. B.; Lewis, R. A.; Murray, R. K.; Mislow, K. *J. Am. Chem. Soc.* **1970**, *92*, 5808.
(24) Beaulieu, W. B.; Rauchfuss, T. B.; Roundhill, D. M. *Inorg. Chem.* **1975**, *14*, 1732.
(25) Li, G. Y. *Angew. Chem. Int. Ed.* **2001**, *40*, 1513.
(26) (a) Dixon, K. R.; Rattray, A. D. *Can. J. Chem.* **1971**, *49*, 3997(b) Silver, B.; Luz, Z. *J. Am. Chem. Soc.* **1962**, *84*, 1091(c) Luz, Z.; Silver, B. *J. Am. Chem. Soc.* **1961**, *83*, 4518(d) Doak, G. O.; Freedman, L. D. *Chem. Rev.* **1961**, *61*, 31.
(27) (a) Pryjomska, I.; Bartosz-Bechowski, H.; Ciunik, Z.; Trzeciak, A. M.; Ziolkowski, J. J. *Dalton Trans.* **2006**, *0*, 213(b) Dubrovina, N. V.; Börner, A. *Angew. Chem. Int. Ed.* **2004**, *43*, 5883(c) Nemoto, T.; Hamada, Y. *The Chemical Record* **2007**, *7*, 150.
(28) Berlin, K. D.; Butler, G. B. *Chem. Rev.* **1960**, *60*, 243.
(29) Kosolapoff, G. M. *J. Am. Pharm.* **1950**, *39*, 704.
(30) Freedman, L. D.; Doak, G. O. *Chem. Rev.* **1957**, *57*, 479.
(31) Burger, A.; Dawson, N. D. *J. Org. Chem.* **1951**, *16*, 1250.
(32) (a) Denney, D. B.; Greenbaum, M. A. *J. Am. Chem. Soc.* **1957**, *79*, 979(b) Greenbaum, M. A.; Denney, D. B.; Hoffmann, A. K. *J. Am. Chem. Soc.* **1956**, *78*, 2563.

(33) Bailey, W. J.; Buckler, S. A. *J. Am. Chem. Soc.* **1957**, *79*, 3567.
(34) Morgan, P. W.; Herr, B. C. *J. Am. Chem. Soc.* **1952**, *74*, 4526.
(35) Burg, A. B.; McKee, W. E. *J. Am. Chem. Soc.* **1951**, *73*, 4590.
(36) Meisenheimer, J.; Casper, J.; Höring, M.; Lauter, W.; Lichtenstadt, L.; Samuel, W. *Justus Liebigs Annalen der Chemie* **1926**, *449*, 213.
(37) Meisenheimer, J.; Lichtenstadt, L. *Berichte der deutschen chemischen Gesellschaft* **1911**, *44*, 356.
(38) Svara, J.; Weferling, N.; Hofmann, T. In *Ullmann's Encyclopedia of Industrial Chemistry*; Wiley-VCH Verlag GmbH & Co. KGaA, 2000.
(39) Kinfe, H. H.; Hamese, A.; Hughes, T.; Omondi, B. *Acta Crystallogr. Sect. E* **2011**, *67*, o3392.
(40) Rahil, J.; Haake, P. *J. Am. Chem. Soc.* **1981**, *103*, 1723.
(41) Bordwell, F. G. *Acc. Chem. Res.* **1988**, *21*, 456.
(42) Balakrishna, M. S.; Reddy, V. S.; Krishnamurthy, S. S.; Nixon, J. F.; Laurent, J. C. T. R. B. S. *Coord. Chem. Rev.* **1994**, *129*, 1.
(43) Ashby, M. T.; Li, Z. *Inorg. Chem.* **1992**, *31*, 1321.
(44) Balakrishna, M. S.; Santarsiero, B. D.; Cavell, R. G. *Inorg. Chem.* **1994**, *33*, 3079.
(45) (a) Newton, M. G.; King, R. B.; Chang, M.; Gimeno, J. *J. Am. Chem. Soc.* **1978**, *100*, 1632(b) Burrows, A. D.; Mahon, M. F.; Palmer, M. T.; Varrone, M. *Inorg. Chem.* **2002**, *41*, 1695.
(46) Wuts, P. G. M.; Greene, T. W. In *Greene's Protective Groups in Organic Synthesis*; John Wiley & Sons, Inc., 2006.
(47) Ona Burgos, P.; Fernandez, I.; Iglesias, M. J.; Garcia-Granda, S.; Lopez Ortiz, F. *Org. Lett.* **2008**, *10*, 537.
(48) Popovici, C.; Oña-Burgos, P.; Fernández, I.; Roces, L.; García-Granda, S.; Iglesias, M. a. J.; Ortiz, F. L. p. *Org. Lett.* **2010**, *12*, 428.
(49) Fernández, I.; Burgos, P. O.; Gómez, G. R.; Bled, C.; García-Granda, S.; López Ortiz, F. *Synlett.* **2007**, *2007*, 0611.
(50) Caravan, P.; Ellison, J. J.; McMurry, T. J.; Lauffer, R. B. *Chem. Rev.* **1999**, *99*, 2293.
(51) Mayer, A.; Neuenhofer, S. *Angew. Chem. Int. Ed.* **1994**, *33*, 1044.
(52) Charbonnière, L. J.; Ziessel, R.; Montalti, M.; Prodi, L.; Zaccheroni, N.; Boehme, C.; Wipff, G. *J. Am. Chem. Soc.* **2002**, *124*, 7779.
(53) Hutchings, G. J. B., M. Schmidbaur, H. *Chem. Soc. Rev.* **2008**, *37*, 1759.
(54) Menard, T.; Vol. 2010.
(55) Bersani, M., University of PADUA, 2008.
(56) Winter, J., 2007.
(57) Ming, M.; Chen, Y.; Katz, A. *Langmuir* **2002**, *18*, 2413.
(58) Imahori, H.; Arimura, M.; Hanada, T.; Nishimura, Y.; Yamazaki, I.; Sakata, Y.; Fukuzumi, S. *J. Am. Chem. Soc.* **2001**, *123*, 335.
(59) Chen, S. W.; Yang, Y. Y. *J. Am. Chem. Soc.* **2002**, *124*, 5280.
(60) Mendes, P. M.; Jacke, S.; Critchley, K.; Plaza, J.; Chen, Y.; Nikitin, K.; Palmer, R. E.; Preece, J. A.; Evans, S. D.; Fitzmaurice, D. *Langmuir* **2004**, *20*, 3766.
(61) Lee, K. Y.; Lee, Y. W.; Kwon, K.; Heo, J.; Kim, J.; Han, S. W. *Chem. Phys. Lett.* **2008**, *453*, 77.
(62) Corti, C. W.; Holliday, R. J.; Thompson, D. T. *Top. Catal.* **2007**, *44*, 331.
(63) Thompson, D. T. *Nano Today* **2007**, *2*, 40.
(64) Zhu, F.-X.; Wang, W.; Li, H.-X. *J. Am. Chem. Soc.* **2011**, *133*, 11632.
(65) Tian, Y.; Tatsuma, T. *J. Am. Chem. Soc.* **2005**, *127*, 7632.
(66) Rothrock, A. R.; Donkers, R. L.; Schoenfisch, M. H. *J. Am. Chem. Soc.* **2005**, *127*, 9362.

(67) Moon, S. Y.; Sekino, T.; Kusunose, T.; Tanaka, S. I. *J. Cryst. Growth* **2009**, *311*, 651.
(68) Corma, A.; Garcia, H. *Chem. Soc. Rev.* **2008**, *37*, 2096.
(69) Bigelow, W. C.; Pickett, D. L.; Zisman, W. A. *J. Colloid Sci.* **1946**, *1*, 513.
(70) Nuzzo, R. G.; Allara, D. L. *J. Am. Chem. Soc.* **1983**, *105*, 4481.
(71) (a) Allara, D. L.; Nuzzo, R. G. *Langmuir* **1985**, *1*, 45(b) Allara, D. L.; Nuzzo, R. G. *Langmuir* **1985**, *1*, 52(c) Schlotter, N. E.; Porter, M. D.; Bright, T. B.; Allara, D. L. *Chem. Phys. Lett.* **1986**, *132*, 93.
(72) (a) Sagiv, J. *J. Am. Chem. Soc.* **1980**, *102*, 92(b) Wasserman, S. R.; Tao, Y. T.; Whitesides, G. M. *Langmuir* **1989**, *5*, 1074.
(73) (a) Brandriss, S.; Margel, S. *Langmuir* **1993**, *9*, 1232(b) Kessel, C. R.; Granick, S. *Langmuir* **1991**, *7*, 532.
(74) Sabatani, E.; Rubinstein, I.; Maoz, R.; Sagiv, J. *J. Electroanal. Chem.* **1987**, *219*, 365.
(75) Dubois, L. H.; Nuzzo, R. G. *Annu. Rev. Phys. Chem.* **1992**, *43*, 437.
(76) Sellers, H.; Ulman, A.; Shnidman, Y.; Eilers, J. E. *J. Am. Chem. Soc.* **1993**, *115*, 9389.
(77) Troughton, E. B.; Bain, C. D.; Whitesides, G. M.; Nuzzo, R. G.; Allara, D. L.; Porter, M. D. *Langmuir* **1988**, *4*, 365.
(78) Sabatani, E.; Cohen-Boulakia, J.; Bruening, M.; Rubinstein, I. *Langmuir* **1993**, *9*, 2974.
(79) Bryant, M. A.; Joa, S. L.; Pemberton, J. E. *Langmuir* **1992**, *8*, 753.
(80) Hill, W.; Wehling, B. *J. Phys. Chem.* **1993**, *97*, 9451.
(81) Li, T. T. T.; Liu, H. Y.; Weaver, M. J. *J. Am. Chem. Soc.* **1984**, *106*, 1233.
(82) Cooper, J. M.; Greenough, K. R.; McNeil, C. J. *J. Electroanal. Chem.* **1993**, *347*, 267.
(83) Ihs, A.; Uvdal, K.; Liedberg, B. *Langmuir* **1993**, *9*, 733.
(84) Arndt, T.; Schupp, H.; Schrepp, W. *Thin Solid Films* **1989**, *178*, 319.
(85) Mielczarski, J. A.; Yoon, R. H. *Langmuir* **1991**, *7*, 101.
(86) Edwards, T. R. G.; Cunnane, V. J.; Parsons, R.; Gani, D. *J. Chem. Soc.* **1989**, *0*, 1041.
(87) Samant, M. G.; Brown, C. A.; Gordon, J. G. *Langmuir* **1992**, *8*, 1615.
(88) Miller, M. S.; Juan, R. R. S.; Ferrato, M.-A.; Carmichael, T. B. *Langmuir* **2011**, *27*, 10019.

CHAPTER 2

The Reactivity of Dinuclear Gold(I) Dithiophosphonate Complexes

2.1 Introduction

Dithio-organophosphorus compounds have found widespread use, not only in basic academic research, but also in diverse and important industrial areas.[1]

2.1.1 Synthesis of dithiophosphonates

The driving force for the preparation of dithiophosphonates is the nucleophillic attack of cyclic dimeric phosphetane disulfides $[RP(S)S]_2$.[2] Currently a commonly used dimer, namely Lawesson's Reagent (LR), is used as a sulfur transfer reagent in organic chemistry that occurs by the conversion of a carbonyl functional group into thiocarbonyl (or thione).[3] Earlier variations of the dimer dates back to 1952, when the reaction of cyclohexene with phosphorus pentasulfide was reported by Fay and Lankelma.[4] Original preparation of the dimer involved the reaction of $PhP(S)Cl_2$ with H_2S gas at 210 °C which results in dimer **A,** shown in **Figure 2.1**. This hazardous undertaking has since been replaced by the reaction of electron rich aromatics with P_4S_{10}, which allows for the synthesis of a multitude of phosphetane dimers. LR is readily prepared from phosphorus pentasulfide and anisole forming **B**.[2] Two significant dimers are the ferrocenyl analogue[5] **E** and selenium analogue[6] **C**, both pioneered by Woollins and co-workers, the latter is commercially available as Woollins' Reagent. Several other derivatives are highlighted in Figure 2.1 below.

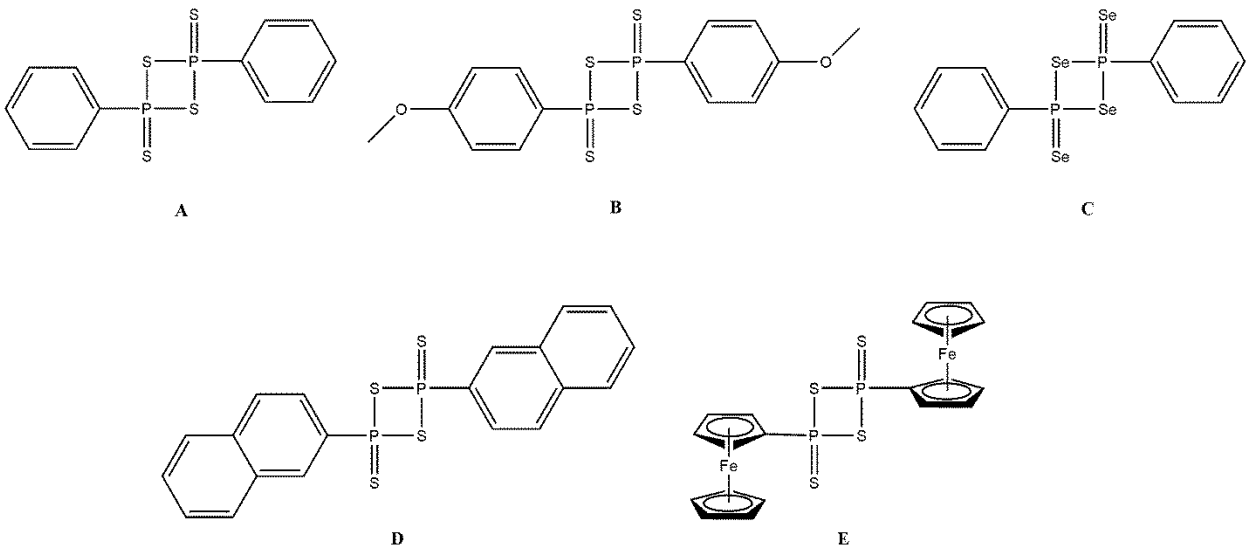

Figure 2.1 Comparison of phosphetane cyclic dimers containing electron rich aromatics and –organometallics

The oxophilic nature of the 4-coordinate phosphorus(V) is the key to the synthetic scheme. The addition of 1° or 2° alcohols to the dimer results in symmetric cleavage and the formation of the corresponding asymmetric dithiophosphonic acid. Therefore a large variety of dithiophosphonate acids can be prepared in a simple manner, **Scheme 2.1**, allowing ligand properties (steric and electronics) to be tuned based on the type of alcohol employed. Alcohols which have a melting point at 70° C or below can be employed to produce ligands *via* a "green" approach, i.e. solvent free. The relative acidity (pKa ~ 2) of the proton allows for deprotonation with a weak base such as ammonia, resulting in the formation of monoanionic salts.

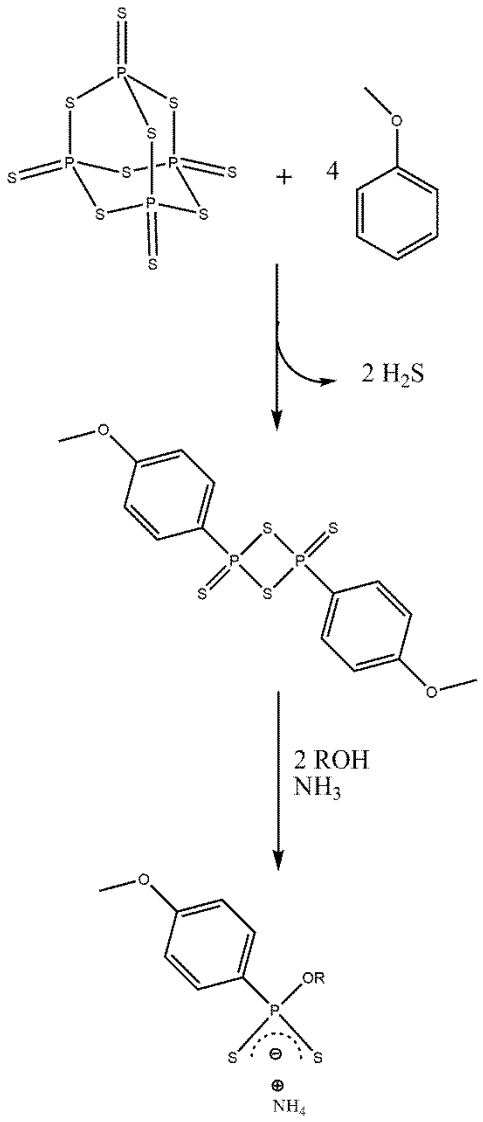

Scheme 2.1 Synthesis of dithiophosphonate ammonium salts

2.1.2 Aurophilicity and its implications on gold(I) chemistry

Closed-shell d^{10} gold(I) metal centres, which typically form linear 14 electron complexes, bind to each other at distances slightly larger than in gold metal, but much smaller than the sum of their van der Waals radii, with energies comparable to that of hydrogen bonding, have created a plethora of coordination compounds which defy conventional geometries.[7] The unique characteristics can be attributed to aurophilic interactions which find their origin in relativistic and polarization effects imposed on relevant orbitals.[8] The relativistic effect experienced by gold are significantly larger than neighbouring elements in the periodic table, and is a local

maximum for the coinage (Group 11) metals.[9] The basis for relativistic effects is the acceleration of the outer electrons to speeds approaching that of light, which arises due to an increase in the proton population of heavier nuclei.[10] This results in the contraction of the *s* and *p* orbitals, and subsequent expansion of the *d* orbital, ultimately reducing the energy gap between the *6s* and *5d* orbitals significantly.[11] Theoretical calculations that have qualitatively and quantitatively reviewed this occurrence are abundant.[8-9,11-12] Since their first discovery, the analogy between Au···Au contacts and hydrogen bonding has been drawn.[13] The most apparent and earliest examples of this phenomenon were demonstrated by Schmidbaur in the late 1980's, in which several auromethanes were synthesized and characterized.[10,14] The formation of hexakis(triphenylphosphaneauro)methane di-cation $[C(Ph_3PAu)_6]^{2+}$ (**Figure 2.2**), whose arrangement consists of linear Ph_3P-Au in a octahedral pattern around a hypervalent carbon, shows the ability of the aurophilic interactions to stabilize the formation of a polyauromethanes.[15]

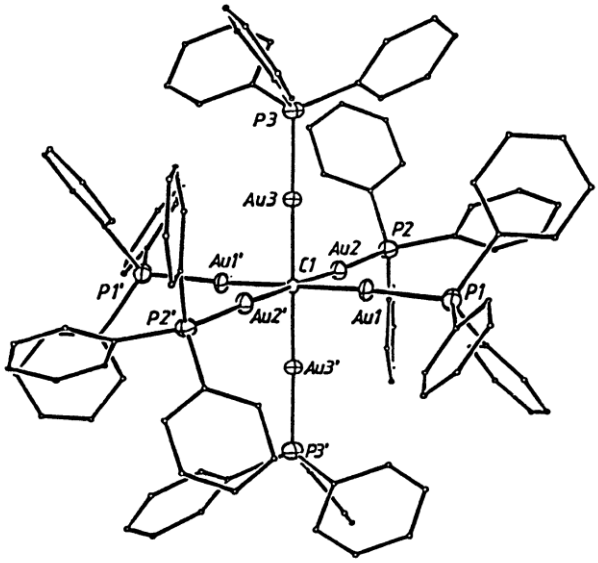

Figure 2.2 Structure of $[C(Ph_3PAu)_6]^{2+}$ isolated by Schmidbaur and co-workers showing an octahedral C atom which defies explanation by simple valence bond theory**[10]**

The isolability of $[AuPR_3]^+$ with H^+ has become apparent with the spectroscopic and theoretical investigations of hyper coordinate gold analogues of the first row elements i.e. ammonium, phosphonium, arsonium, and oxonium cations, which possess remarkable stability.[15b,16] An

examination of the gold structures, deposited in the Cambridge Structural Database, shows a range of 2.5 – 4 Å for Au-Au contacts, whilst up to 3.5 Å is considered aurophilic.[17]

Two-coordinate, linear gold(I) complexes (illustrated in **Figure 2.3**) are the most studied compounds in gold chemistry.[18] Due to its low coordination, gold(I) forms neutral and ionic complexes of the general formula X-Au-Y (X=Y=neutral or anionic ligands).[11] The intermolecular Au···Au interactions results in the formation of polymeric chains, which in turn allows these interactions to become more pronounced in dinuclear units that form these polymeric chains.

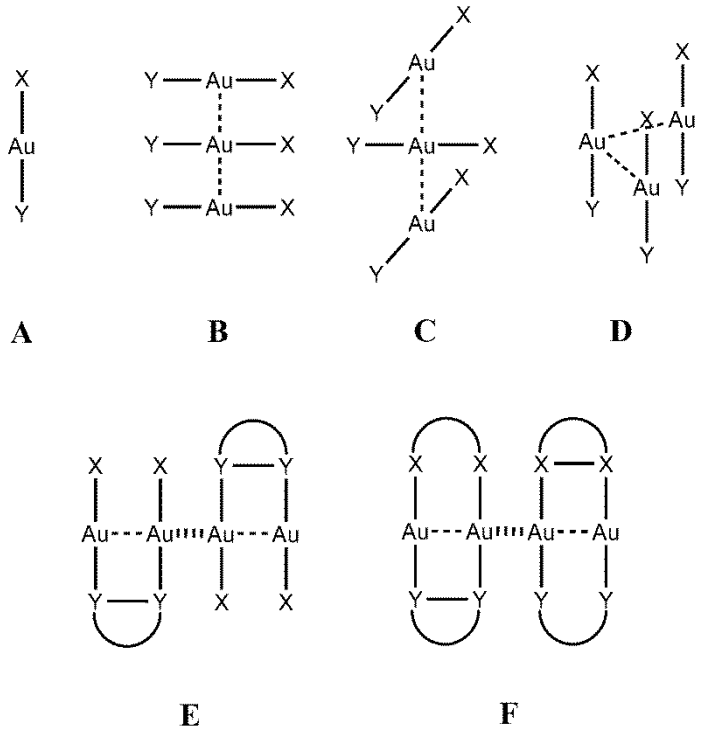

Figure 2.3 Common binding motifs in gold(I) complexes. Unsupported ligands: A, B, C, D Semi supported: E Fully supported: F[19]

This is due to the possibility of both inter- and intramolecular Au···Au interactions induced with di- and poly-nuclear gold(I) complexes.[19-20] Dinuclear gold(I) complexes are of particular interest due to the close proximity of two Au(I) metal centers in the same molecule; this facilitates the study of Au···Au interactions.[19] The luminescence properties for this distinct class of gold(I) complexes have also been studied and for certain ligands revealed the interesting

feature that the presence or absence of intermolecular Au···Au interactions could be predicted based solely on an analysis of the solid-state emission profiles.[21]

Since the initial report on dinuclear gold(I) dithiophosphonate complexes of the type $[AuS_2PR(OR')]_2$ in 1998,[22] a significant number of new dithiophosphonate derivatives with Group 11 metals have been reported.[23] The number of gold(I) dinuclear dithiophosphonate complexes supersede any other metal in terms of nuclearity and oxidation state studies, for this ligand class.[23]

The primary focus of this section is to introduce an auxiliary coordination structure into the dithiophosphonate, which would be capable of creating novel gold(I) dinuclear complexes, with the inherent ability of producing larger molecular assemblies. The auxiliary constituent is to be introduced *via* the parent alcohol leading to the dithiophosphonic acid. Phenylmethanol and butanol, provides novelty and versatility in the coordination patterns of gold complexes[24].

2.1.3 Silver dithiophosphonate complexes

Silver dithiophosphonate complexes have always been superseded by its gold derivatives and only recently was the first *mono*nuclear silver(I) dithiophosphonate complexes reported.[25] Dinuclear silver(I) complexes aid in illustrating the differences between gold and silver namely the relativistic effects in the "coinage metals".[9] A Dinuclear silver(I) complex $[Ag\{S_2P(OMe)(4\text{-}C_6H_4OEt)\}\{PPh_2\}]_2$, containing an eight-membered $Ag_2S_4P_2$ ring was synthesized by Haiduc *et al*.[26]

2.2 Results and Discussion

The results herein depict the study of dithiophosphonate gold(I) and silver(I) complexes and the reactivity of dithiophosphonate gold(I) complexes toward bis(diphenylphosphine) methane. Two dithiophosphonate ligands where synthesized and these were further reacted with a gold(I) and silver(I) precursors, thereafter these complexes were further reacted and analysed.

2.2.1 Ligand preparation

The 2,4-diaryl-1,3-dithiadiphosphetane disulfide dimer, reacts with two stoichiometric equivalents of phenylmethanol or 1-butanol, symmetrically cleaving the dimer, to produce the two ligands $(NH_4)[(S_2P\text{-}1,4\text{-}C_6H_4OEt)(OCH_2C_6H_5)]$ (**Scheme 2.2**) and $(NH_4)[(S_2P\text{-}1,4\text{-}C_6H_4OEt)(OCH_2CH_2CH_2CH_3)]$ (**Scheme 2.3**).

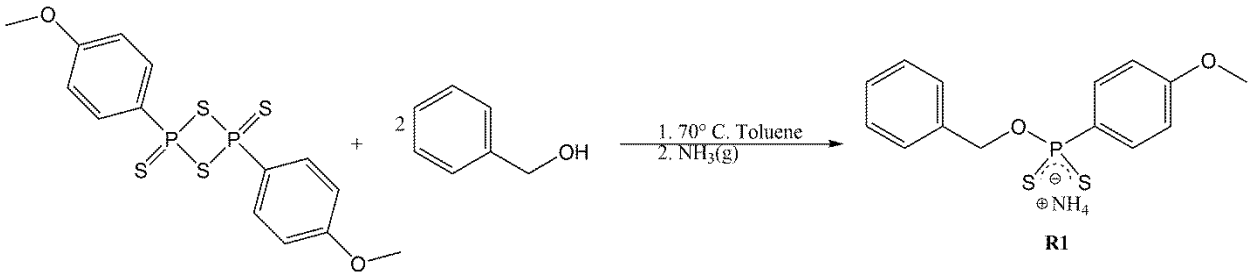

Scheme 2.2 Symmetric cleavage of Lawesson's reagent with phenylmethanol

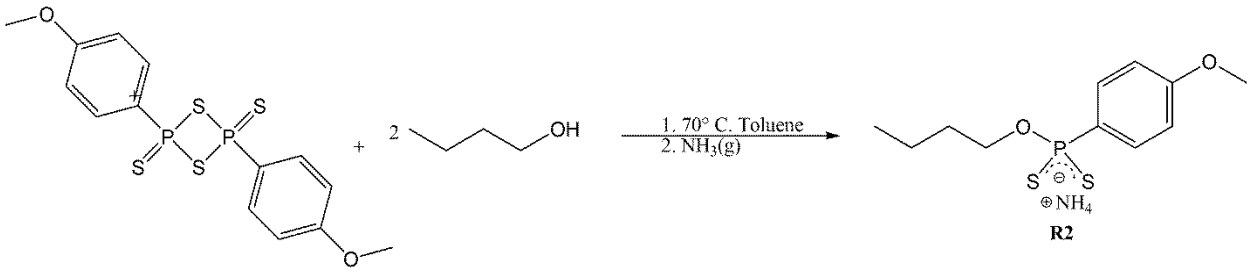

Scheme 2.3 Symmetric cleavage of Lawesson's reagent with 1-butanol

Full elucidation by solution NMR spectroscopy (^1H, ^{31}P and ^{13}C) was conducted in methanol-D4 as the ammonium dithiophosphonate salts proved insoluble in $CDCl_3$.

The reaction occurs due the oxophilic nature of the 4-coordinate phosphorus. In ^{31}P NMR, the isolated dithiophosphonate ligands show a single resonance peak at 106 ppm and 108 ppm for **R1** and **R2** derivatives, respectively. Peaks for such ligand derivatives typically fall within the region, 90 to 112 ppm.[2] The ^1H and ^{13}C NMR spectra of the salts were consistent with the

presence of both methyl and the respective alkoxy moieties, (see experimental **section 2.34** and **2.35**).

Infrared spectra of the dithiophosphonate salts show distinct bands at 1101 and 1111 cm^{-1}, 1018 and 1006 cm^{-1}, 680 and 660 cm^{-1} and 554 and 545 cm^{-1}, corresponding to ν[(P)–O–C], ν[P–O–(C)], $\nu(PS)_{asym}$ and $\nu(PS)_{sym}$ stretches, respectively.[27] The broad bands at 2960 and 3467 cm^{-1} corresponded to the N-H stretching bands and provided an indication that an ammonium salt was present.[28] Melting point analysis was also carried out and sharp melting point ranges in each case were obtained. Further proof of ligand formation was afforded by the subsequent complexation reactions of each ligand and X-ray crystallographic studies of the gold(I) complexes.

2.2.2 Gold(I) dinuclear dithiophosphonate complexes

The reaction of $(NH_4)[(S_2P\text{-}1,4\text{-}C_6H_4OEt)(OCH_2C_6H_5)]$ or $(NH_4)[(S_2P\text{-}1,4\text{-}C_6H_4OEt)(OCH_2CH_2CH_2CH_3)]$ with [AuCl(tht)] (tht = tetrahydrothiophene) in THF (molar ratio 1:1) led to the formation of new dinuclear gold(I) complexes, **Schemes 2.4** and **2.5**. The dinuclear gold(I) macro cycles with S-P-S bridging moieties follow coordination patterns observed previously in literature.[22]

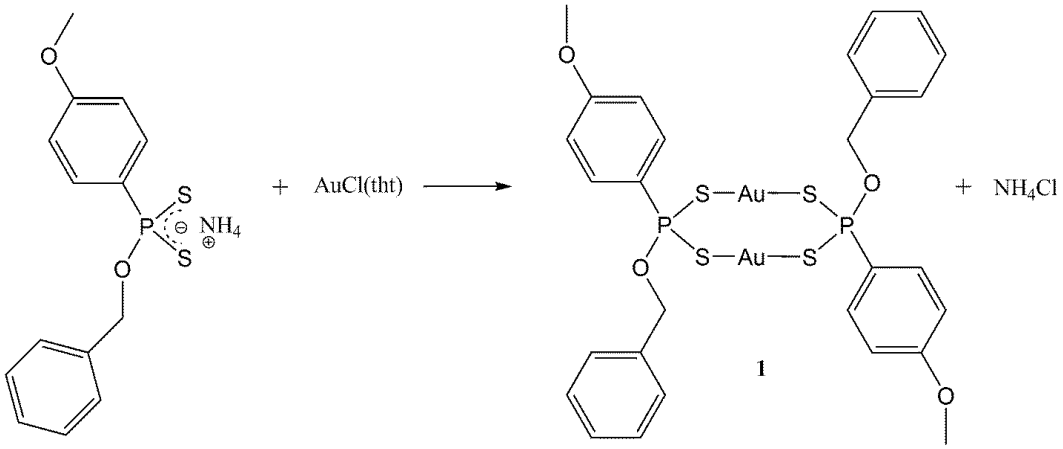

Scheme 2.4 Formation of a linear gold(I) metallacyclic complex **1**

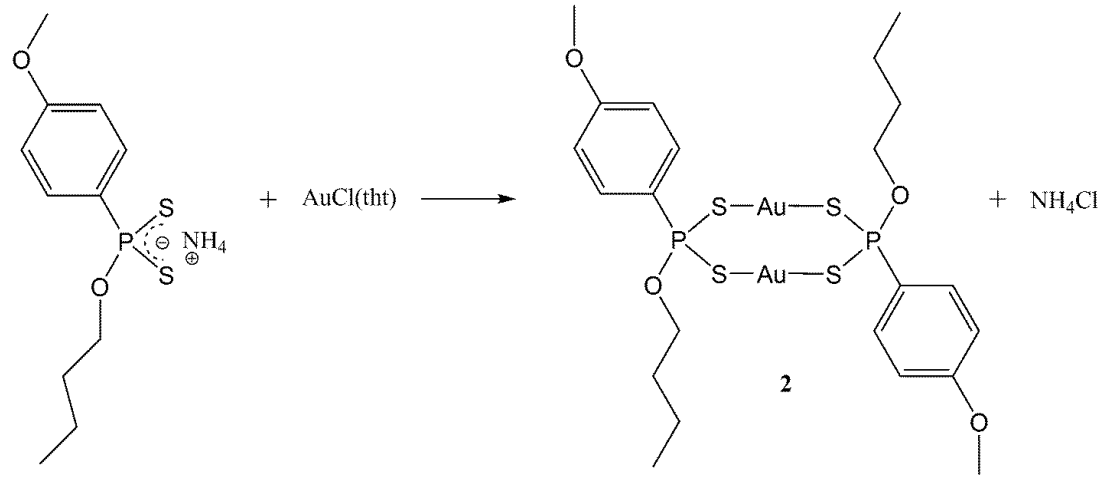

Scheme 2.5 Formation of a linear gold(I) complex **2**

Infrared spectra of the complexes formed were consistent with data previously discussed for the ligand IR assignment (**see experimental section 2.36 and 2.37**), a notable feature of the complex IR spectra, however, was the disappearance of the broad N-H stretching bands associated with the dithiophosphonate salt, indicating removal of the ammonium ion and thus binding of the ligand to the metal nucleus. The dinuclear gold(I) dithiophosphonate complexes were all subjected to solution NMR examination (^{1}H, ^{31}P and ^{13}C) in $CDCl_3$. The complexes, unlike their respective parent ligands, were readily soluble in deuterated chloroform. The ^{1}H and ^{13}C spectra confirmed the presence of the methyl and respective alkoxy groups. The asymmetrical nature of the ligand induces isomerisation and two well resolved resonance peaks for complex **1** were observed at 105 and 103 ppm and for complex **2**, these peaks were observed at 104 and 102 ppm.

These peaks are assigned to *anti* and *syn* configurations, relative to substitution of the four coordinate phosphorus atom, as shown in **Scheme 2.6** below. The energy barrier between the isomeric forms in solution is sufficiently small to allow for rapid transition between isomers; however, the residence time of each can be monitored on the NMR time-scale. The *anti* isomer contains an inversion centre between the gold centres which is lost upon reconfiguration to the *syn* isomer.

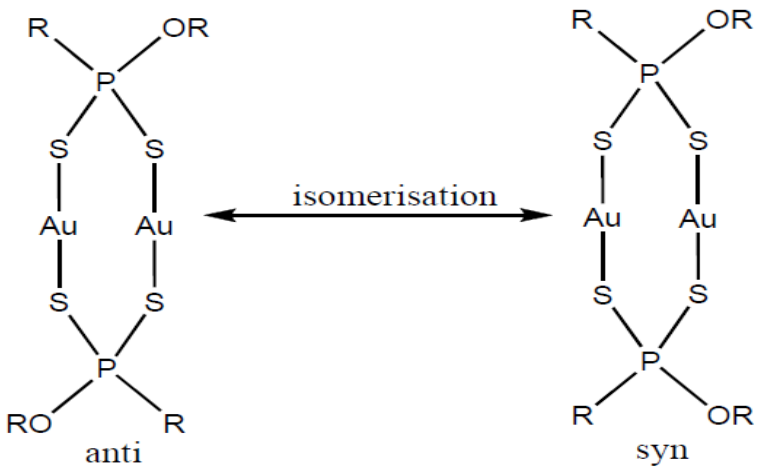

Scheme 2.6 Isomerisation present in solution

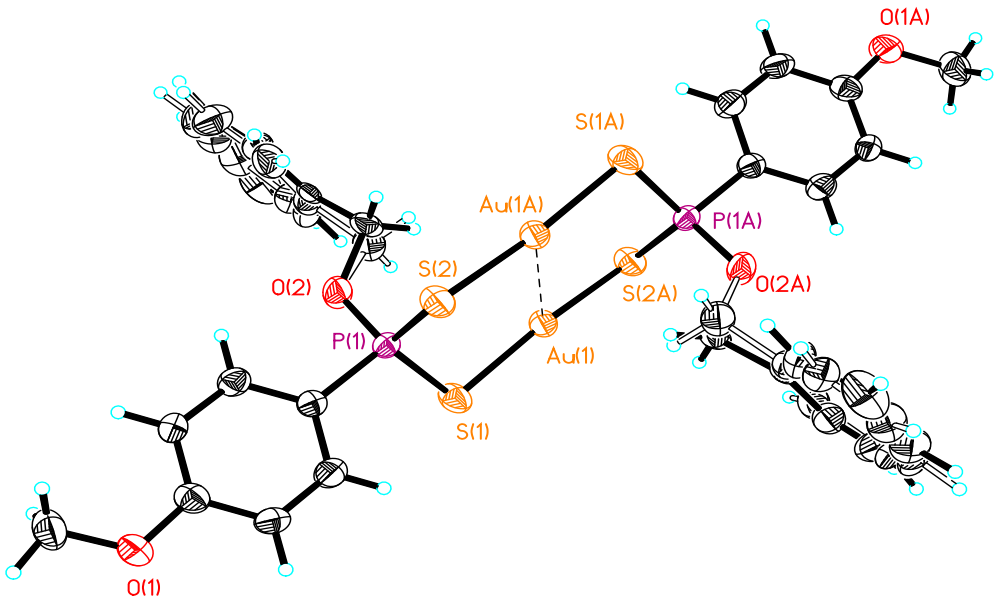

Figure 2.4 Molecular structure of complex **1.** Thermal ellipsoids are drawn at the 50% probability level

The neutral 8-membered macrocycle adopts an elongated chair conformation. The structure crystallized in the triclinic crystal system and was solved in the P -1 space group with the centre

of inversion situated in the middle of the Au_2S_4 manifold. The trans-annular distance between the S-S atoms is *ca.* 3.422 Å. The fully supported intramolecular Au···Au distance is 3.0923(5) Å which caused a slight distortion from an ideal linear geometry expected for this 2-coordinate system, resulting in an S-Au-S bond angle of 171.71(4)°. Intermolecular Au···Au contacts are absent. The S-P bond lengths are 2.0134(15) and 2.0182(16) Å, which reflects coordination with delocalization of the charge over the whole S-P-S fragment. The tetrahedral geometry of the P atom shows a small deviation from the expected 109.5°.

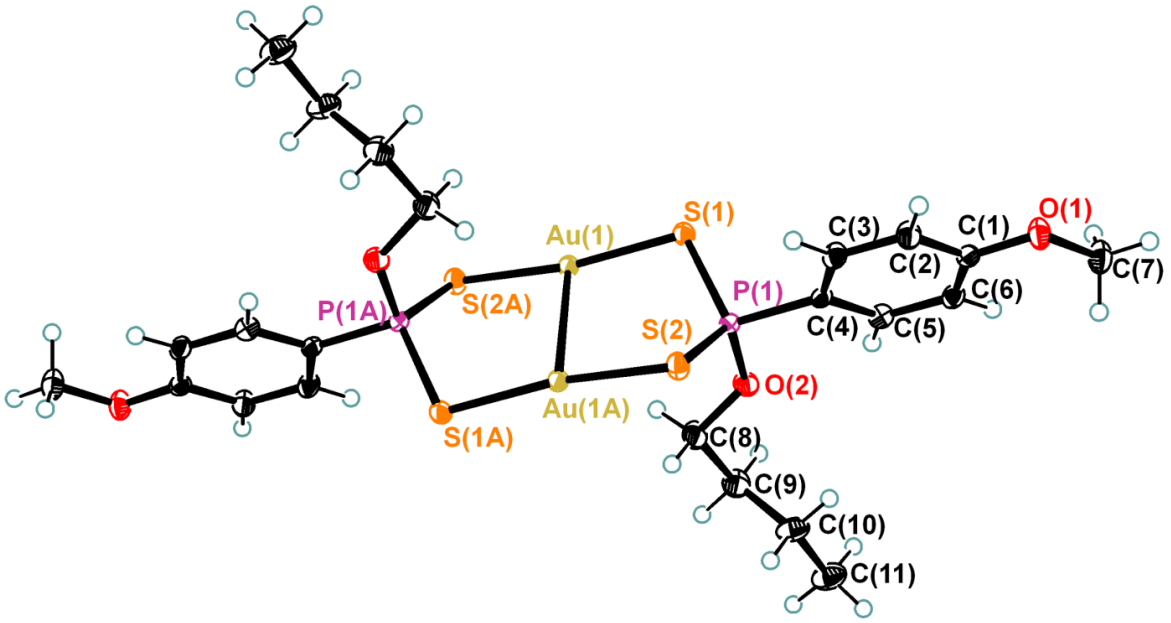

Figure 2.5 Molecular structure of complex **2.** Thermal ellipsoids are drawn at the 50% probability level

Complex **2** adopts the same elongated chair conformation as complex **1**. However, complex **2** crystallized in the monoclinic crystal system and was solved in the $P2_{1/c}$ space group with the centre of inversion situated in the middle of the Au_2S_4 manifold, as for 1. In this instance the trans-annular distance between the S-S atoms is *ca.* 3.435 Å and the fully supported intramolecular Au···Au distance is 3.0613(7) Å which causes a similar distortion from the ideal linear geometry, also resulting in the S-Au-S bond angle of 170.472(17)°. From complex **2** intermolecular Au···Au contacts are also absent, as for **1**. The S-P bond lengths are 2.0290(10) and 2.0117(9) Å, which reflects a similar coordination mode to complex **1**.

Table 2.1 Selected Bond lengths [Å] and angles [°] for complex **1**

Au(1)-Au(1A)	3.0923(5)	S(1)-Au(1)-S(2)	171.71(4)
Au(1)-S(1)	2.2908(11)	S(1)-Au(1)-Au(1A)	94.00(3)
Au(1)-S(2A)	2.2930(11)	S(2A)-Au(1)-Au(1A)	94.25(3)
P(1)-C(1)	1.789(4)	P(1)-S(1)-Au(1)	103.60(5)
S(1)-P(1)	2.0134(15)	P(1)-S(2)-Au(1A)	103.64(6)
S(2)-P(1)	2.0182(16)	O(2)-P(1)-C(1)	101.47(17)
S(2)-Au(1A)	2.2930(11)	O(2)-P(1)-S(1)	112.61(15)
P(1)-O(2)	1.578(3)	C(4)-O(1)-C(7)	118.0(3)
		O(2)-P(1)-S(2)	111.72(15)
		C(1)-P(1)-S(2)	106.33(14)
		S(1)-P(1)-S(2)	116.17(7)
		C(1)-P(1)-S(1)	107.14(14)

Table 2.2 Selected Bond lengths [Å] and angles [°] for complex 2

Au(1)-Au(1A)	3.0613(7)	S(1)-Au(1)-S(2A)	170.472(17)
Au(1)-S(1)	2.2909(9)	S(1)-Au(1)-Au(1A)	91.74(3)
Au(1)-S(2A)	2.3026(10)	S(2)-Au(1A)-Au(1)	97.56(3)
P(1)-C(4)	1.787(2)	P(1)-S(1)-Au(1)	106.01(4)
S(1)-P(1)	2.0290(10)	P(1)-S(2)-Au(1A)	101.98(3)
S(2)-P(1)	2.0117(9)	O(2)-P(1)-C(4)	101.18(9)
S(2)-Au(1A)	2.3026(10)	O(2)-P(1)-S(1)	111.39(7)
P(1)-O(2)	1.5808(17)	C(1)-O(1)-C(7)	116.53(17)
		O(2)-P(1)-S(2)	112.70(7)
		C(4)-P(1)-S(2)	107.72(7)
		S(2)-P(1)-S(1)	116.42(5)
		C(4)-P(1)-S(1)	105.97(7)

There are no distinct Au···Au intermolecular attractions holding the molecules in the crystal structure together for complexes **1** or **2**, however, in complex **1** there is intermolecular hydrogen bonding between the sulfur S(2) and hydrogen H(2) with a contact measuring *ca.* 2.895 Å to an adjacent aromatic hydrogen, shown in **Figure 2.6**.

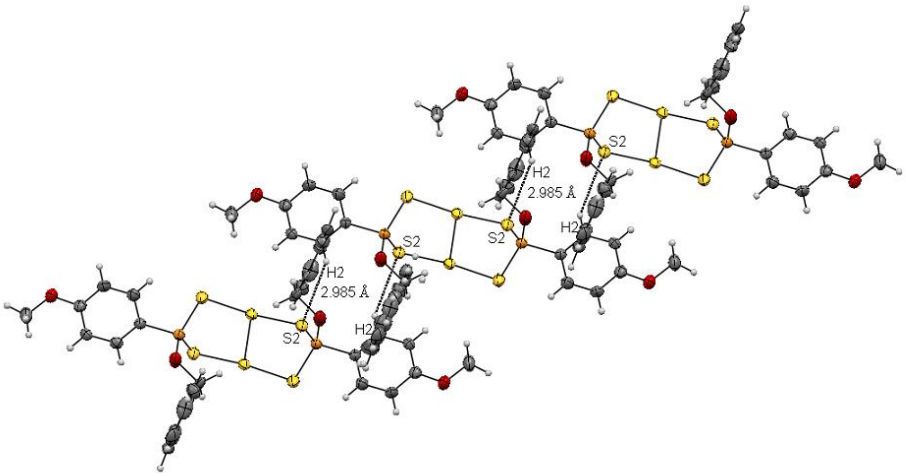

Figure 2.6 Structure of complex **1** showing the H-bonding present

This secondary interaction is of sufficient energy to direct crystal packing forces in the crystal lattice, and possibly actively inhibit weaker intermolecular Au···Au contacts. The resulting stacked configuration, shown in **Figure 2.7**, of the molecules in the crystal lattice is not due to aurophilic interactions but due to hydrogen bonding. The eight-member metallocycle of **1** is arranged in parallel chains normal to the (001) plane. **Figure 2.8** shows the orientation of Complex **2** in a zigzag manner with the 8 member manifold situated in the (101) plane.

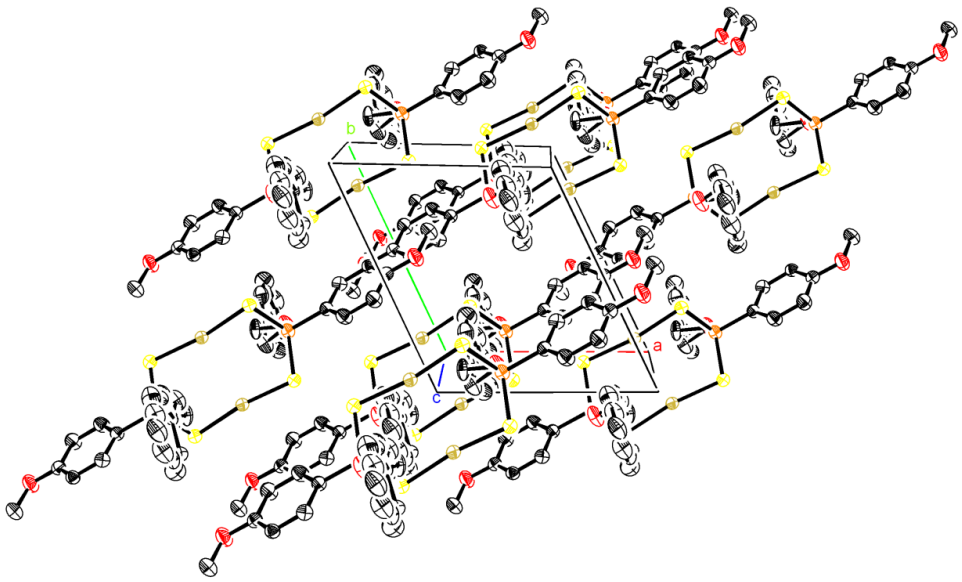

Figure 2.7 Crystal packing of **1** as seen along the *c* axis

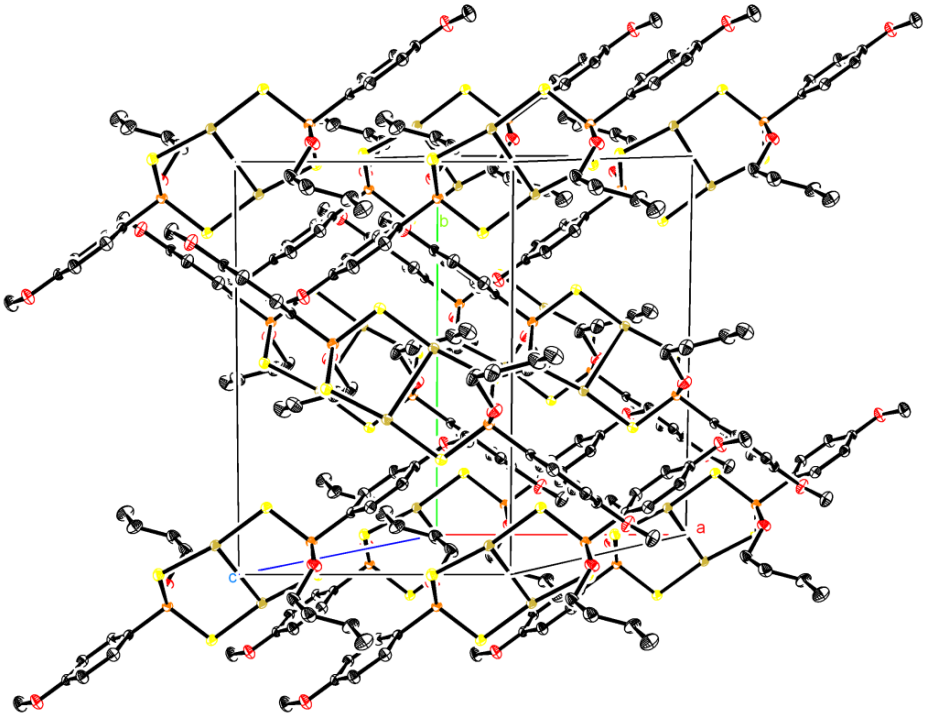

Figure 2.8 Crystal packing of **2** as seen down the *b* axis

Table 2.3 Crystal data and structure refinement for **1**

Empirical formula	C28 H28 Au2 O4 P2 S4	
Formula weight	1012.62	
Temperature	173(2) K	
Wavelength	0.71073 Å	
Crystal system	Triclinic	
Space group	P -1	
Unit cell dimensions	a = 8.8664(11) Å	α= 97.3090(10)°.
	b = 9.6680(12) Å	β= 106.2380(10)°.
	c = 10.8408(13) Å	γ = 114.4670(10)°.
Volume	780.05(17) $Å^3$	
Z	1	
Density (calculated)	2.156 Mg/m^3	
Absorption coefficient	9.796 mm^{-1}	
Crystal size	0.24 x 0.12 x 0.05 mm^3	
Theta range for data collection	2.04 to 25.42°.	
Index ranges	-10<=h<=10, -11<=k<=11, -13<=l<=13	
Reflections collected	12798	
Independent reflections	2866 [R(int) = 0.0308]	
Completeness to theta = 25.42°	99.5 %	
Absorption correction	Semi-empirical from equivalents	
Max. and min. transmission	0.6560 and 0.2039	
Refinement method	Full-matrix least-squares on F^2	
Goodness-of-fit on F^2	1.040	
Final R indices [I>2sigma(I)]	R1 = 0.0216, wR2 = 0.0535	
R indices (all data)	R1 = 0.0244, wR2 = 0.0553	
Largest diff. peak and hole	1.531 and -0.613 $e.Å^{-3}$	

Table 2.4 Crystal data and structure refinement for **2**

Empirical formula	C22 H32 Au2 O4 P2 S4	
Formula weight	944.59	
Temperature	173(2) K	
Wavelength	0.71073 Å	
Crystal system	Monoclinic	
Space group	P21/c	
Unit cell dimensions	a = 9.811(5) Å	α = 90°.
	b = 14.727(5) Å	β = 126.52(3)°.
	c = 12.220(4) Å	γ = 90°.
Volume	1418.9(10) $Å^3$	
Z	2	
Density (calculated)	2.211 Mg/m^3	
Absorption coefficient	10.762 mm^{-1}	
Crystal size	0.42 x 0.21 x 0.17 mm^3	
Theta range for data collection	2.49 to 28.43°.	
Index ranges	-13<=h<=13, -19<=k<=19, -16<=l<=16	
Reflections collected	30880	
Independent reflections	3556 [R(int) = 0.0298]	
Completeness to theta = 28.43°	99.5 %	
Absorption correction	Semi-empirical from equivalents	
Max. and min. transmission	0.2620 and 0.0931	
Refinement method	Full-matrix least-squares on F^2	
Goodness-of-fit on F^2	1.731	
Final R indices [I>2sigma(I)]	R1 = 0.0140, wR2 = 0.0361	
R indices (all data)	R1 = 0.0160, wR2 = 0.0366	
Largest diff. peak and hole	1.003 and -0.998 $e.Å^{-3}$	

2.2.3 Silver(I) dinuclear dithiophosphonate complex

The reaction of $(NH_4)[(S_2P\text{-}1,4\text{-}C_6H_4OEt)(OCH_2CH_2CH_2CH_3)]$ with $[Ag(NO_3)]$ in THF (molar ratio 1:1) led to the formation of new dinuclear silver(I) complex, **Schemes 2.7**. The dinuclear silver(I) macro cycle with S-P-S bridging moieties, follow the predictable NMR and IR patterns as illustrated by dinuclear gold(I) macro cycles.

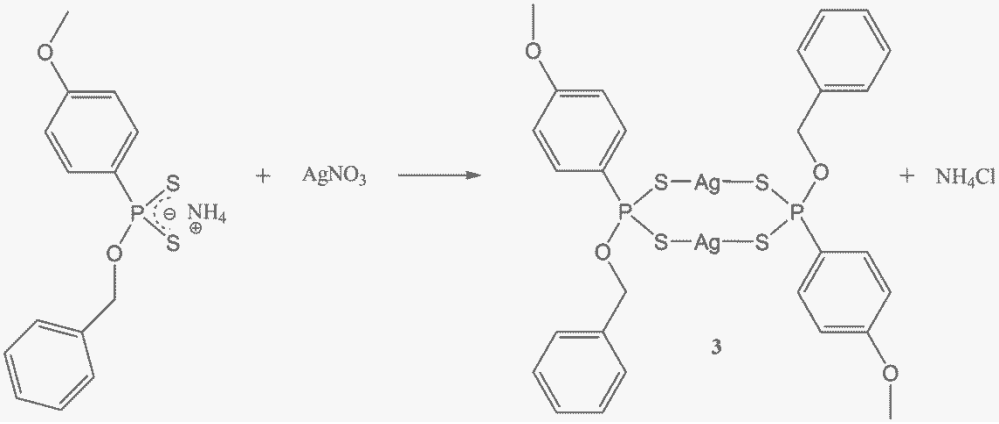

Scheme 2.7 Formation of a linear silver(I) metallacyclic complex **3.**

Infrared spectra of complex **3** formed were consistent with data previously discussed for the ligand and gold(I) complex IR assignment (see experimental **Section 2.3.8**). The notable feature of the complex IR spectrum was the disappearance of the broad N-H stretching bands associated with the dithiophosphonate salt, indicating removal of the ammonium ion and thus binding of the ligand to the metal nucleus.

The Ag(I) dithiophosphonate complex was subjected to solution NMR examination (^1H, ^{31}P and ^{13}C) in $CDCl_3$. The complex, unlike the respective parent ligand, was again, readily soluble in deuterated chloroform. The ^1H and ^{13}C spectra confirmed the presence of the methyl and respective alkoxy group. Due to the asymmetrical nature of the ligand which induces isomerisation, two well resolved resonance peaks for complex **3**, which were observed at 105 and 107 ppm.

2.2.4 Reactivity studies

Previous studies have shown the reaction of bis-phosphines with dinuclear gold(I) dithiophosphonates complexes such as **1** and **2** results in the formation of bridged open-ended and closed 8-membered dinuclear unit complexes of the type $Au_2dppm(dtp)_2$, **A** and $Au_2dppm(dtp{=}O)$, **B** (dtp = dithiophosphonate) as shown in **Scheme 2.8**.[29]

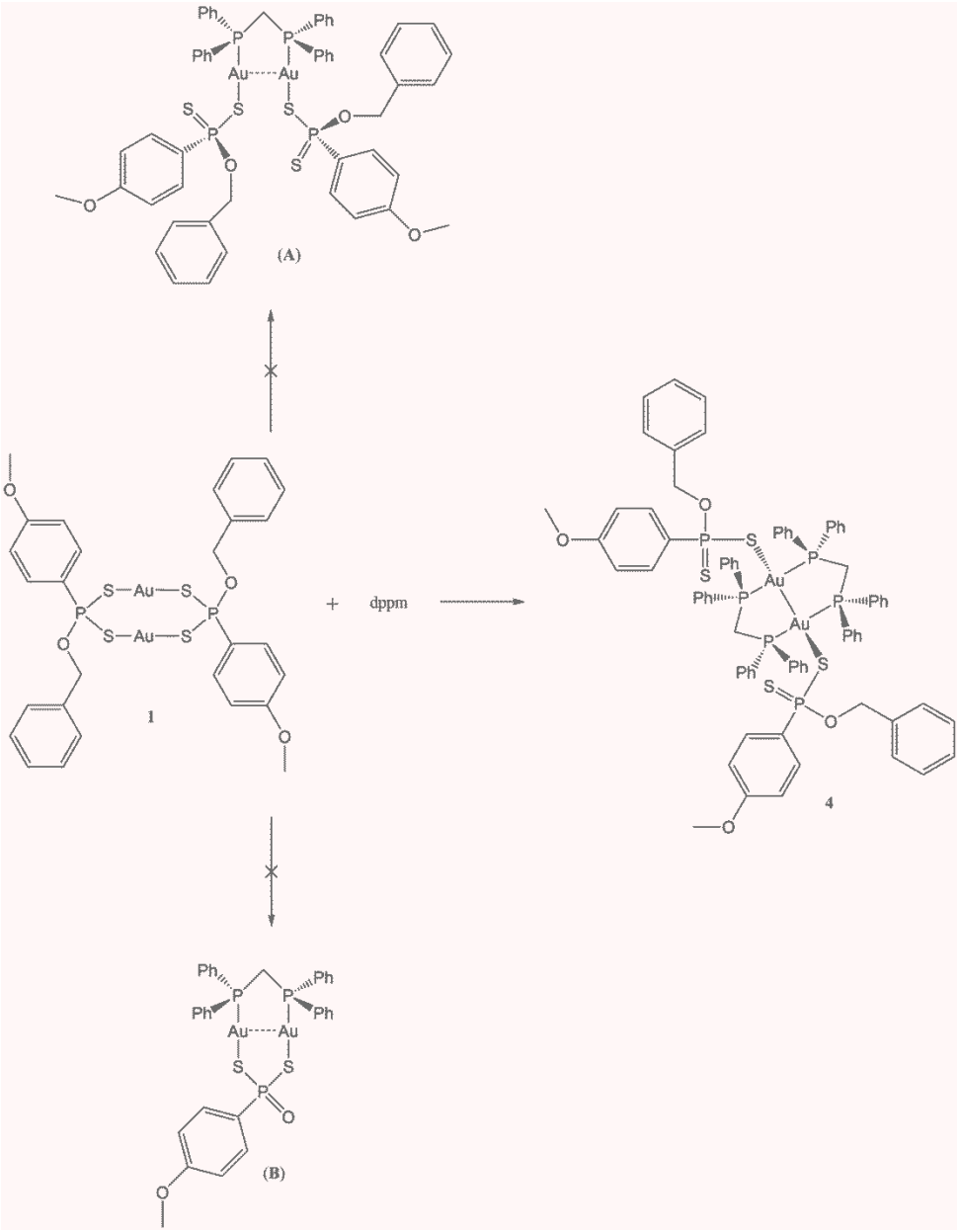

Scheme 2.8 Reaction of dinuclear units with dppm, (**A** and **B**) predicted product, (**4**) actual product

This study hypothesized that the alcohol groups used to synthesize the dithiophosphonate moiety leads to the formation of different complexes, as seen in **Scheme 2.8**. In particular, alcohols that have the ability to form stable carbo-cations (such aromatic derivatives) lead to the formation of **B** and those that do not form stable carbo cations (such as straight chain alkyls) lead to the formation of **A**. Using the two alcohols used in this study the postulated formation of the two forms are shown in **Scheme 2.9**.

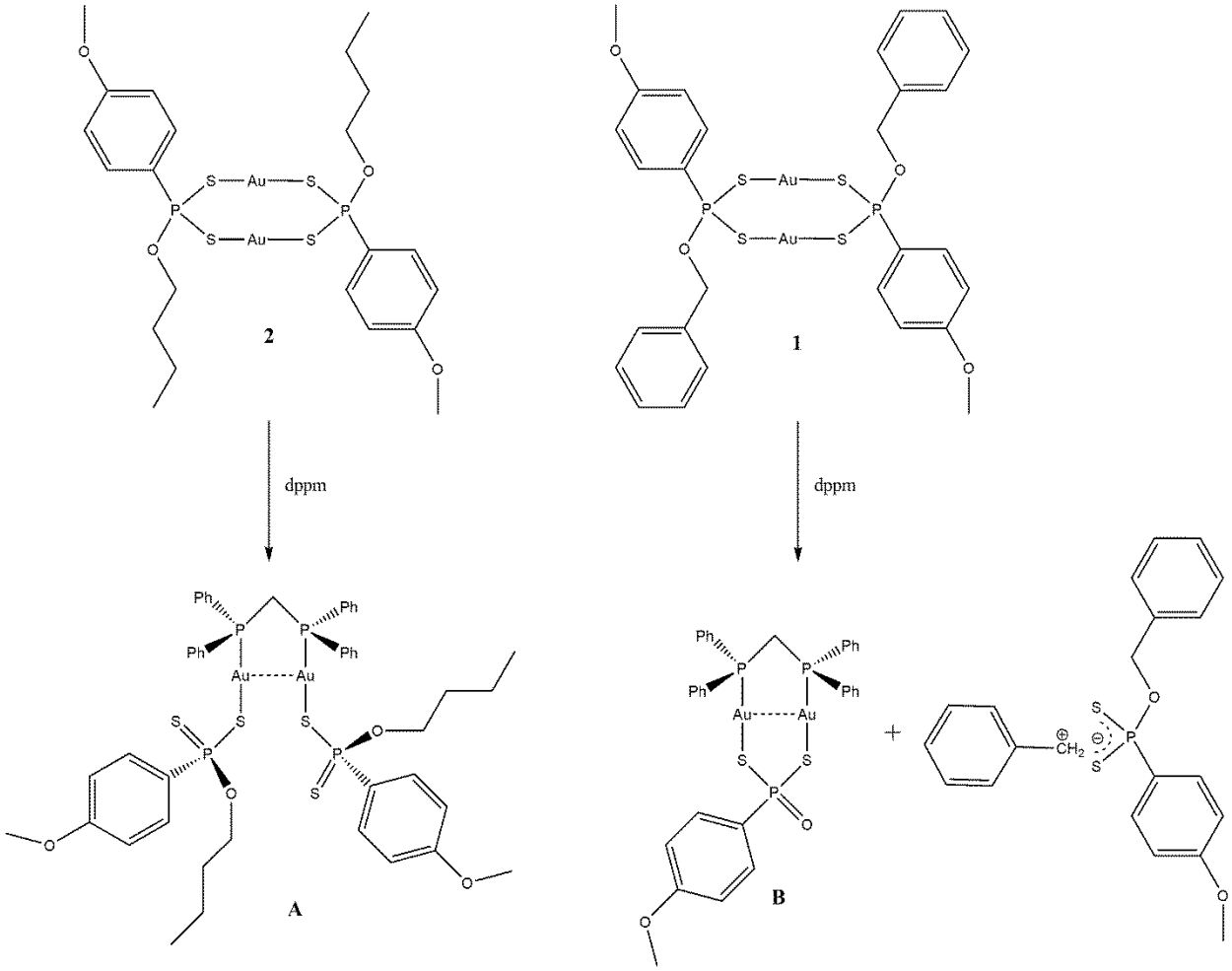

Scheme 2.9 Reaction of dinuclear units with dppm, (**A** and **B**) postulated products

Eventually, this study demonstrated that the results obtained deviates from the stated hypothesis, which must be revisited. For example, the reaction of **1** with one molar equivalent of dppm, in dichloromethane solution for 4 hrs at room temperature resulted in neither **A** nor **B** type structures, but produced **4** (**Scheme 2.8**), a closed 8-membered dinuclear unit with two bonded dppm ligands. The ^{31}P NMR showed two resonance peaks at 30 and 96 ppm, the former

assigned to the P atoms in dppm (free dppm P atoms resonates at -22.5 ppm as determined by NMR experiment) and the latter corresponding to the two equivalent P atoms of the bonded ligands. A NMR study was conducted (**Figure 2.9**) to try to monitor the progress of the reaction and try to deduce the possible structural forms

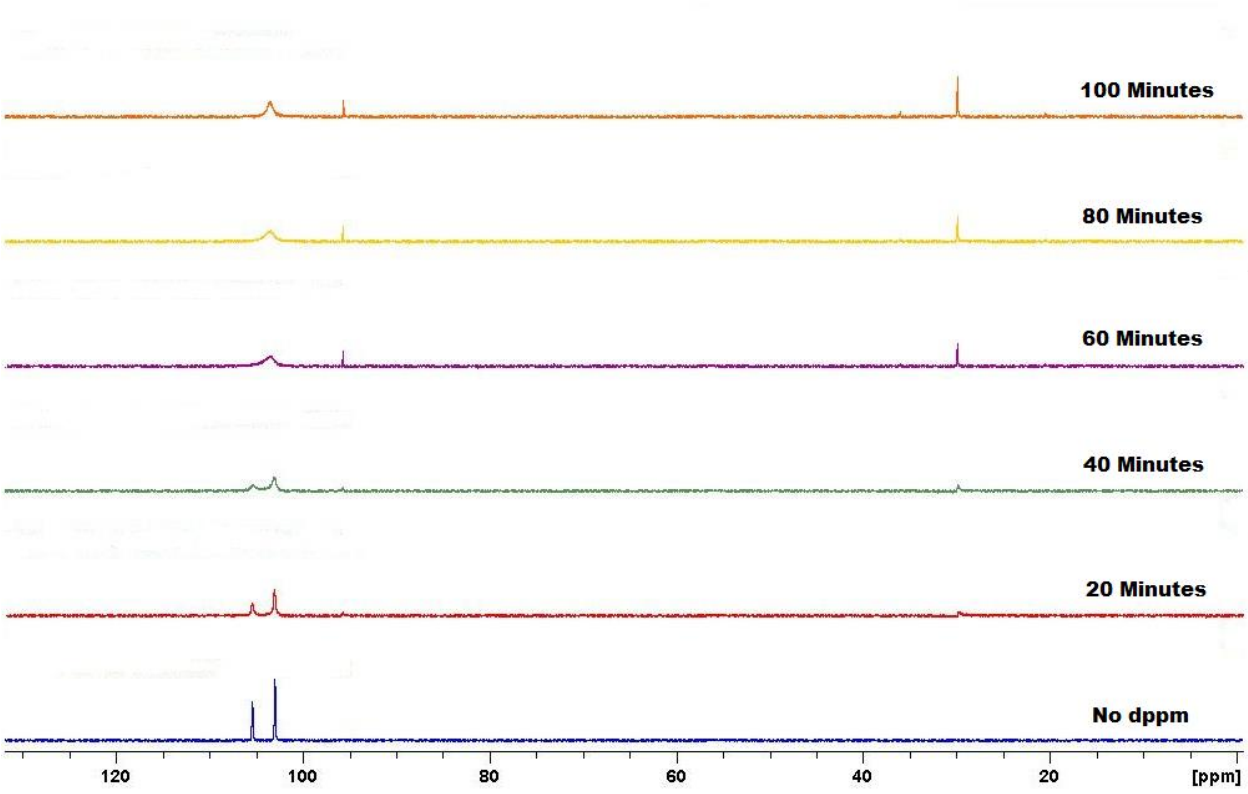

Figure 2.9 ^{31}P NMR study showing changes in structures upon addition of dppm to **1**. The lowest (blue) spectrum corresponds to the ^{31}P spectrum of complex **1** only

The NMR study showed two initial peaks corresponding to complex **1**. On addition of dppm the appearance of peaks at 30 and 96 ppm is evident after 20 minutes, were the former corresponds to the bound dppm and the latter to the bound dtp ligands. This also led to a key observation namely the concomitant disappearance of the two initial peaks of complex **1**. Of the two initial peaks (representing two isomers), it was seen that after 60 minutes a single isomer is consumed. From this it was concluded that the less abundant cis isomer was consumed first, followed by the more abundant *trans* isomer. The *trans* isomer is considered more abundant as it was shown to be the sole isomer in solid state with solid state MAS ^{31}P NMR, and only upon dissolution does the other (*cis*) isomer appear.

The possible cause of the deviation could be assigned to several factors, some of which may include: i) solvent effects ii) the purity of the bulk powder of complex **1,** iii) and the addition of excess dppm. The structure shown in **Figure 2.10**, shows complex **4**, with a $[Au_2(dppm)_2]$ species clearly present.

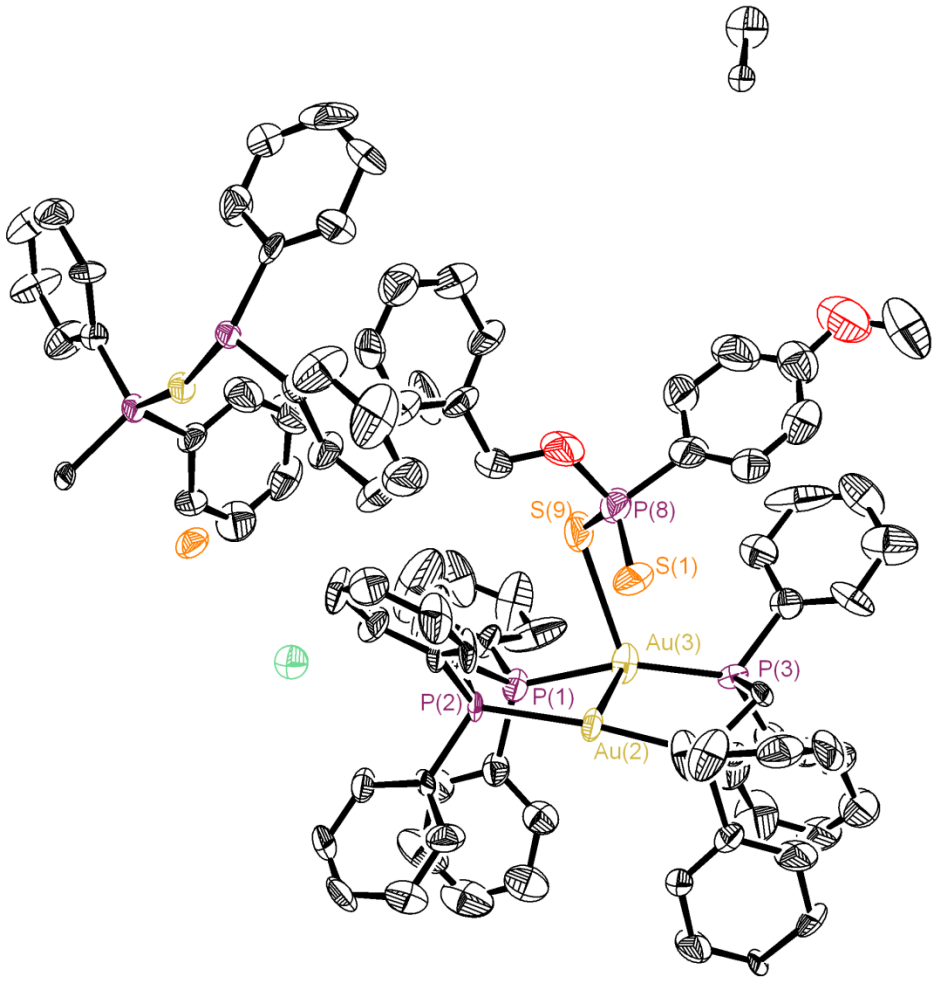

Figure 2.10 Molecular structure of an unrefined asymmetric unit of complex **4**. Thermal ellipsoids are drawn at the 50% probability level

From the **Figure 2.10**, evidence of distortion of the phenyl rings are present. Although this structure is unrefined, the neutral dppm 8-membered dinuclear $[Au_2(dppm)_2]$ aids in the visualization of the complex. On interpretation of the ^1H NMR results, which correlates to the synthesized structure, it is evident that the complex was synthesized.

Although crystals of the reaction product of complex **2** with dppm were not obtained, a NMR study was performed to predict the structure. The NMR study showed two initial peaks corresponding to that of complex **2**, shown in **Figure 2.11.** On addition of dppm the appearance of a peak at 30 ppm is evident after 40 minutes, which corresponds to bonded dppm. Following the similar pattern of **Figure 2.9**, disappearance of the initial two peaks of complex **2** is seen. Of these two initial peaks, (two isomers of complex **2**) it is seen that after 60 minutes a single isomer is consumed. This leads to the deduction that the lower abundant isomer is totally consumed, followed by more abundant isomer. From the spectra below it is observed that the two peaks of complex **2** disappear completely giving rise to the single peak at 101 ppm.

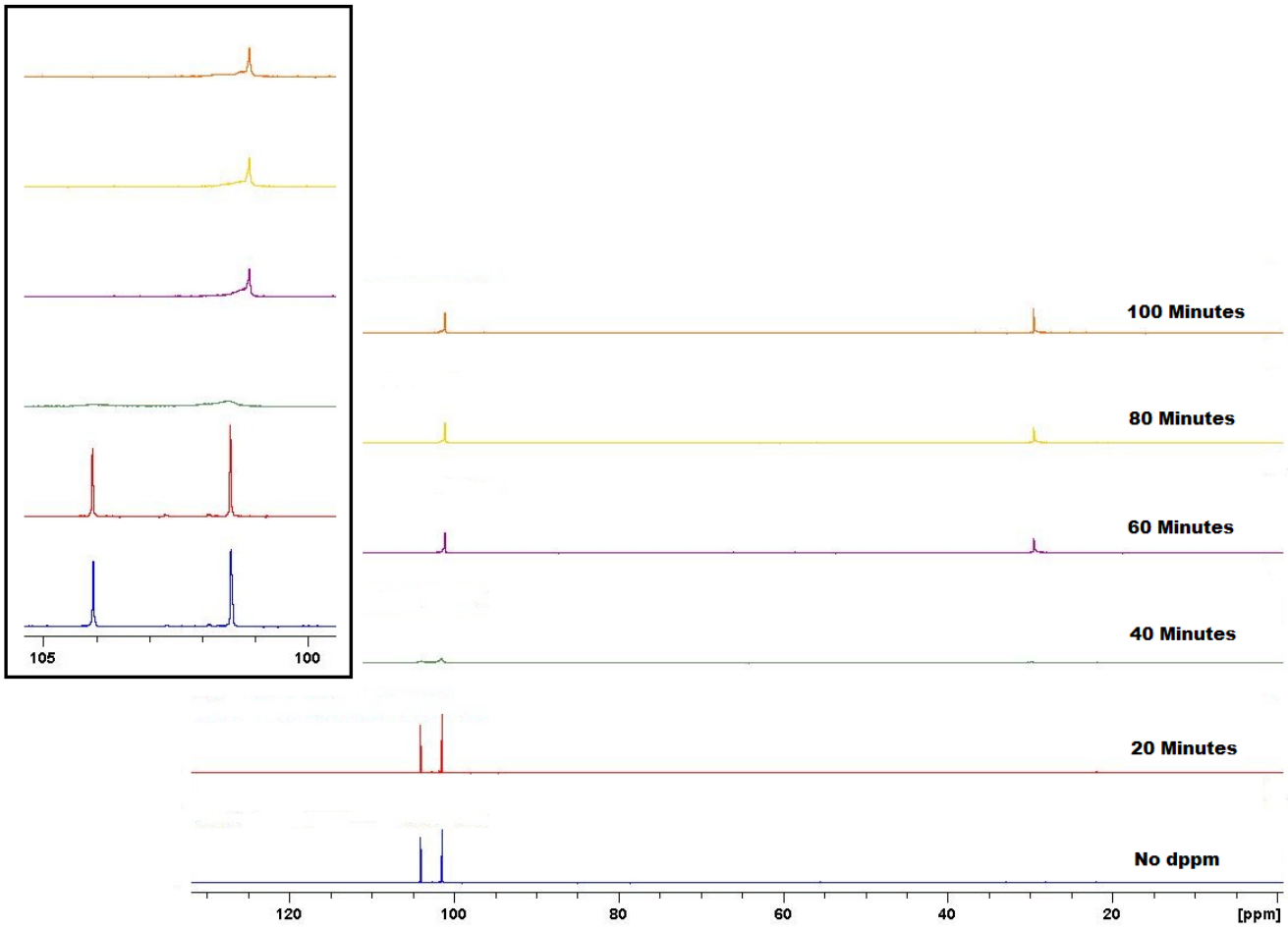

Figure 2.11 ^{31}P NMR study of the treatment of **2** with dppm. The blue spectra corresponds to the 31P spectra of complex **2** only

It is difficult to observe the appearance of the peak at 101 ppm, which corresponds to the bound ligand molecule. On closer inspection it is seen that the two peaks of complex **2** which are seen at 102 and 104 ppm, are observed in the expanded spectra in insert. The postulated structure of the reaction of dppm with complex **2** is that of **A** in **Figure 2.7**, which is a bridged open-ended dinuclear unit observed previously.[29]

In summary, this chapter introduced the concept of aurophilicity, which had been subsequently demonstrated in the two crystal structures which contain intramolecular Au···Au interactions. The reactivity of the dinuclear complex towards bis-phosphines showed a deviation from previously reported results, and led to the isolation of an 8-membered dinuclear dppm closed-structure with two open ended singly bound ligand molecules, in contrast to the expected, bridged open-ended or closed 8-membered dinuclear unit complexes of the type Au_2dppm$(dtp)_2$, and Au_2dppm(dtp=O), respectively.

2.3 Experimental

Herein the general considerations, instrumentation, and experimental procedures will be outlined.

2.3.1 General considerations

Unless otherwise stated, all reactions were carried out under an inert atmosphere of positive nitrogen gas flow (predried by Drierite/anhydrous $CaSO_4$ column) using standard Schlenk techniques. Reactions were stirred magnetically with a Teflon coated stirrer-bar. Glassware was dried for a minimum period of 24 hrs at 160 °C and assembled hot under a stream of dinitrogen gas. Diethyl ether, tetrahydrofuran, and hexane were distilled over sodium wire under nitrogen until the purple colour of benzophenone-ketyl was persistent. Dichloromethane and toluene were distilled over anhydrous calcium hydride. Alcohols were distilled over magnesium turnings/iodine. All solvents were degassed by freeze-thaw cycles prior to immediate use. Room temperature refers to 23-25 °C; temperatures above were obtained with the use of a silicone-based oil bath. The following chemicals were purchased from the Sigma-Aldrich company: tetrahydrothiophene, phosphorus pentasulfide, anisole, cholorodiphenylphosphine, phenylmethanol, butanol, bis(diphenylphosphino)methane, 4-bromobenzaldehyde, ethanol amine, t-butyl amine, silver nitrate, and silver triflouoromethanesulfonate. Deuterated solvents were obtained from Merck. Nitrogen, argon and ammonia gas was obtained from Afrox. Gold solution [pre-dissolved in aqua regia (3HCl: HNO_3)] was used as basis in preparation of all gold(I) starting materials and was a generous gift from Rand Refineries.

2.3.2 Instrumentation

Nuclear Magnetic Resonance: All NMR was carried out at ambient conditions (temperature = 298 K). Solution NMR experiments was carried out on a Bruker Avance 400 MHz spectrometer. ^{1}H spectra, expressed in parts per million (ppm), are referenced internally to residual proton impurity in the deuterated solvents and reported as (δ_H) multiplicity(**s** = singlet; **d** = doublet; **dd=** doublet of doublets; **t** = triplet; **dt** = doublet of triplets; **p** = pentet; **sx** = sextet and **m**= multiplet). ^{31}P nuclei chemical shifts were referenced relative to an 85% H_3PO_4 in D_2O external standard solution.

X ray Crystallography: Data were collected using a Bruker CCD (charge coupled device) based diffractometer equipped with an Oxford Cryostream low-temperature apparatus operating at 173 K. Data were measured using omega and phi scans of 0.5° per frame for 10 s. The total number of images was based on results from the program COSMO[31] where redundancy was expected to be 4.0 and completeness of 100% out to 0.83 Å. Cell parameters were retrieved using APEX II software[32] and refined using SAINT on all observed reflections. Data reduction was performed using the SAINT software[33] which corrects for Lp. Scaling and absorption corrections were applied using SADABS[34] multi-scan technique, supplied by George Sheldrick. The structures are solved by the direct method using the SHELXS-97 program and refined by least squares method on F^2, SHELXL- 97, which are incorporated in SHELXTL-PC V 6.10.[35]

Infrared spectra were collected on a Perkin Elmer Spectrum 100 FTIR spectrophotometer.

Elemental analyses were performed at the University of Kwazulu-Natal Pietermaritzburg campus using a Thermo Scientific Flash 2000 elemental analyzer.

2.3.3 Preparation of starting materials

Caution! Tetrahydrothiophene has a foul smell and inhalation can have adverse effects. The organophosphorus compounds isolated in this study slowly releases H_2S gas upon exposure to the atmosphere and must be treated with caution. Reagents and manipulations described herein should be approached with caution and performed in an appropriate well ventilated fume-hood.

2.3.3.1 Synthesis of $(4\text{-}C_6H_4OMeP(S)S)^2$

A 500-mL three-neck round bottom flask, with a nitrogen inlet was charged with P_4S_{10} (16 g, 0.04 mol) with anisole (excess). The resulting suspension was refluxed until complete dissolution of solids was observed, *ca* 6 hrs. The resulting solution was then allowed to cool to room temperature. The resulting microcrystalline material was filtered under vacuum and washed with portions of toluene and diethyl ether. The highly insoluble and foul smelling compound was stored in a vacuum desiccator. Melting point: 227 °C (decompose). No NMR data available due to insolubility in deuterated solvents.

2.3.3.2 Synthesis of [AuCl(tht)][30]

A beaker was charged with freshly prepared solution of $H[AuCl_4]\cdot 3H_2O$ (7.66 g, 0.0194 mol) in $EtOH/H_2O$ (9:1 v/v). To this solution, tht was added drop wise and the solution formed a yellow precipitate $[AuCl_3(tht)]$. With continuous stirring more tht was added until a white precipitate was obtained. The addition of tht was ceased and the white precipitate collected through filtration and the product washed with portions of cold EtOH (3 x 5 mL). The product was obtained as a free flowing white powder, and was placed in a vial after purging with nitrogen gas and placed in the fridge for further use. Yield: (5.76 g, 0.0180 mol) 92%.

2.3.4 Synthesis of $(NH_4)[S_2P(_4\text{-}C_6H_4OMe)(OCH_2C_6H_5)]$

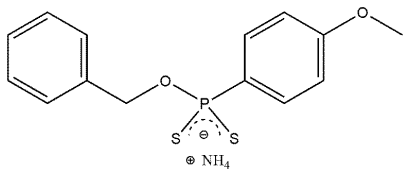

A Schlenk flask was charged with $(4\text{-}C_6H_4OMeP(S)S)_2$ (2.5 g, 6.19 mmol) and placed under vacuum for 30 minutes. The solid was heated to 70 °C, phenylmethanol (1.46 g, 12.96 mmol) and toluene (2 mL) was added. The temperature was maintained at 70 °C for 60 minutes, until dissolution of all the solids had been observed. The clear residue was cooled to room temperature, before being placed in an ice bath for 10 minutes. Anhydrous NH_3 gas was bubbled through the residue with vigorous agitation, which caused the immediate precipitation of a white salt. Yield 3.786g (94%). Melting point: 89.4-91.2 °C. ^{1}H-NMR (Methanol-D4) ppm: 3.68 (s, 3H), 4.83 (d, 2H, J = 8.08 Hz), 6.81 (dd, 2H, J = 8.87, 2.62 Hz), 7.13 (d, 2H, J = 7.20 Hz), 7.18 (t, 1H, J = 8.49 Hz), 7.98 (dd, 2H, J = 13.43, 8.71 Hz). ^{13}C NMR (Methanol-D4): δ (ppm): 55.78 (CH_3), 66.55 ($ArOCH_2$), 113.61 (*meta*-ArC), 128.40 (*para*-ArC), 128.80 (*meta*-ArC), 129.17 (*ortho*-ArC), 132.94 (*ortho*-ArC), 137.26(*ipso*-ArC), 139.87 (*ipso*-ArC), 162.53 (*ipso*-ArC). ^{31}P NMR (Methanol-D4) ppm: 108 (s). Anal. calc. for $C_{10}H_{17}NO_2PS_2$: C 51.36, H 5.54; N 4.28 %. Found: C 51.54, H 5.64, N 4.22 %.

Selected IR data ν/cm^{-1}: 3467 (b), 1111 (m), 1006 (m), 660 (s), 545 (s).

2.3.5 Synthesis of $(NH_4)[S_2P(_4\text{-}C_6H_4OMe)(OCH_2CH_2CH_2CH_3)]$

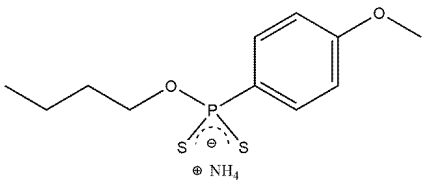

A Schlenk flask was charged with (4-$C_6H_4OMeP(S)S)_2$ (2.50 g, 6.19 mmol) and placed under vacuum for 30 minutes. The solid was heated to 70 °C, 1-butanol (0.918 g, 12.37 mmol) and toluene (2 mL) was added. The temperature was maintained at 70 °C for 60 minutes, until dissolution of all the solids had been observed. The clear residue was cooled to room temperature, before being placed in an ice bath for 10 minutes. Anhydrous NH_3 gas was bubbled through the residue with vigorous agitation, which caused the immediate precipitation of a white coloured salt. Yield 3.544g (98%). Melting Point: 88.3-90.1 °C. ^{1}H-NMR (Methanol-D4) ppm: 0.83 (t, 3H, J = 7.38 Hz), 1.31 (m, 2H), 1.52 (m, 2H), 3.75 (s, 3H), 3.80 (dt, 2H, J = 8.13, 6.64 Hz), 6.85 (dd, 2H, J = 13.41, 8.81 Hz), 7.97 (dd, 2H, J = 8.845, 2.60 Hz). ^{13}C NMR (Methanol-D4): δ (ppm): 14.23 ($ArOCH_2CH_2CH_3$), 20.05 ($ArOCH_2CH_2CH_2$), 33.66 ($ArOCH_2CH_2$), 55.92 (CH_3), 64.87 ($ArOCH_2$), 113.61 (*ortho*-ArC), 132.94 (*meta*-ArC), 162.48 (*ipso*-ArC). ^{31}P NMR (Methanol-D4) ppm: 106 (s). Anal. calc. for $C_{10}H_{17}NO_2PS_2$: C 43.15, H 6.16; N 5.03 %. Found: C 43.21, H 6.24, N 5.16 %.

Selected IR data ν/cm^{-1}: 3126-2960 (b), 1101 (m), 1018 (m), 680 (s), 554 (s).

2.3.6 Synthesis of $[AuS_2P(_4\text{-}C_6H_4OMe)(OCH_2C_6H_5)]_2$

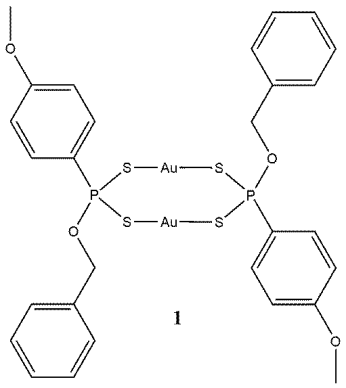

1

A Schlenk flask was charged with $(NH_4)[S_2P(4\text{-}C_6H_4OMe)(OCH_2C_6H_5)]$ (400 mg, 1.227 mmol) and dry tetrahydrofuran (40 mL). To the clear solution [AuCl(tht)] (392 mg, 1.227 mmol) (tht = tetrahydrothiophene) was added and the reaction stirred for 30 min, resulting in the formation of a turbid yellow solution. The solvent was removed in *vacuo*, followed by extraction with dichloromethane (40 mL). The extract was filtered through a composite of Celite/anhydrous $MgSO_4$. The volume of the filtrate was reduced in *vacuo*. A yellow powder was consolidated and washed with diethyl ether (2 x 5 mL). Yield 572 mg (91 %) of yellow powder soluble in

chlorinated organic solvents. Single crystals suitable for X-ray diffraction studies were grown by slow diffusion of hexane layered onto a concentrated DCM solution of **1**. Melting point: 119.3-122.2 °C. Anal. calc. for $C_{28}H_{28}Au_2O_4P_2S_4$: C 33.21; H 2.79 %. Found: C 33.24; H 2.77 %. ^{1}H-NMR ($CDCl_3$) ppm: 3.74 (m, 6H, CH_3,), 5.28 (m, 4H, CH_2), 6.85 (s, 4H, ArH), 7.26 (m, 8H, ArH), 7.33 (m, 2H), 7.93 (dd, 4H, J = 8.66, 4.44 Hz). ^{13}C NMR ($CDCl_3$): δ (ppm): 55.46 (CH_3), 69.11 (CH_2), 114.08 (*meta*-ArC), 128.47 (ArC), 129.41 (*para*-ArC), 132.48 (*ortho*-ArC), 162.48 (*ipso*-ArC), 165.66 (*ipso*-ArC), 177.42 (*ipso*-ArC). ^{31}P NMR ($CDCl_3$) ppm: 103 (s), 105 (s). Selected IR data ν/cm^{-1}: 1181 (m), 1024(m), 591 (s), 539 (s).

2.3.7 Synthesis of $[AuS_2P(_4\text{-}C_6H_4OMe)(OCH_2CH_2CH_2CH_3)]_2$

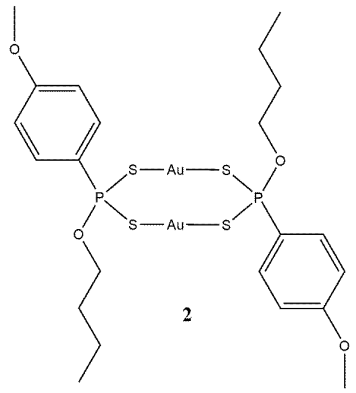

2

A Schlenk flask was charged with $(NH_4)[S_2P(4\text{-}C_6H_4OMe)(OCH_2CH_2CH_2CH_3)]$ (400 mg, 1.437 mmol) and dry tetrahydrofuran (40 mL). To the clear solution [AuCl(tht)] (460 mg, 1.437 mmol) (tht = tetrahydrothiophene) was added and the reaction stirred for 30 min, resulting in the formation of a turbid yellow mixture. The solvent was removed in *vacuo,* followed by extraction with dichloromethane (40 mL). The extract was filtered through a composite of Celite/anhydrous $MgSO_4$. The volume of the filtrate was reduced in *vacuo*. A yellow powder was consolidated and washed with diethyl ether (2 x 5 mL). Yield 536 mg (79 %) of yellow powder soluble in chlorinated organic solvents. Single crystals suitable for X-ray diffraction studies were grown by slow diffusion of hexane layered onto a concentrated DCM solution of **2**. Melting point: 110.8-112.7.1 °C. Anal. calc. for $C_{22}H_{32}Au_2O_4P_2S_4$: C 27.97; H 3.41 %. Found: C 27.84; H 3.45 %. ^{1}H-NMR ($CDCl_3$) ppm: 0.93 (t, 6H, J = 7.54 Hz), 1.44 (m, 4H), 1.71 (m, 4H), 3.85 (s, 6H), 4.32 (q, 4H, J = 14.40, 6.46 Hz), 6.95 (m, 4H), 7.98 (m, 4H). ^{13}C NMR ($CDCl_3$): δ (ppm): 13.72 ($OCH_2CH_2CH_2CH_3$), 19.01 ($OCH_2CH_2CH_2$), 32.26 (OCH_2CH_2), 55.49

(OCH_3), 67.69 (OCH_2), 113.97 (*ortho*-ArC), 132.46 (*meta*-ArC), 163.15 (*ipso*-ArC). ^{31}P NMR($CDCl_3$) ppm: 102 (s), 104 (s).

Selected IR data ν/cm^{-1}: 1180 (m), 1029(m), 683 (s), 558 (s).

2.3.8 Synthesis of $[AgS_2P(_4\text{-}C_6H_4OMe)(OCH_2CH_2CH_2CH_3)]_2$

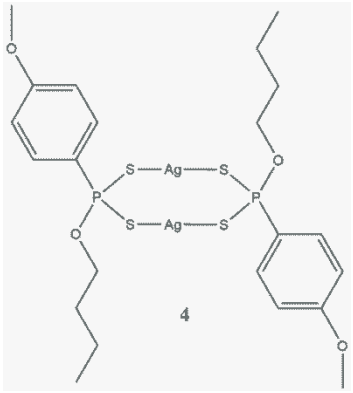

A Schlenk flask was charged with $(NH_4)[S_2P(4\text{-}C_6H_4OMe)(OCH_2CH_2CH_2CH_3)]$ (596 mg, 2.314 mmol) and dry tetrahydrofuran (40 mL). To the clear solution $[Ag(NO_3)]$ (343 mg, 2.314 mmol) was added and the reaction stirred for 30 min, resulting in the formation of a turbid yellow mixture. The solvent was removed in vacuo, followed by extraction with dichloromethane (40 mL). The extract was filtered through a composite of Celite/anhydrous $MgSO_4$. The volume of the filtrate was reduced in vacuo. A yellow powder was consolidated and washed with diethyl ether (2 x 5 mL). Yield 582 mg (75 %) of yellow powder soluble in chlorinated organic solvents. Single crystals suitable for X-ray diffraction studies were grown by slow diffusion of hexane layered onto a concentrated DCM solution of **4**. Melting point: 111.6-112.4 °C. Anal. calc. for $C_{22}H_{32}Ag_2O_4P_2S_4$: C 34.48 %; H 4.21 %. Found: C 34.34; H 4.28 %. ^{1}H-NMR ($CDCl_3$) ppm: 0.81 (t, 6H, J = 7.22 Hz), 1.29 (m, 4H), 1.59 (m, 4H), 3.77 (s, 6H), 3.93 (s, 4H), 6.84 (m, 4H), 7.87 (m, 4H). ^{13}C NMR ($CDCl_3$): δ (ppm): 13.75 ($OCH_2CH_2CH_2CH_3$), 18.97 ($OCH_2CH_2CH_2$), 32.26 (OCH_2CH_2), 55.40 (OCH_3), 66.93 (OCH_2), 113.59 (*ortho*-ArC), 132.47 (*meta*-ArC), 162.30 (*ipso*-ArC). ^{31}P NMR($CDCl_3$) ppm: 105 (s), 107 (s).

Selected IR data ν/cm^{-1}: 1178 (m), 1018 (m), 603 (s), 526 (s).

2.3.9 Synthesis of $[Au_2(dppm)_2\{S_2P(_4\text{-}C_6H_4OMe)(OCH_2C_6H_5)\}_2]$

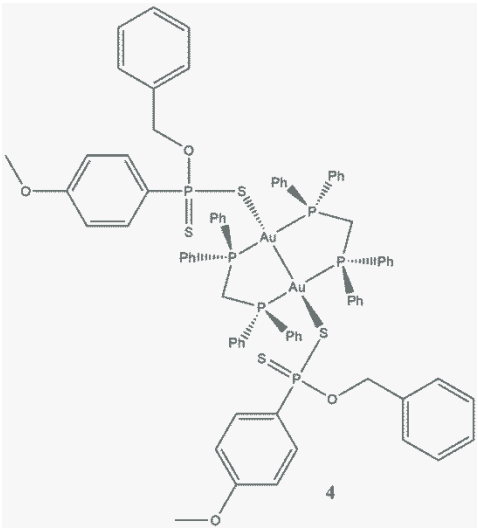

A Schlenk flask was charged with $[AuS_2P(4\text{-}C_6H_4OMe)(OCH_2C_5H_6)]_2$ (118mg, 0.117mmol) and dichloromethane (40 mL). To the solution dppm (48mg, 0.117mmol) was added and stirred for 4 hours. The solvent was removed *in vacuo*, and powder consolidated with diethyl ether. Yield 127mg (80 %) of pale yellow powder soluble in chlorinated organic solvents. Single crystals suitable for X-ray diffraction studies were grown by slow diffusion of hexane layered onto a concentrated DCM solution of **4**. Melting point: 148.6-151.4 °C. Anal. calc. for $C_{78}H_{72}Au_2O_4P_6S_4$: C 52.59 %; H 4.07 %. Found: C 52.48; H 4.03 %. ^{1}H-NMR ($CDCl_3$) ppm: 1.27 (s, 4H), 3.80 (s, 6H), 4.72 (s, 4H), 6.78 (d, 4H, J = 6.60), 7.23 – 7.26 (m, 10H), 7.32 – 7.41 (m, 40H), 7.90 - 7.95 (m, 4H). ^{31}P NMR($CDCl_3$) ppm: 30 (s), 96 (s).

Selected IR data ν/cm^{-1}: 3047 (m), 1435 (m), 688 (s), 512 (s).

2.4 References

(1) van Zyl, W. E.; Woollins, J. D. *Coord. Chem. Rev.* **2013**, *257*, 718.
(2) van Zyl, W.; Fackler, J. P. *Phosphorous, Sulfur and Silicon* **2000**, *167*, 117.
(3) Ozturk, T.; Ertas, E.; Mert, O. *Chem. Rev.* **2007**, *107*, 5210.
(4) Fay, P.; Lankelma, H. P. *J. Am. Chem. Soc.* **1952**, *74*, 4933.
(5) Foreman, M. R. S. J.; Slawin, A. M. Z.; Woollins, J. D. *Dalton Trans.* **1996**, 3653.
(6) Wood, P. T.; Woollins, J. D. *J. Chem. Soc., Chem. Comm.* **1988**, 1190.
(7) Grohmann, A.; Schmidbaur, H. I. G. S. *Gold: Progress in Chemistry, Biochemistry and technology.*; John Wiley & Sons Ltd.: West Sussex, England, 1999.
(8) Pyykkö, P. *Angew. Chem. Int. Ed.* **2004**, *43*, 4412.
(9) Pyykkö, P. *Angew. Chem. Int. Ed.* **2002**, *41*, 3573.
(10) Scherbaum, F.; Grohmann, A.; Huber, B.; Krüger, C.; Schmidbaur, H. *Angew. Chem. Int. Ed.* **1988**, *27*, 1544.
(11) Schmidbaur, H. *Gold Bulletin* **1990**, *23*, 11.
(12) (a) Schmidbaur, H. *Gold Bulletin* **2000**, *33*, 3(b) Schwerdtfeger, P. *Heteroatom Chemistry* **2002**, *13*, 578.
(13) Rapson, W. *Gold Bulletin* **1989**, *22*, 19.
(14) (a) Scherbaum, F.; Huber, B.; Müller, G.; Schmidbaur, H. *Ang. Chem. Int. Ed* **1988**, *27*, 1542(b) Schmidbaur, H.; Graf, W.; Müller, G. *Angew. Chem. Int. Ed.* **1988**, *27*, 417.
(15) (a) Schmidbaur, H.; Weidenhiller, G.; Steigelmann, O. *Angew. Chem. Int. Ed.* **1991**, *30*, 433(b) Schmidbaur, H. *Pure and Applied chemistry* **1993**, *65*, 691.
(16) (a) Li, J.; Pyykko, P. *Inorg. Chem.* **1993**, *32*, 2630(b) Haeberlen, O. D.; Schmidbaur, H.; Rosch, N. *J. Am. Chem. Soc.* **1994**, *116*, 8241.
(17) Pathaneni, S. S.; Desiraju, G. R. *J. Chem. Soc., Dalton Trans.* **1993**, 319.
(18) Gimeno, M.; Laguna, A. *Gold Bulletin* **2003**, *36*, 83.
(19) Schmidbaur, H.; Schier, A. *Chem. Soc. Rev.* **2012**, *41*, 370.
(20) Lawton, S. L.; Rohrbaugh, W. J.; Kokotailo, G. T. *Inorg. Chem.* **1972**, *11*, 2227.
(21) van Zyl, W. E.; López-de-Luzuriaga, J. M.; Mohamed, A. A.; Staples, R. J.; Fackler, J. P. *Inorg. Chem.* **2002**, *41*, 4579.
(22) van Zyl, W. E.; Staples, R. J.; Fackler, J. J. P. *Inorg. Chem. Comm.* **1998**, *1*, 51.
(23) Van Zyl, W. E. *Comm. Inorg. Chem.* **2010**, *31*, 13.
(24) Vaughan, L. G. *J. Am. Chem. Soc.* **1970**, *92*, 730.
(25) Sun, D.; Huang, R.-B. *Acta Crystallog. Sect. C* **2011**, *67*, m315.
(26) Haiduc, I.; Mezei, G.; Micu-Semeniuc, R.; Edelmann, F. T.; Fischer, A. *Z. Anorg. Allg. Chem.* **2006**, *632*, 295.
(27) Thomas, L. C.; Chittenden, R. A. *Spectrochimica Acta* **1964**, *20*, 489.
(28) Coates, J. In *Encyclopedia of Analytical Chemistry*; John Wiley & Sons, Ltd, 2006.
(29) Maspero, A.; Kani, I.; Mohamed, A. A.; Omary, M. A.; Staples, R. J.; Fackler, J. P. *Inorg. Chem.* **2003**, *42*, 5311.
(30) Usón, R.; Laguna, A.; Laguna, M. *Inorg. Syn.* **1989**, *26*, 85.

(31) COSMO V1.61, *Software for the CCD Detector Systems for Determining Data Collection Parameters*. Bruker Analytical X-ray Systems, Madison, WI (**2009**).
(32) APEX2 V2010.11-3. Software *for the CCD Detector System*; Bruker Analytical X-ray Systems, Madison, WI (**2010**).
(33) SAINT V 7.68A Software *for the Integration of CCD Detector System* Bruker Analytical X-ray Systems, Madison, WI (**2010**).
(34) SADABS V2.008/2 Program for absorption corrections using Bruker-AXS CCD based on the method of Robert Blessing; Blessing, R.H. Acta Cryst. A51, **1995**, 33.
(35) Sheldrick, G.M. "A short history of SHELX". *Acta Cryst*. A64, **2008**, 112-122.

CHAPTER 3

Synthesis of a Phosphinamide and its Derived Silver Complex

3.1 Phosphinamide

3.1.1 Preparative methods of phosphinamides and phosphine oxides

Numerous methods to prepare phosphine oxides have been outlined in literature, and most involve the use of an oxidising agent.[1] Among the numerous preparative methods, use of equimolar amounts of H_2O_2 in aqueous solution under mild conditions leads to formation the corresponding phosphinamides and phosphine oxides.[2]

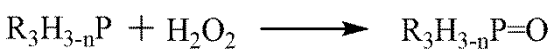

Scheme 3.1 Use of H_2O_2 in the preparation of phosphine oxides

Solvolysis of P–Cl compounds, usually monohalophosphines, occurs *via* the reaction of these monohalophosphines with water or alcohols to give phosphinamides (If the halo phosphine is nitrogen substituted) and phosphine oxides.

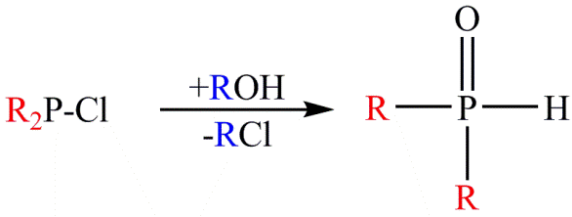

Scheme 3.2 Solvolysis of P–Cl compound

Another synthesis procedure is using a phase transfer catalyst, which improves yields and reduces the formation of side products. This procedure is known as the Todd—Atherton reaction and allows for the attachment of the phosphoryl to the amine nitrogen *via* the use of a phase transfer catalyst.[3]

Apart from the above mentioned synthesis routes, another prominent method that has been demonstrated by Priya *et al.* is the reaction of aminophosphines with aldehydes and ketones.[4]

3.1.2 Metal complexes of phosphinamide and phosphine oxides

Phosphinamides and phosphine oxides readily react with oxophilic metals to give coordination complexes.[4] The binding modes are generally via the lone pairs on the N or O atoms on the phosphinyl group.

Recently, phosphine oxide research in bis-phosphine monoxides (BPMOs) has developed into an exciting field of research and has garnered great interest in phosphine oxides and their uses in catalysis.[5] The general considerations to follow are that of the Hard and Soft, Acid and Base principle (SHAB) which predicts that the soft P center of BPMOs would prefer to bind to softer metals in low oxidation states, such as Hg^{2+}, Pd^{0}, Pd^{2+}, Pt^{2+}, Au^{+}, and the like, whereas the hard O donor atom should have a higher affinity for hard Lewis acids such as the lanthanides in the high oxidation state of +3 (**Table 3.1**).[6,7] However, in the presence of two donor atoms as on a BPMO, the binding of *both* the P and O atoms to one metal center, forming a chelate, is possible.[5]

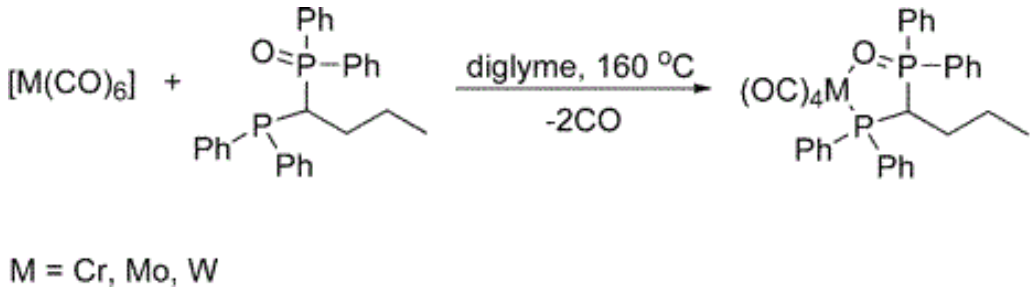

Scheme 3.3 The chelating ability of BMPOs[5]

Table 3.1 Table of hard and soft, acids and bases[8]

HARD ACIDS	SOFT ACIDS
H^+, Na^+, Ca^{2+}, Mn^{2+}, Al^{3+}, N^{3+}, Cl^{3+}, Gd^{3+}, Cr^{3+}, Co^{3+}, Fe^{3+}, BF_3, $B(OR)_3$, $AlCl_3$, SO_3, CO_2, RCO^+, RPO_2^+, NC^+	M^0 (metal atoms), Cu^+, Ag^+, Hg^+, Pd^{2+}, Pt^{2+}, $Co(CN)_5^{2-}$, $InCl_3$, BH_3, RS^+, Br_2, $RO\cdot$, $RO_2\cdot$, carbenes
HARD BASES	**SOFT BASES**
H_2O, OH^-, F^-, $CH_3CO_2^-$, SO_4^{2-}, CO_3^{2-}, NO_3^-, PO_4^{3-} ,ClO_4^-, NH_3, RNH_2, ROH, R_2O, RO^-	R_2S, RSH, I^-, SCN^-, $S_2O_3^{2-}$, R_3P, $(RO)_3P$, CN^-, RNC, CO, C_2H_4, C_6H_6, H^-, R^-
BORDERLINE ACIDS	**BORDERLINE BASES**
Fe^{2+}, Co^{2+}, Ni^{2+}, Sn^{2+}, Ru^{2+} Rh^{3+}, Ir^{3+}, SO_2, $B(CH_3)_3$, R_3C^+, $C_6H_5^+$	$C_6H_5NH_2$, C_6H_5N, N_2, N_3^-, Br^-, NO_2^-, SO_3^{2-}

However, when considering phosphinamides, the binding ability of the P atom is hindered as it is in the +5 oxidation state, but the N atom has the potential to bind to metal centers due to its basicity.[6] There have been a number of phosphine oxide complexes reported in the literature,[4,6-7] but only one report on a phosphine oxide silver complex (specifically the formation of Ag···O=P bond) *via* N-(6-methyl-2-pyridinyl)-P,P-diphenyl-phosphinic amide as the ligand, is known (**Figure 3.1**).[9]

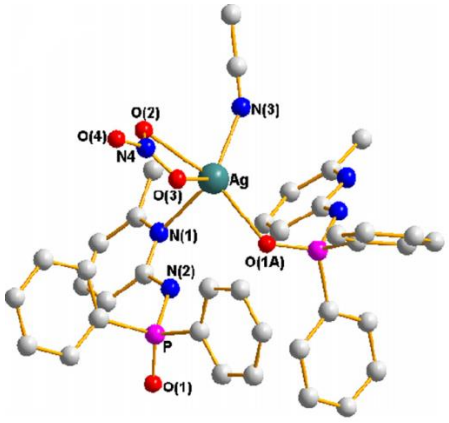

Figure 3.1 X-ray structure of silver complex containing a Ag···O=P bond[9]

3.1.3 Lanthanide complexes

Lanthanide complexes attract growing interest due to their potential role as photoluminescent probes,[10] materials for Organic LED technology,[11] medical diagnostics[12] and lasing systems.[13] The use of ‘‘inorganic analogs’’ of 1,3-diketonates, namely tetraarylimidodiphosphinates (tpip), which provides an O=P–N–P=O binding site, has sparked major interest and such ligands are prepared *via* organophosphorous chlorides. The ligand (tpip) forms a complex with Eu(III) ions as seen in **Figure 3.2**.[14]

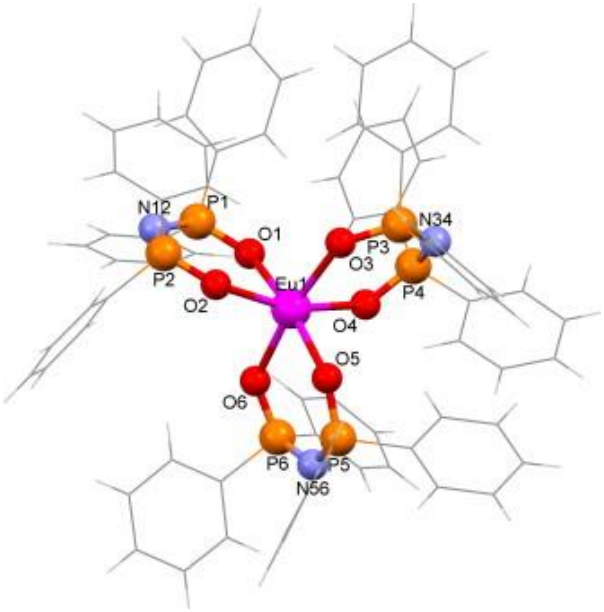

Figure 3.2 X-ray structure of europium tris(tetraphenylimidodiphosphinate)[14]

3.2 Results and discussion of the synthesized phosphinamide ligand and complex

The preparation of N-tert-butyl-P-diphenylphosphinic amide was accomplished, and a corresponding silver complex synthesized.

3.2.1 Preparation of N-tert-butyl-P-diphenylphosphinic amide ligand

N-tert-butyl-P-diphenylphosphinic amide was isolated as the oxidation product of $(C_6H_5)_2PONH$-*t*-C_4H_9 upon exposure to air or moisture (**Scheme 3.6**) (presumably during re-crystallization) in reasonable yield (70 %). The structure is a polymorph of a previously

reported structure[15] which contains three molecules in the asymmetric unit while the structure in the present study contains only two molecules.

The reaction of tertiary-butyl amine with chlorodiphenyl phosphine in ether, in a 1:1 molar ratio, resulted in the formation of N-tert-butyl-P-diphenylphosphinic amide. Tertiary-butyl amine was deprotonated using butyl lithium at -78 °C in ether (**Scheme 3.4**).

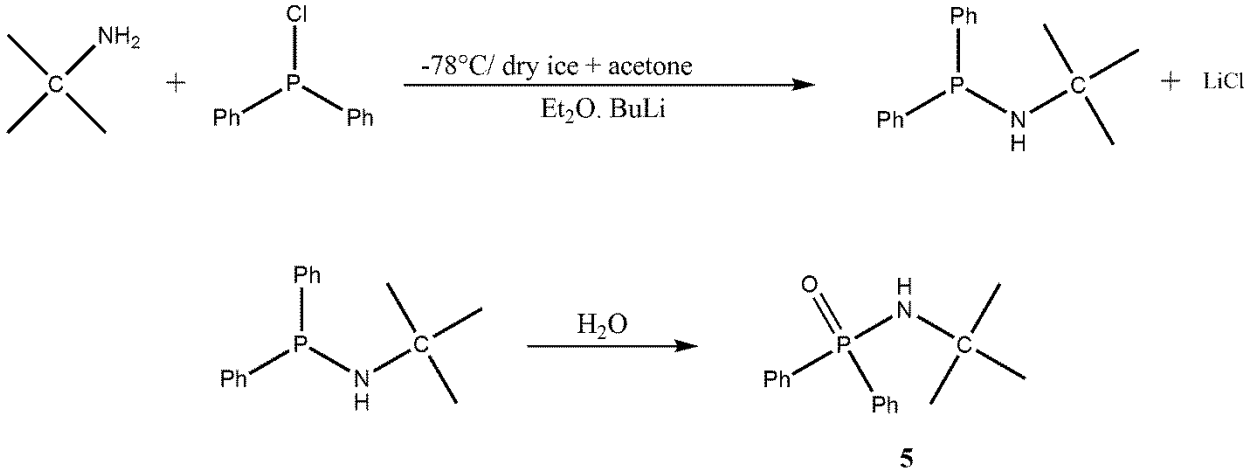

Scheme 3.4 Formation of N-tert-butyl-P-diphenylphosphinic amide ligand (**5**)

The solution structure of **5** shows a single peak in the ^{31}P NMR spectrum at 19.51 ppm for the oxidised P atom and this is further characterised by IR which shows a strong band at 1175 cm^{-1}. The ^{1}H and ^{13}C NMR spectra of the ligand were consistent with the presence of both methyl and phenyl moieties. Initially, it was postulated that the starting material chlorodiphenyl phosphine was oxidised, however it proved false on inspection of a ^{31}P NMR experiment. The oxidation must have happened in air only during crystallization to form the present phosphinamide (**5**).

The solid-state structure crystallized in a triclinic crystal system and contains two molecules in an asymmetric unit linked by hydrogen bonds, with the unit cell containing four ligand molecules. The structure of the hydrogen-bonded dimer with the atom-numbering scheme is shown in **Figure 3.3** and the packing of the phosphinamide is shown in **Figure 3.5**. The two molecules constituting the asymmetric unit have essentially the same bonding parameters (See **Table 3.3**). The geometry of each P atom can be described as a distorted tetrahedron as seen by angles O(1)-P(1)-C(1) and O(1)-P(1)-N(1) as 109.51(5) and 115.29(5)°, respectively, for one molecule and O(2)-P(2)-C(23) and O(2)-P(2)-N(2) as 108.77(5) and 117.15(5)°, respectively for the second molecule. The P=O bond lengths for the two molecules are

1.4900(8) and 1.4911(9) Å respectively, and is in good agreement with the literature values of the similar compounds.[15] The P–N and P–C bond distances are comparable to similar synthesized compounds in literature.[4,15-16]

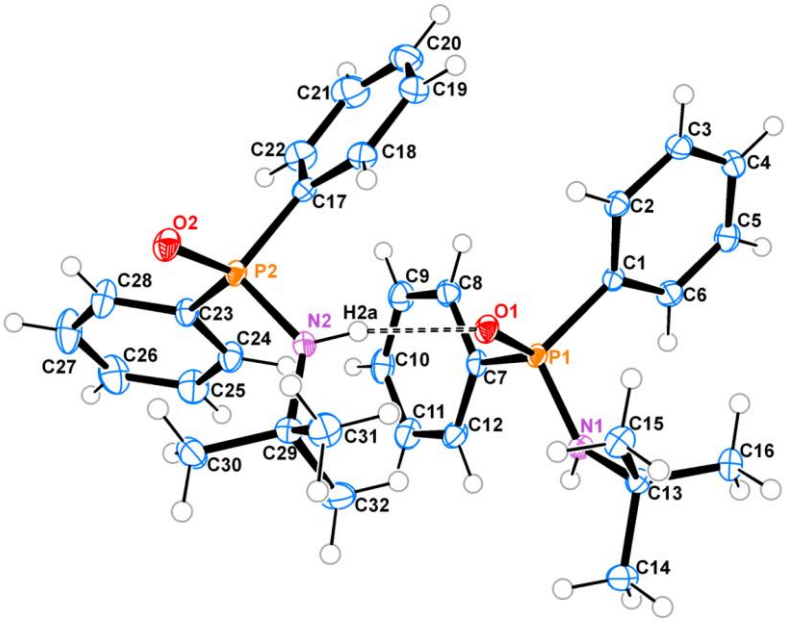

Figure 3.3 Compound 5 with the atom labelling scheme. The displacement ellipsoids are shown at the 50% probability level

The two asymmetric units are held together by the N(2)—H(2A)···O(1) hydrogen bonding interaction (**Table 3.2**) of moderate strength to form the dimeric unit (**Figure 3.3** and **3.4**). In the structure, the dimeric units in turn are held together by a network of weak N(1)—H(1)···O(2) interactions which extend across the *bc* plane (**Figure 3.5**).

Table 3.2 Hydrogen-bond geometry

D-H···A [Å]	D-H [Å]	H···A [Å]	D···A [Å]	D-H···A angle [°]
N(2)-H(2A) ··O(1)	0.88	2.03	2.8891 (13)	172
N(1)-H(1) ··O(2)	0.88	2.28	2.8932 (13)	127

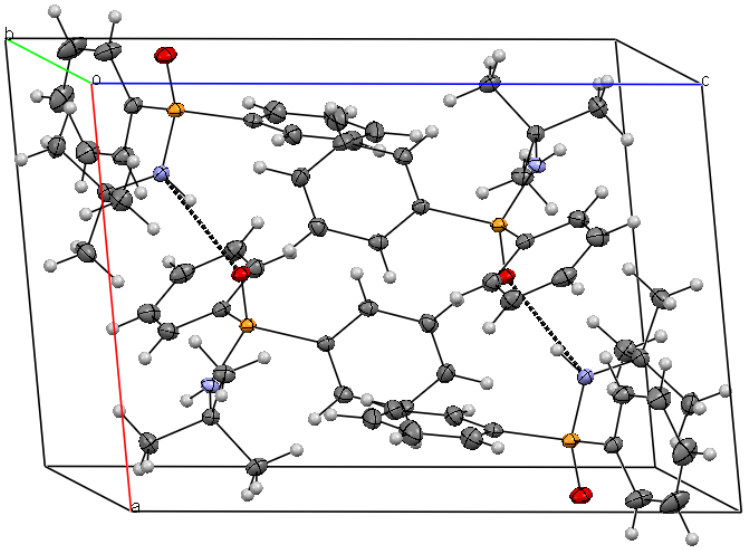

Figure 3.4 Packing diagram of Compound **5** showing the hydrogen bonding between the two molecules of the asymmetric unit, seen along the ***c*** axis

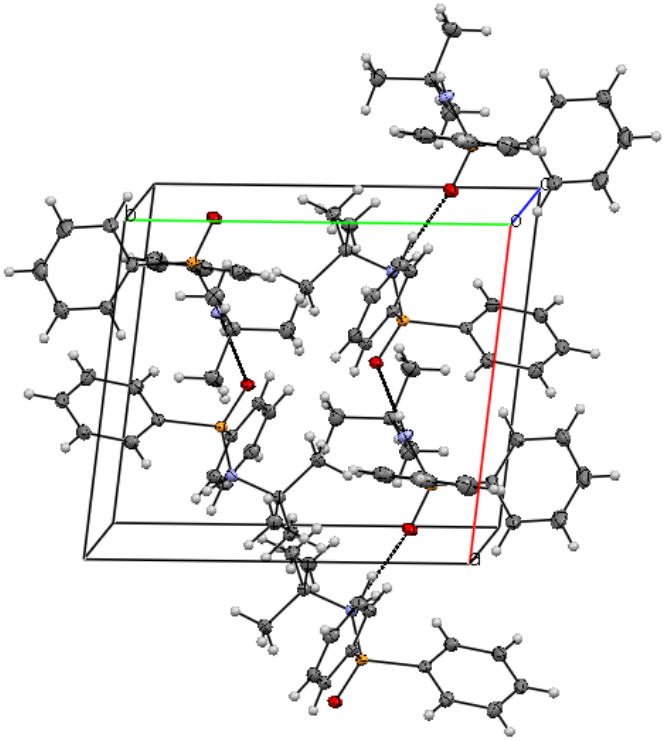

Figure 3.5 Packing within the structure of Compound **5** showing the hydrogen bonding between the molecules outside of the asymmetric unit, seen along the ***b*** axis

From **Figures 3.4** and **3.5** the two molecules within the asymmetric unit interact *via* intramolecular hydrogen bonding interactions and these molecules pack *via* similar

intermolecular interactions. Compound **5** was reacted further with silver trifluoromethanesulfonate to yield a silver(I) complex of **6**.

Table 3.3 Selected Bond lengths [Å] and angles [°] for complex **5**

N(1)-P(1)	1.6434(10)	P(2)-N(2)-H(2A)	115.5
N(1)-H(9)	0.8800	O(1)-P(1)-N(1)	115.29(5)
N(2)-P(2)	1.6357(10)	O(1)-P(1)-C(7)	112.71(5)
N(2)-H(2A)	0.8800	N(1)-P(1)-C(7)	103.33(5)
P(1)-O(1)	1.4900(8)	O(1)-P(1)-C(1)	109.51(5)
P(2)-O(2)	1.4911(9)	N(1)-P(1)-C(1)	109.81(5)
C(23)-P(2)	1.8080(12)	C(7)-P(1)-C(1)	105.65(5)
C(13)-N(1)	1.4898(14)	O(2)-P(2)-N(2)	117.15(5)
C(7)-P(1)	1.8073(12)	O(2)-P(2)-C(17)	112.96(5)
C(1)-P(1)	1.8112(11)	N(2)-P(2)-C(17)	101.05(5)
		O(2)-P(2)-C(23)	108.77(5)
		N(2)-P(2)-C(23)	108.23(5)
		C(17)-P(2)-C(23)	108.18(5)
		C(29)-N(2)-P(2)	128.98(8)
		C(13)-N(1)-P(1)	126.99(7)
		C(13)-N(1)-H(1)	116.5
		P(1)-N(1)-H(1)	116.5
		N(1)-C(13)-C(14)	105.96(9)
		N(1)-C(13)-C(15)	111.80(9)
		C(2)-C(1)-P(1)	119.63(9)
		C(6)-C(1)-P(1)	120.77(9)

Table 3.4 Crystal data and structure refinement for **5**

Empirical formula	(C16 H20 N O P)	
Formula weight	273.30	
Temperature	173(2) K	
Wavelength	0.71073 Å	
Crystal system	Triclinic	
Space group	P-1	
Unit cell dimensions	a = 9.9212(2) Å	α= 89.3440(10)°.
	b = 10.9651(2) Å	β= 82.3230(10)°.
	c = 13.9669(3) Å	γ = 83.0590(10)°.
Volume	1494.75(5) $Å^3$	
Z	4	
Density (calculated)	1.214 Mg/m^3	
Absorption coefficient	0.176 mm^{-1}	
F(000)	584	
Crystal size	0.27 x 0.25 x 0.21 mm^3	
Theta range for data collection	1.87 to 28.31°.	
Index ranges	-13<=h<=13, -13<=k<=14, -18<=l<=18	
Reflections collected	47775	
Independent reflections	7384 [R(int) = 0.0189]	
Completeness to theta = 28.31°	99.0 %	
Absorption correction	Semi-empirical from equivalents	
Max. and min. transmission	0.9639 and 0.9540	
Refinement method	Full-matrix least-squares on F^2	
Data / restraints / parameters	7384 / 0 / 349	
Goodness-of-fit on F^2	1.040	
Final R indices [I>2sigma(I)]	R1 = 0.0331, wR2 = 0.0856	
R indices (all data)	R1 = 0.0388, wR2 = 0.0895	
Largest diff. peak and hole	0.633 and -0.741 $e.Å^{-3}$	

3.2.2 N-tert-butyl-P-diphenylphosphinic amide silver(I) complex

The reaction of $[OP(C_6H_5)_2(NH\text{-}tert\text{-}C_4H_9)]$ (**5**) with $[Ag(CF_3SO_3)]$ (molar ratio 2:1) in THF led to the formation of a novel dinuclear silver(I) complex with a T-shape geometry, $[Ag(CF_3SO_3)(OPPh_2N(H)CMe_3)_2\}\{Ag(OPPh_2N(H)CMe_3)_2\}]SO_3CF_3$ (**6**) illustrated in Scheme 3.7

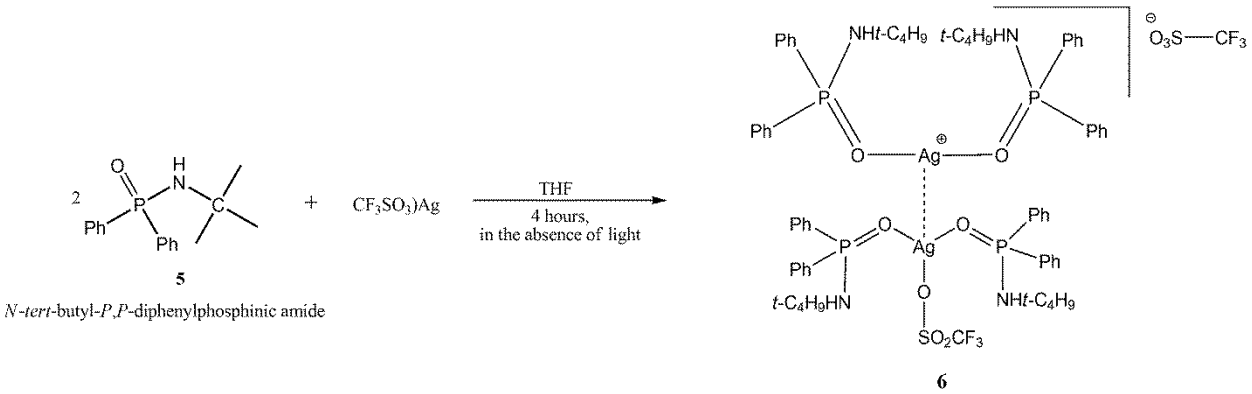

Scheme 3.5 Formation of $[Ag(CF_3SO_3)(OPPh_2N(H)CMe_3)_2\}\{Ag(OPPh_2N(H)CMe_3)_2\}]$-$SO_3CF_3$ (**6**)

Reported results of coordinative phosphinamides were on group 12 metals and lanthanides which are highly oxophillic in nature.[4,7] The aforementioned complex **6** shows a coordination system that contains a dinuclear unit of silver(I) atoms that are each bound to two ligand molecules (**5**) *via* a dative O···Ag bond. One of the Ag atoms is bound to the trifluoromethanesulfonate group while the other Ag atom forms a cationic species that is stabilized by the second trifluoromethanesulfonate moiety.

The solution structure of **6** shows a downfield shift in the ^1H spectrum; with a shift of 0.1 ppm over the resultant spectra of ligand **5** and the ^{31}P NMR spectrum of complex **6** shows a single peak at 19.4 ppm. This result further illustrated that the P atom was oxidized which does not allow further binding of the P atom. Infrared spectra of complex **6** show distinct bands at 3181 and 1172 cm^{-1}, corresponding to Oxygen-Metal and Phosphorous-Oxygen stretch respectively.

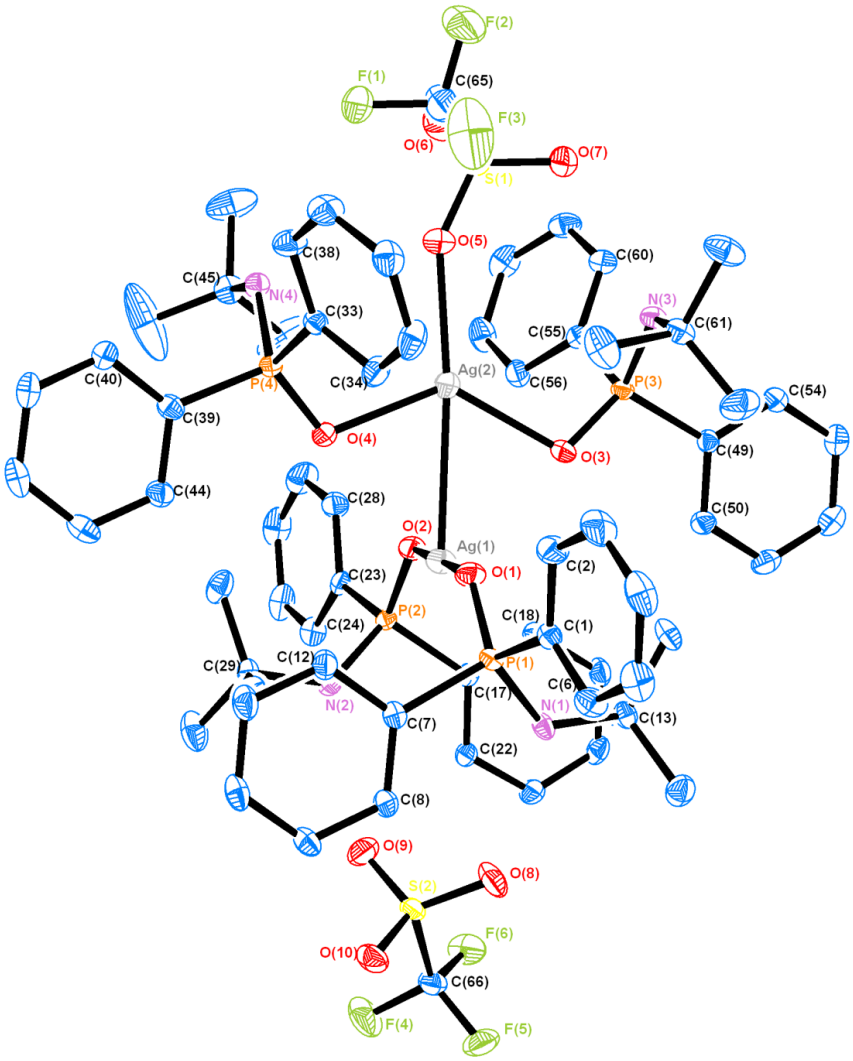

Figure 3.6 Complex **6** with the atom labeling scheme. The displacement ellipsoids are shown at the 50% probability level. Hydrogen atoms are excluded for clarity.

In the solid-state the complex crystallized in the monoclinic system in the *Cc* symmetry space group. There is a distinct covalent bond between Ag(2) and O(5) from the trifluoromethanesulfonate moiety, measuring 2.370(2) Å which impacts on the geometry of the molecule around the Ag(2) atom. In comparison the distance between Ag(1) and O(9) is *ca.* 5.078 Å. The geometry around the Ag(2) atom is seen to adopt a distorted trigonal planar geometry which is confirmed by the angles between the O atoms and the Ag(2) atom which was found to be 129.69(6), 107.77 and 122.20(8)° for O(3)-Ag(2)-O(4), O(4)-Ag(2)-O(5), O(3)-Ag(2)-O(5), respectively. This geometry allows the respective bond lengths of Ag(2)-O(3), Ag(2)-O(4) and Ag(2)-O(5) to be approximately equidistant and this is seen with the bond lengths of 2.2472(19), 2.2475(18) and 2.370(2) Å, respectively. In comparison, the

atoms O(2)-Ag(1)-O(1) adopt a linear geometry and this is confirmed by the angle of 179.56(7)° between these atoms. The bond lengths for the related atoms are seen to be 2.0900(18) and 2.101(2) Å for Ag(1)-O(1) and Ag(1)-O(2), respectively. The P=O bonds of P(1)-O(1), P(2)-O(2), P(4)-O(4) P(3)-O(3) were found to be 1.5076(19), 1.509(2), 1.5107(18) and 1.5115(19) Å respectively, which is longer than that of the free ligand. This is due to the Ag atom pulling electron density away from the O atom and therefore elongates the bond between phosphorous and oxygen. Another feature of the above structure is that the two silver units that make up the dinuclear molecule sit at approximate right angles to each other and this is seen in the packing diagram of the above structure (**Figure 3.7**).

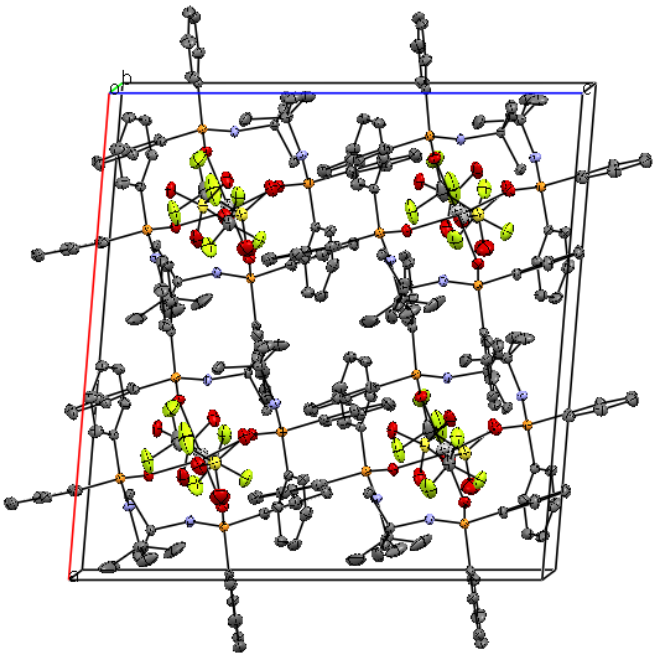

Figure 3.7 Packing diagram of Complex **6** seen along the ***b*** axis

The bond angles between O(1)-Ag(1)-Ag(2) and O(2)-Ag(1)-Ag(2) which is 94.19(5) and 85.82(5)° serves to illustrate this. Apart from these features of the solid state structure, there is also an interaction between the two silver atoms Ag(1)-Ag(2), with a bond distance of 2.8979(3) Å which coincides with previously reported bond distances that are reported in a range of 2.869(5) to 2.981(5) Å.[17] This bond length is also below the sum of van der Waals radii of 3.44 Å for silver, which infers a strong interaction of Ag(1)-Ag(2) atoms in complex **6**.[18]

On inspection of complex **6** there are four uncoordinated N atoms which could be further reacted to form a supramolecular heterometallic system. The preferential binding of the silver to oxygen over nitrogen can perhaps be rationalised by the hard and soft acid-base (SHAB) theory where Ag^{+} is a relatively soft acid and N and O donor atoms are relatively hard bases. However of the two, oxygen donor atoms are softer than their nitrogen counterparts.[8]

Table 3.5 Selected Bond lengths [Å] and angles [°] for complex **6**

Ag(1)-Ag(2)	2.8979(3)	O(5)-Ag(2)-Ag(1)	174.67(5)
O(5)-Ag(2)	2.370(2)	O(4)-Ag(2)-Ag(1)	66.89(4)
O(5)-S(1)	1.449(2)	O(3)-Ag(2)-Ag(1)	63.11(4)
O(4)-Ag(2)	2.2475(18)	O(4)-Ag(2)-O(5)	107.77(7)
O(4)-P(4)	1.5107(18)	O(3)-Ag(2)-O(5)	122.20(7)
O(3)-Ag(2)	2.2472(18)	O(3)-Ag(2)-O(4)	129.68(6)
O(3)-P(3)	1.5115(18)	O(2)-Ag(1)-Ag(2)	85.82(5)
O(2)-Ag(1)	2.1011(19)	O(1)-Ag(1)-Ag(2)	94.19(5)
O(2)-P(2)	1.5091(18)	O(1)-Ag(1)-O(2)	179.56(8)
O(1)-Ag(1)	2.0900(18)	C(7)-P(1)-C(1)	108.74(10)
O(1)-P(1)	1.5076(18)	N(1)-P(1)-C(1)	110.20(11)
N(4)-P(4)	1.648(2)	O(1)-P(1)-C(1)	105.14(11)
N(3)-P(3)	1.655(2)	N(1)-P(1)-C(7)	103.71(10)
N(2)-P(2)	1.633(2)	O(1)-P(1)-C(7)	109.71(11)
N(1)-P(1)	1.630(2)	O(1)-P(1)-N(1)	119.09(11)
C(1)-P(1)	1.802(2)	S(1)-O(5)-Ag(2)	150.98(14)
		P(4)-O(4)-Ag(2)	110.16(9)
		P(3)-O(3)-Ag(2)	107.33(9)
		P(2)-O(2)-Ag(1)	118.24(11)
		P(1)-O(1)-Ag(1)	122.56(11)

Table 3.6 Crystal data and structure refinement of complex **6**

Empirical formula	C66 H76 Ag2 F6 N4 O10 P4 S2	
Formula weight	1603.05	
Temperature	173(2) K	
Wavelength	0.71073 Å	
Crystal system	Monoclinic	
Space group	*Cc*	
Unit cell dimensions	a = 17.8630(3) Å	α = 90°.
	b = 22.8841(4) Å	β = 94.7690(10)°.
	c = 17.3304(3) Å	γ = 90°.
Volume	7059.8(2) $Å^3$	
Z	4	
Density (calculated)	1.508 Mg/m^3	
Absorption coefficient	0.779 mm^{-1}	
Crystal size	0.35 x 0.34 x 0.22 mm^3	
Theta range for data collection	1.78 to 28.29°.	
Reflections collected	84418	
Independent reflections	17258 [R(int) = 0.0238]	
Absorption correction	Semi-empirical from equivalents	
Refinement method	Full-matrix least-squares on F^2	
Data / restraints / parameters	17258 / 2 / 860	
Goodness-of-fit on F^2	1.039	
Final R indices [I>2sigma(I)]	R1 = 0.0277, wR2 = 0.0839	
R indices (all data)	R1 = 0.0288, wR2 = 0.0850	
Largest diff. peak and hole	0.997 and -0.606 $e.Å^{-3}$	

In summary, this chapter introduced the concept of phosphinamide ligand formation, which had been subsequently demonstrated in the ligand crystal structure of **4**. This structure displays hydrogen bonding interactions. The reaction of **4** with silver trifluoromethanesulfonate resulted in the formation of a novel complex **5** which displays a number of interesting structural properties. One of these is the geometry around the two silver atoms, where one Ag centre adopts a distorted trigonal planar geometry and the other a linear geometry.

3.3 Preparation of compounds

All compounds were prepared using the same characterization techniques as outlined in chapter **2**

3.3.1 Synthesis of $[(C_6H_5)_2PO(NH\text{-}t\text{-}C_4H_9)]$

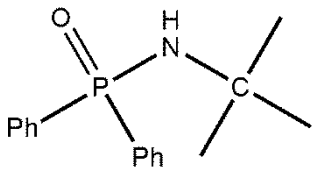

5

To a flame-dried Schlenk tube, *t*-butylamine (0.332 g, 4.53 mmol) was added to ether (30 mL) with stirring. The Schlenk tube was immersed into a dry ice/acetone bath at -78 ^{0}C, thereafter BuLi (2.84 mL, 1.6 M) was added drop-wise and stirred for 20 minutes. The solution was then warmed to room temperature and further stirred for 30 minutes.

A prepared solution of chlorodiphenylphosphine (0.974 g, 4.415 mmol) in ether was added to the Schlenk tube at -78^{0}C and stirred for 20 minutes. The reaction was warmed to room temperature and stirred for 20 minutes. LiCl was filtered off under vacuum through a septum of $MgSO_4$ and Celite (filter-aid). The ensuing filtrate was further stirred at room temperature for 30 minutes, followed by the removal of solvent under reduced pressure which resulted in a white precipitate. The resulting precipitate was dissolved in dichloromethane and the solution filtered through anhydrous $MgSO_4$ and Celite (filter-aid). Solvent was removed under reduced pressure to a volume of 5 mL and hexane was added to precipitate out the product. The resulting mixture was then stirred for 10 minutes, thereafter the solvent was

removed under reduced pressure and a white powder was isolated. Yield: 0.826 g, 70%; Melting point: 133 – 136 ^{0}C. ^{1}H NMR: δ (ppm): 1.29 (*1H*, s, NH), 1.27 (9*H*, s), 7.33 (8*H*, m), 7.41 (2*H*, dd, J = 6.72, 1.54 Hz). ^{13}C NMR ($CDCl_3$): δ (ppm): 32.28 (CH_3), 53.09 ($C(CH_3)$), 128.30 (*ortho*-ArC), 131.74 (*meta*-ArC), 135.70 (*para*-ArC). ^{31}P NMR: δ: 19.51ppm. Anal. calc. for $C_{16}H_{20}NOP$: C 70.31, H 7.38; N 5.12 %. Found: C 70.4, H 7.32, N 5.08 %.

Selected IR data *v*/cm^{-1}: 1175 (s), 1109(s), 692 (s), 522 (s).

3.3.2 Synthesis of $[Ag(CF_3SO_3)(OPPh_2N(H)CMe_3)_2\}\{Ag(OPPh_2N(H)CMe3)_2\}]SO_3CF_3$

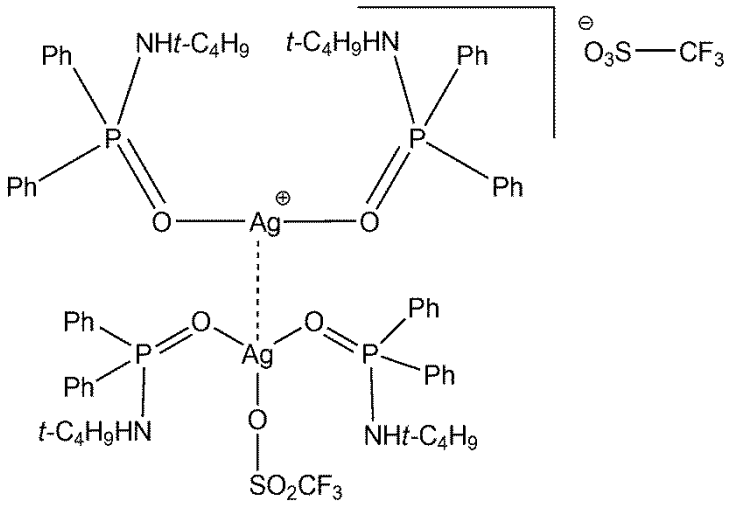

6

To a solution of *N*-*tert*-butyl-*P*,*P*-diphenylphosphinic amide (0.197 g, 0.248 mmol) in THF (20 mL), silver trifluoromethanesulfonate (0.0646 g, 0.251 mmol) was added in a 2:1 molar ratio in a pre-dried Schlenk tube under nitrogen while stirring. The Schlenk tube was covered in foil to avoid light as silver is sensitive to light. The mixture was stirred for 4 hours at room temperature and solvent was removed under reduced pressure. Dichloromethane was added and stirred for an additional 10 minutes, and filtered through $MgSO_4$ and Celite. Solvent was removed *in vacuuo* to obtain a white powder. Yield: 0.069 g, 35% yield. Melting point at 147.6 – 149.4 ^{0}C. ^{1}H NMR: δ (ppm): 1.64 (*4H*, s), 1.300 (36*H*, s), 7.44 (32*H*, m), 7.89 (8*H*, dd, J = 6.68, 1.20 Hz). ^{13}C NMR ($CDCl_3$): δ (ppm): 32.29 (CH_3), 53.00 ($C(CH_3)$), 128.29 (*ortho*-ArC), 131.42 (*meta*-ArC), 135.70 (*para*-ArC). ^{31}P NMR: δ: 19.49 ppm. Anal. calc. for $C_{62}H_{76}Ag_2F_6N_4O_{10}P_4S_2$: C 47.89, H 4.93; N 3.60 %. Found: C 47.90, H 4.83, N 3.68 %.

Selected IR data *v*/cm^{-1}: 3181(m), 1172 (s), 1122(s), 678 (s), 542 (s).

3.4 References

(1) (a) Berlin, K. D.; Butler, G. B. *Chem. Rev.* **1960**, *60*, 243 (b) Pietrusiewicz, K. M.; Zablocka, M. *Chem. Rev*. **1994**, *94*, 1375 (c) Bloomfield, A. J.; Qian, J. M.; Herzon, S. B. *Organomet.* **2010**, *29*, 4193.

(2) Svara, J.; Weferling, N.; Hofmann, T. In *Ullmann's Encyclopedia of Industrial Chemistry*; Wiley-VCH Verlag GmbH & Co. KGaA, 2000.

(3) Bondarenko, N.; Kharlamov, A.; Vendilo, A. *Russ. Chem. Bull.* **2009**, *58*, 1872.

(4) Priya, S.; Balakrishna, M. S.; Mobin, S. M. *Polyhedron* **2005**, *24*, 1641.

(5) Grushin, V. V. *Chem. Rev.* **2004**, *104*, 1629.

(6) Charbonnière, L. J.; Ziessel, R.; Montalti, M.; Prodi, L.; Zaccheroni, N.; Boehme, C.; Wipff, G. *J. Am. Chem. Soc.* **2002**, *124*, 7779.

(7) Priya, S.; Balakrishna, M. S.; Mague, J. T.; Mobin, S. M. *Inorg. Chem.* **2003**, *42*, 1272.

(8) Pearson, R. G. *J. Chem. Educ.* **1968**, *45*, 581.

(9) Yeh, C.-W.; Chang, K.-H.; Hu, C.-Y.; Hsu, W.; Chen, J.-D. *Polyhedron* **2012**, *31*, 657.

(10) Soini, E.; Lövgren, T.; Reimer, C. B. *C R C Critical Reviews in Anal. Chem.* **1987**, *18*, 105.

(11) Kido, J.; Okamoto, Y. *Chem. Rev.* **2002**, *102*, 2357.

(12) Thompson, K. H.; Orvig, C. *Chem. Soc. Rev.* **2006**, *35*, 499.

(13) Hasegawa, Y.; Kawai, H.; Nakamura, K.; Yasuda, N.; Wada, Y.; Yanagida, S. *J. Alloys Compd.* **2006**, *408–412*, 669.

(14) Pietraszkiewicz, M.; Pietraszkiewicz, O.; Karpiuk, J.; Karpiuk, E.; Borowiak, T.; Dutkiewicz, G. *Inorg. Chim. Acta* **2012**, *387*, 426.

(15) Han, W. S.; Lee, S. W. *J. Korean Chem. Soc.* **2001**, *45*, 264.

(16) Kinfe, H. H.; Hamese, A.; Hughes, T.; Omondi, B. *Acta Crystallog. Sect. E* **2011**, *67*, o3392.

(17) Li, B.; Zang, S.-Q.; Li, H.-Y.; Wu, Y.-J.; Mak, T. C. W. *J. Organomet. Chem.* **2012**, 112, *708–709*.

(18) H. Zhu, X. Z., X. Liu,X. Wang,G. Liu, A. Usman ,H. Fun. *Inorg. Chem. Comm.* **2003**, 1113.

CHAPTER 4

Synthesis of Gold Nanoparticles (AuNPs) and the formation of Self Assembled Monolayers (SAMs)

4.1 Introduction

4.1.1 Synthesis of gold nanoparticles

Colloidal gold, also known as gold nanoparticles, is a suspension (or colloid) of nanometer-sized particles (1-100 nm) of gold in a fluid, and is observed in different shapes and sizes. The colour of the nanoparticles depends on the shape and size of the nanoparticles.[1] There are various shapes that are noted, but the two that are most common are the nanorods [**Figure 4.1(b)**] and nanospheres [**Figure 4.1(a)**].

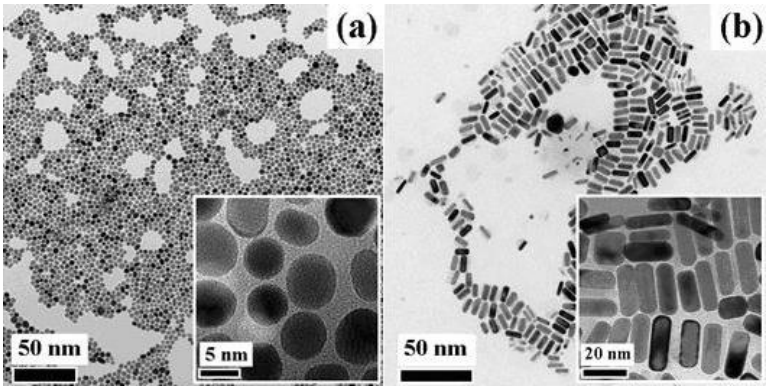

Figure 4.1 Transmission electron micrograph of (a) Nanospheres, (b) Nanorods[2]

4.1.1.1 Faraday Method

In 1857, Faraday reported the formation of deep red solutions of colloidal gold by reduction of an aqueous solution of tetrachloroaurate ($AuCl_4^-$) using phosphorus in CS_2 in a two phase system.[3]

4.1.1.2 Citrate Reduction Method (Turkevitch Method)

Among the numerous methods of synthesis of AuNPs, the most popular has been that of citrate reduction of $H[AuCl_4]$in water, which was introduced by Turkevitch in 1951.[4] It leads to AuNPs of 10 - 20 nm in diameter. It entails the reaction of small amounts of hot tetrachloroauric acid with small amounts of sodium citrate solution. The AuNPs will form because the citrate ions act as a reducing agent.[5]

4.1.1.3 The Brust-Schiffrin Method

This method involves the synthesis of AuNPs using a two-phase synthesis and stabilization using thiols. This type of synthesis uses Faraday's two phase synthesis,[3] as well as using thiol ligands which bind strongly to gold. $AuCl^-$ is transferred to toluene using tetra-octylammonium bromide as the phase-transfer reagent and reduced by $NaBH_4$ in the presence of dodecanethiol (**Figure 4.2**).[6]

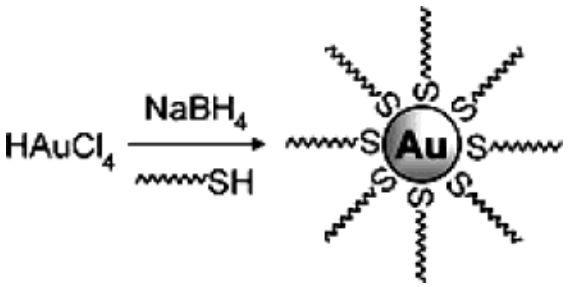

Figure 4.2 Formation of AuNPs coated with organic shells by reduction of Au(III) compounds in the presence of thiols[7]

This method yields diameters in the range of 1-3 nm, with a maximum in the particle size distribution at 2.0-2.5 nm.[8]

4.1.2 Use of SiO_2 as a solid support

SiO_2 is used in a variety of industrial applications. It is used as a catalytic support and a filler in fused SiO_2 wares in optical glasses.[9] SiO_2 is a porous material with large surface areas. It is through this large surface area and porosity that gold nanoparticles are allowed to form and thus the gold nanoparticles are stabilized preventing aggregation.[10]

4.1.3 Gold nanoparticles/SiO_2 nanocomposites (AuNP/SiO_2)

The nanoparticles found on a SiO_2 substrate provide a high surface area and possess chemical and physical properties that are distinct from those of both the bulk phase. The importance of the surface structure of nanoparticles has led to a new class of materials through the modification of surface structure. Fabrication of metal coated SiO_2 materials is of special interest due to their stability and inactivity with reactant.[10]

It has been suggested that the role of the support aids in the stabilization of the gold nanoparticles. SiO_2 is used as a support due to its inert character, which allows investigation of the effect of the metal, minimizing the effect of the metal-support interaction. The strong interaction between SiO_2 surfaces and Au particles makes SiO_2 supports very convenient for studying the size effect of the gold nanoparticles, minimizing the disturbance of the support interaction.[11] It is shown that SiO_2 suppresses the sintering of gold nanoparticles preventing aggregation.[12]

Through the properties of the SiO_2 and the intrinsic properties of gold, hybrids known as gold nanoparticle/SiO_2 composites have emerged. The nanocomposites posseses an array of properties not seen individually and from these combined properties an array of applications are seen. There are various methods in which these gold nanoparticle/SiO_2 composites are prepared, of which deposition of gold nanoparticles on SiO_2 spheres done by a sonochemical approach,[10] controlled functionalization of the SiO_2 surface with a Au(I) complex,[13] and deposition–precipitation method,[14] are examples.

There have been numerous methods for the synthesis of gold nanoparticles, these include multi-step synthesis. In the present study an uncomplicated two step synthesis of AuNP/SiO_2 nanocomposites has been undertaken. It involves the *in situ* thermal reduction of tetrachloroauric acid, H[$AuCl_4$]. The composites were characterized by the following methods: Brunauer, Emmet and Teller surface area analysis (BET), Scanning Electron Microscopy (SEM) with Energy dispersive X-ray spectroscopy (EDX), Transmission Electron Microscopy (TEM) and X-Ray Diffraction (XRD).

4.1.4 Formation and Properties of Self Assembled Monolayers (SAMs)

The formation of monolayers by self-assembly of surfactant molecules at surfaces is one example of the general phenomena of self-assembly. In nature, self-assembly results in supramolecular organizations of interlocking components that provides very complex systems.[18]

SAMs offer unique opportunities in increasing the fundamental understanding of self-organization, structure-property relationships, and interfacial phenomena. The ability to tailor both head and tail groups of the constituent molecules makes SAMs excellent systems for a deeper fundamental understanding of phenomena affected by competing intermolecular, molecular-substrates and molecule-solvent interactions, like ordering and growth, wetting, adhesion, lubrication, and corrosion. SAMs are well-defined and accessible, which makes them good model systems for studies of physical chemistry and statistical physics in two dimensions, and the crossover to three dimensions.[19]

The fabrication and manipulations of molecular assemblies, molecular recognition, bio-mineralization, hierarchical structure and function, and computational chemistry to elucidate structure-function relationships have become central themes in modern chemistry.[19]

4.1.5 Cholesterol and related alcohols towards derived dithiophosphonic acids

Steroids, which are mostly of eukaryotic origin and contain primary alcohol functionalities, are derivatives of cyclopentano-perhydrophenanthrene, a compound that consists of four fused, non-planar rings. Cholesterol, the most abundant steroid in animals, is the major component of animal plasma membranes, with its polar hydroxyl group responsible for its amphiphilic character, while the fused rings provides the molecule with greater rigidity over other membrane lipids.[20]

Cholesterol is also the metabolic precursor of steroid hormones, substrates that regulate a great variety of physiological responses. Androgens and oestrogens affect sexual development and function, which includes estradiol and estrone, the most important female sex hormone.[21]

In this study, cholesterol was used to form a dithiophosphonate salt, which was used in the preparation of the SAMs.

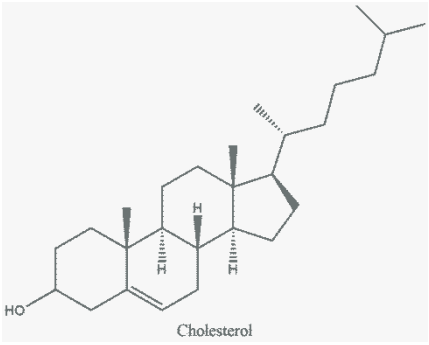

Figure 4.3 The structure of cholesterol

4.1.6 Parameters involved in the formation of nanocomposites

The concentration of the tetrachloroauric acid was varied, namely: 0.01 M, 0.5 M and 1.25 M**.** The temperatures to be used were 50 °C, 100 °C, 200 °C and 300 °C. Herein the following sample codes (**Table 4.1**) will be used in analysis of results obtained.

Table 4.1 Sample codes for the proceeding nanocomposites synthesized

	50°C	100°C	200°C	300°C
0.01 M	AuNP 1	AuNP 2	AuNP 3	AuNP 4
0.5 M	AuNP 5	AuNP 6	AuNP 7	AuNP 8
1.25 M	AuNP 9	AuNP 10	AuNP 11	AuNP 12

4.2 Results and Discussion

The surface structures of nanoparticles lead to a new class of materials through the modification of surface structure, thus the importance of these composites has become vast. AuNP/SiO_2 composites were prepared via the *in-situ* thermal reduction of tetrachloroauric

acid, without the use of a reducing or stabilizing agent, thereafter self assembled monolayers were synthesized via simple immersion.

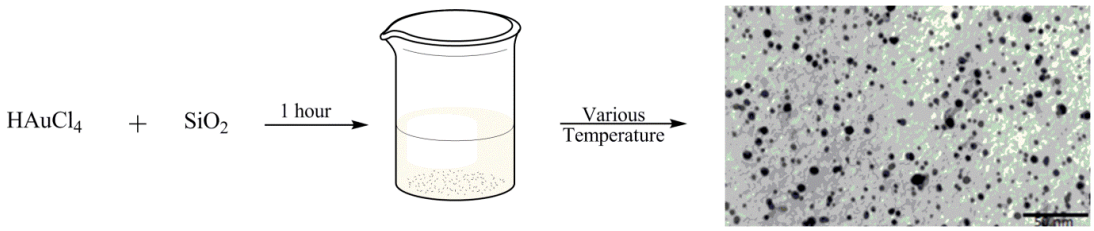

Scheme 4.1 Preparation of AuNP/SiO_2 nanocomposites

4.2.1 SEM and EDX results of AuNP/SiO_2 composites

The results obtained suggests that the AuNP where synthesized on the SiO_2 support. Through SEM and EDX analysis it was possible to quantify the gold present on SiO_2. The SEM results follow a similar generalised pattern and only results for composites synthesized at 300 °C and 50 °C are shown.

Figure 4.4 to **Figure 4.9** show results for composites synthesized at 300 °C at various concentrations of gold solution. The images obtained are as follows:

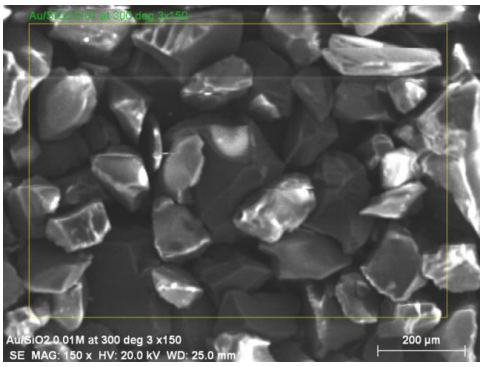

Figure 4.4 SEM image of **AuNP 4**

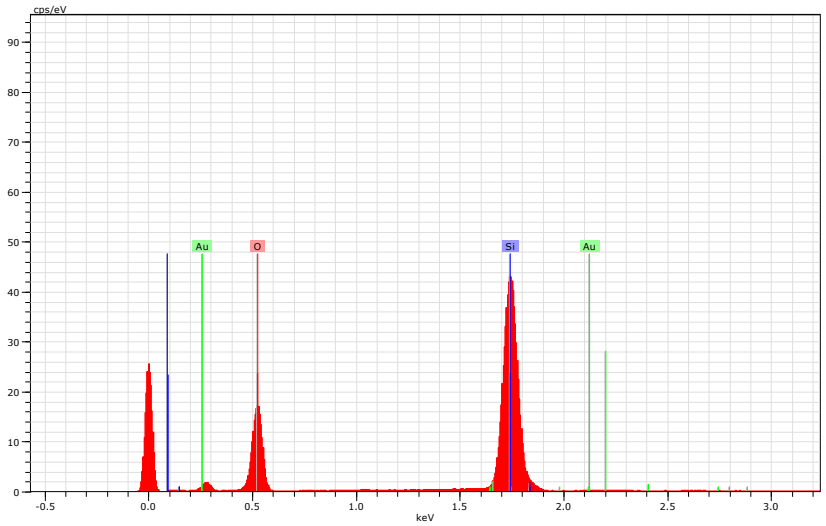

Figure 4.5 EDX spectrum of **AuNP 4**

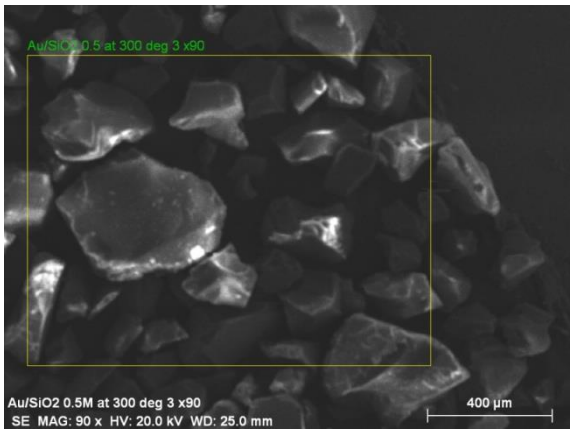

Figure 4.6 SEM image of **AuNP 8**

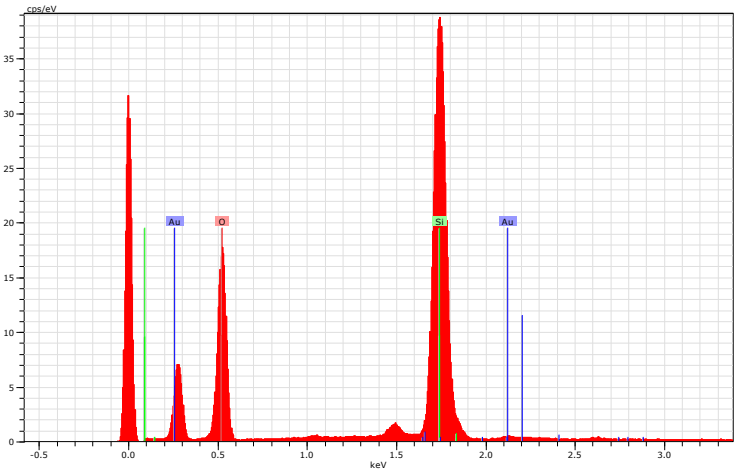

Figure 4.7 EDX spectrum of **AuNP 8**

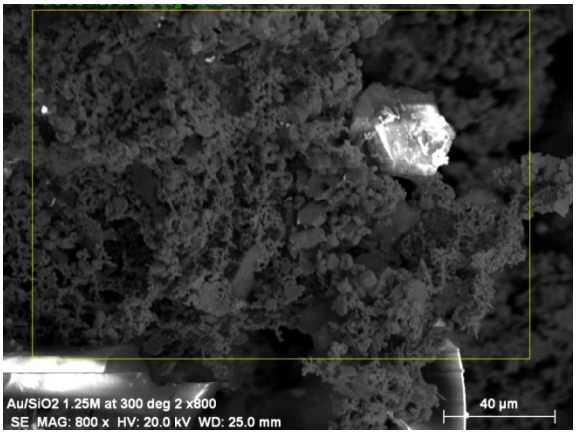

Figure 4.8 SEM image of **AuNP 12**

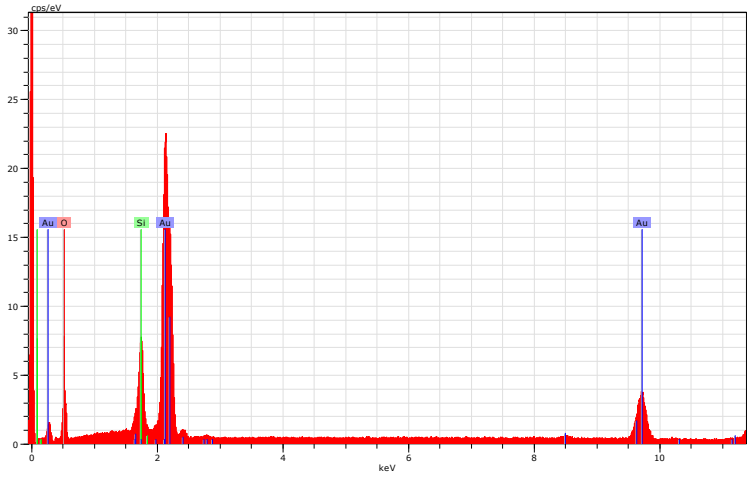

Figure 4.9 EDX spectrum of **AuNP 12**

The percentages show that as concentration of gold in solution increases, so too does the weight percentage of gold on silica. However, this is not representative due to analysis of a single sampling site.

From **Figures 4.4** and **4.6** it is not evident that gold is present on **AuNP 4** and **AuNP 8**, but from the EDX spectra (**Figures 4.7** and **4.9**) there is evidence of gold present in small amounts due to the lower concentrations. From **Figure 4.9** it is seen that gold is deposited on the surface of the SiO_2, and the higher concentration of 1.25 M presumably accounts for this. The characteristic peak of gold seen in the EDX spectrum is 0.25, 2.1, and 2.2 eV.

Figure 4.10 and **Figure 4.11** show results for 50 °C at the various concentrations. The images obtained are as follows:

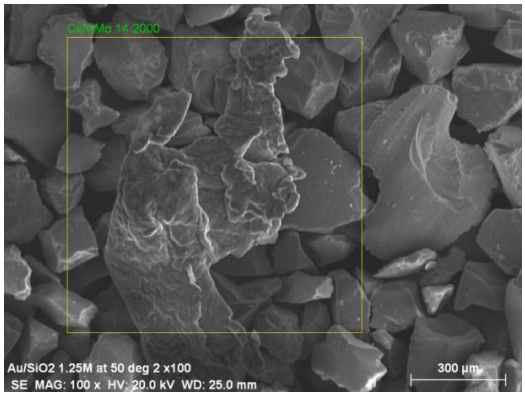

Figure 4.10 SEM image of **AuNP 9**

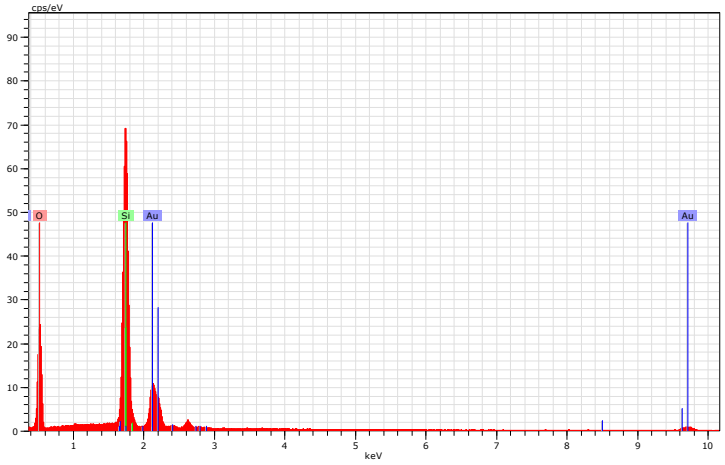

Figure 4.11 EDX spectrum of **AuNP 9**

It is seen from the above image and EDX spectra that gold is present. Weight percentage of gold present increases as concentration of gold increases, and the 50 °C set of samples follow a similar trend to the 300 °C set of samples in that, there is an increase of the deposition of gold on SiO_2 surface with the respective increase in concentration.

4.2.2 TEM results of AuNP/SiO_2 composites

A key factor of solid supports is the stabilization of nanoparticles. Common supports such as SiO_2, titanium dioxide, and zeolites partially prevent the aggregation of gold nanoparticles, this is due to the porosity of supports. Shape and structure of the Au particles correlate with the catalytic activity.[22] Through the use of solid supports, many properties can be fine-tuned, as well as the ability to control shape and size.[23]

Through varying the concentration of $H[AuCl_4]$, the size and shape of the gold nanoparticles can be varied.[2] Literature reports that nanoparticle size increases with increased concentration. However, this applies to specific supports, preparative methods and approaches.[22,24]

TEM images reveal that AuNPs were present and were deposited on the surface of the SiO_2 gel. The shape of the nanoparticles was generally circular and the size varied with the concentration. Low concentration samples did show aggregation.

Image analysis was carried out digitally by counting particles manually. The particle diameter, standard deviation, and particle count where generated. Due to difficulties encountered while conducting TEM analysis, the requisite particle count of 250 needed for statistical evaluation was not achieved for all samples.

4.2.2.1 TEM results of AuNP/SiO_2 composites samples at 300 °C.

Figure 4.12 to **Figure 4.17** show results for 300 °C at the various concentrations. The images obtained are as follows:

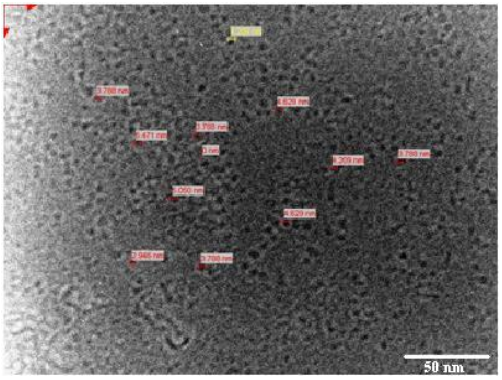

Figure 4.12 TEM image of **AuNP 4**

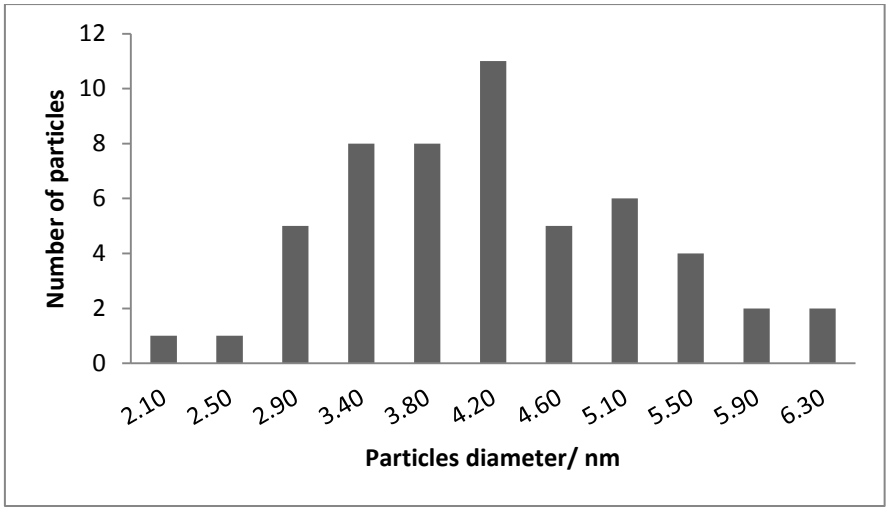

Figure 4.13 Particle size distribution histogram of **AuNP 4**

From **Figure 4.12** and **4.13** it is seen that **AuNP 4** TEM images, reveal a mean diameter of 4 nm. The highest number of AuNPs with the same diameter was 11 with a diameter of 4 nm. The AuNPs showed an even distribution on the SiO_2 gel and varied from 2 nm to 6 nm.

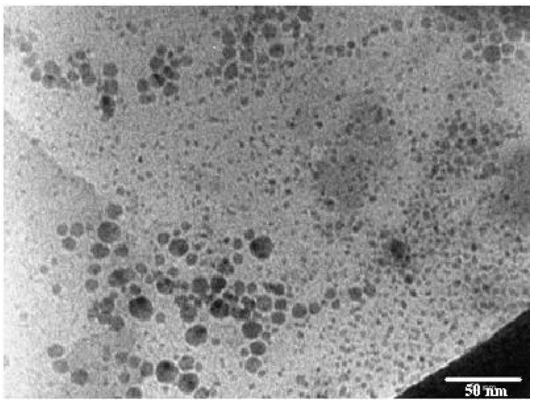

Figure 4.14 TEM image of **AuNP 8**

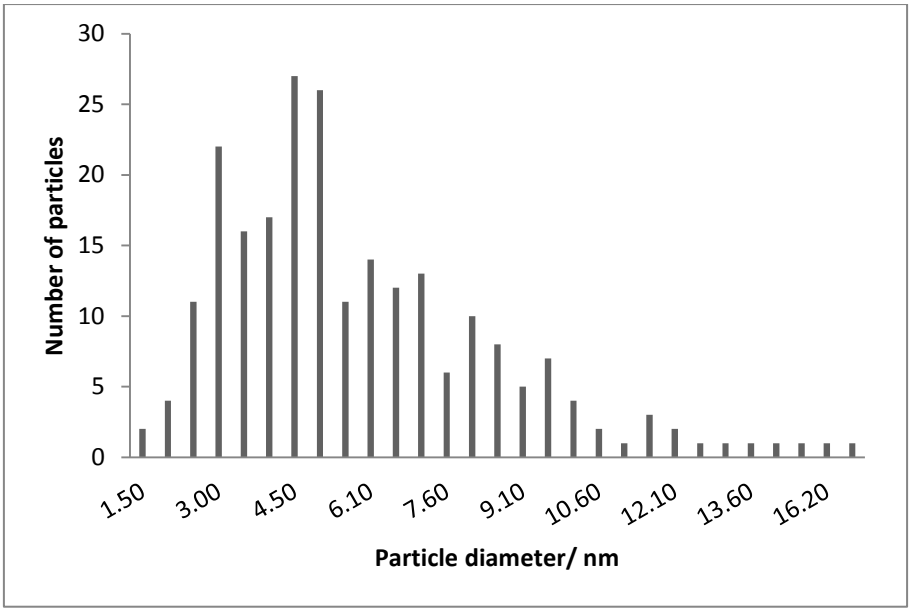

Figure 4.15 Particle size distribution histogram of **AuNP 8**

From **Figure 4.14** and **4.15** it is seen that **AuNP 8** TEM images, reveal a mean diameter of 6 nm. The highest number of AuNPs with the same diameter was 27, with a diameter of 5 nm. The AuNPs showed an even distribution on the SiO_2 gel and varied from 2 nm to 18 nm.

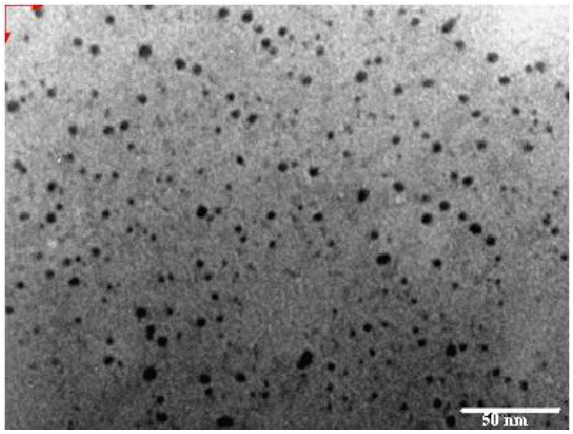

Figure 4.16 TEM image of **AuNP 12**

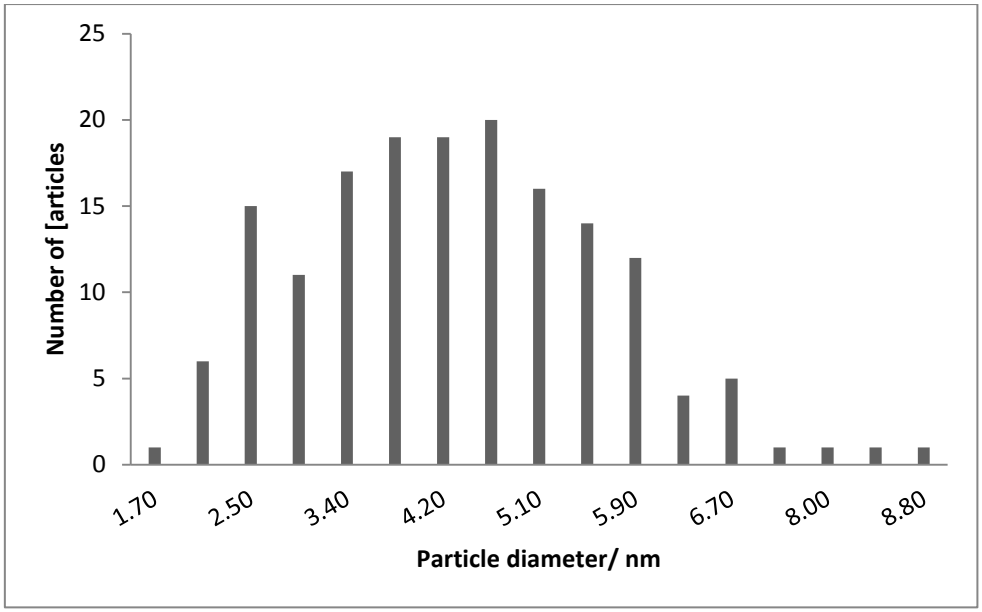

Figure 4.17 Particle size distribution histogram of **AuNP 12**

From **Figure 4.16** and **4.17** it is seen that **AuNP 12** TEM images, reveal a mean diameter of 4 nm. The highest number of AuNPs with the same diameter was 20 with a diameter of 5 nm. The AuNPs showed an even distribution on the SiO_2 gel and varied from 2 nm to 9 nm.

When comparing the three different concentrations, there is no apparent trend seen with regard to the mean particle diameter, namely 4 nm for **AuNP 4**, 6 nm for **AuNP 8** and 4 nm for **AuNP 12**. The deposition of gold to the surface seems to decrease with a decrease in concentration, with regard to the count of particles.

The results can be rationalised as follows. With increase in concentration of Au^{3+}, there is an increase in the magnitude of Au^0 deposited on the surface. With the increase of deposition, there should be an increase in the amount of gold nanoparticles. The increase in number of particles could lead to the stabilization of the gold nanoparticles depending on the support, or it could lead to the aggregation of gold nanoparticles to form larger particles. SiO_2 is a porous material and due to this porosity, it is postulated that a significant number of AuNPs accumulate in these pores. The AuNPs are thus stabilized in this manner. That is, they enter the pore and reside there, thus preventing the aggregation of the AuNPs.

AuNP 4, with a count of 54 nanoparticles, and a mean diameter of 4 nm, showed stable nanoparticles formation and no indication of aggregation. **AuNP 8** with a count of 227 nanoparticles and a mean of 5 nm shows homogenous dispersion of gold nanoparticles and stable gold nanoparticles. **AuNP 12** with a count of 163 nanoparticles and a mean of 4 nm

shows even distribution and the nanoparticles fall within a very small range making them excellent choice for requirements of AuNPs of a size less than 10 nm.

This count is justified as the concentration increase from 0.01 M to 0.5 M the count increases from 54 nanoparticles to 227 nanoparticles, however, once the concentration reaches a maximum (between 0.5 M and 1.25 M), the count was shown to decrease and aggregation occurs. Aggregation is visible for all samples but nanoparticles found in the pores are seen.

It should be noted that the above results follow a different trend to increase in particle size with the increase of concentration. This arises from the fact that SiO_2 stabilizes the AuNPs through the presence of pores and the following postulation can be made: as the total number of pores exposed to gold increase (or the total number of pores occupied by gold), the number of smaller AuNPs formed increases. As the concentration increases the total number of nanoparticles formed increases, until a maximum concentration is reached and the pores reach saturation.

4.2.2.2 TEM results of AuNP/SiO_2 composites for samples at 200 °C

Figure 4.18 to **Figure 4.23** show results for 200 °C at the various concentrations. The images obtained are as follows:

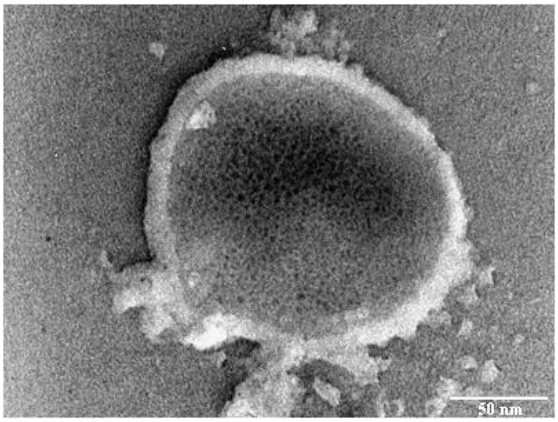

Figure 4.18 TEM image of **AuNP 3**

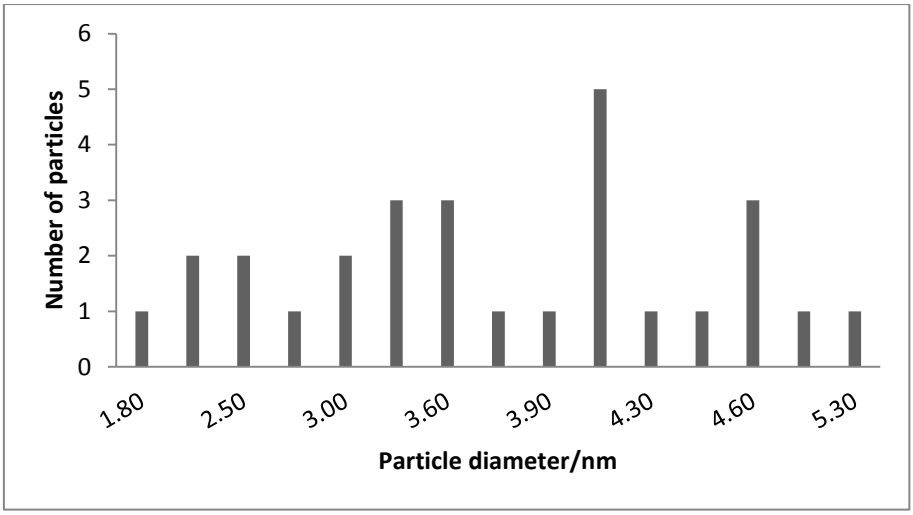

Figure 4.19 Particle size distribution histogram of **AuNP 3**

From **Figure 4.18** and **4.19** it is seen that **AuNP 3** TEM images reveal a mean diameter of 4 nm. The highest number of AuNPs with the same diameter was 5 with a diameter of 4 nm. The AuNPs showed an even distribution on the SiO_2 gel and varied from 2 nm to 5 nm.

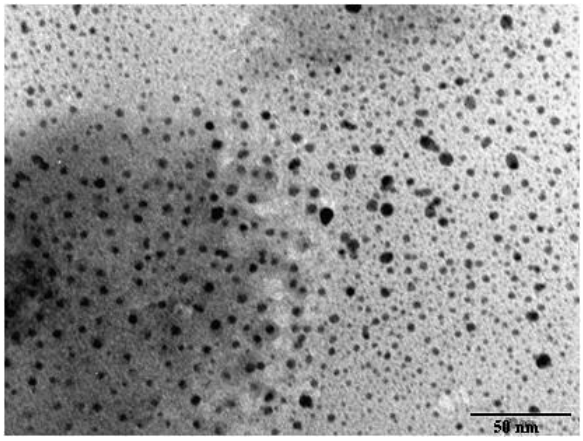

Figure 4.20 TEM image of **AuNP 7**

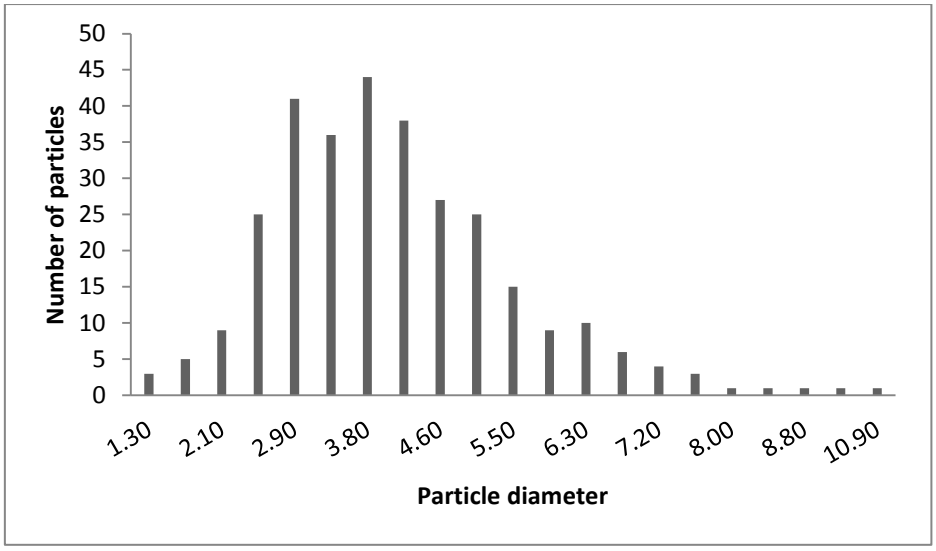

Figure 4.21 Particle size distribution histogram of **AuNP 7**

From **Figure 4.20** and **4.21** it is seen that **AuNP 7** TEM images reveal a mean diameter of 4 nm. The highest number of AuNPs with the same diameter was 44 with a diameter of 4 nm. The AuNPs showed an even distribution on the SiO_2 gel and varied from 1 nm to 11 nm.

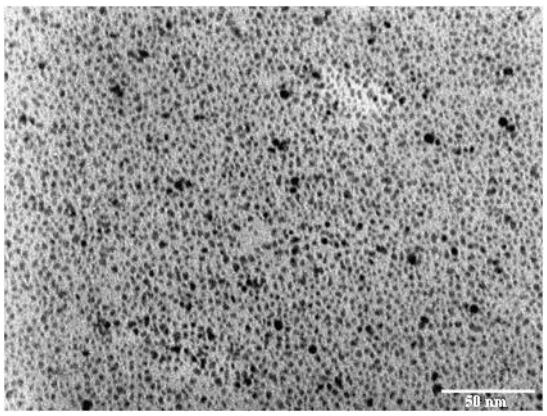

Figure 4.22 TEM image of **AuNP 11**

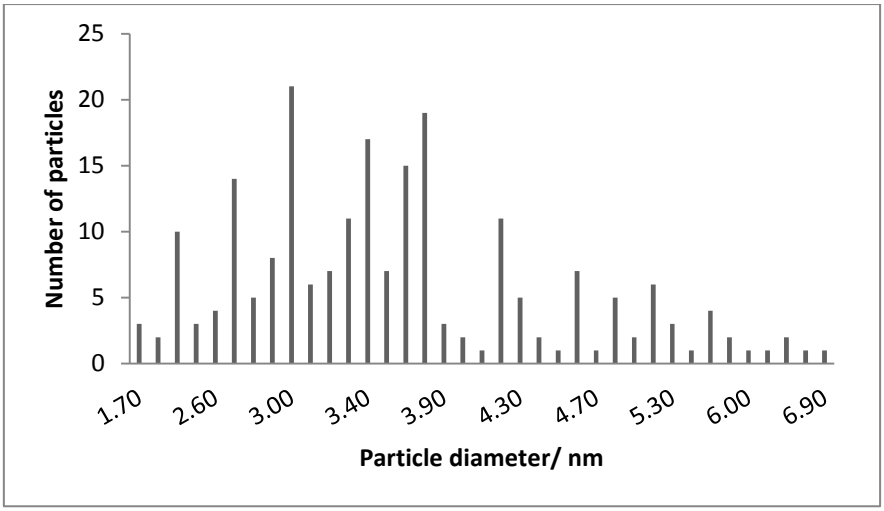

Figure 4.23 Particle size distribution histogram of **AuNP 11**

From **Figure 4.22** and **4.23** it is seen that **AuNP 11** TEM images reveal a mean diameter of 4 nm. The highest number of AuNPs with the same diameter was 21 with a diameter of 3 nm. The AuNPs showed an even distribution on the SiO_2 gel and varied from 2 nm to 7 nm.

From **Figure 4.18** it was seen that aggregation occurs rapidly under the electron beam of the Transmission Electron Microscope. These results follow the same trend as the 300 °C samples. **AuNP 3** with a count of 28 nanoparticles, and a mean diameter of 4 nm. **AuNP 7** with a count of 305 nanoparticles and a mean of 4 nm shows even dispersal of AuNPs. **AuNP 11** with a count of 216 nanoparticles and a mean of 4 nm shows even distribution. Again, as the total number of pores exposed to gold increase, the number of smaller AuNPs formed increases and as the concentration increases the total number of nanoparticles formed increases, until a maximum concentration is reached and the pores reach saturation.

4.2.2.3 TEM results of AuNP/SiO_2 composites for 100 °C samples

Figure 4.24 to **Figure 4.29** show results for 100 °C at the various concentrations. The images obtained are as follows:

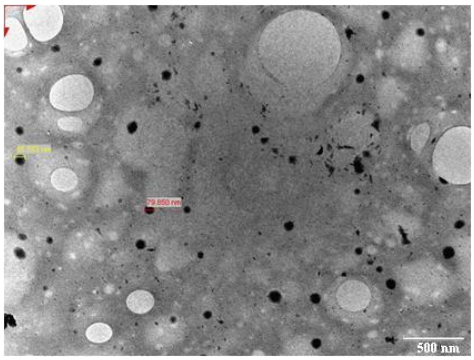

Figure 4.24 TEM image of **AuNP 2**

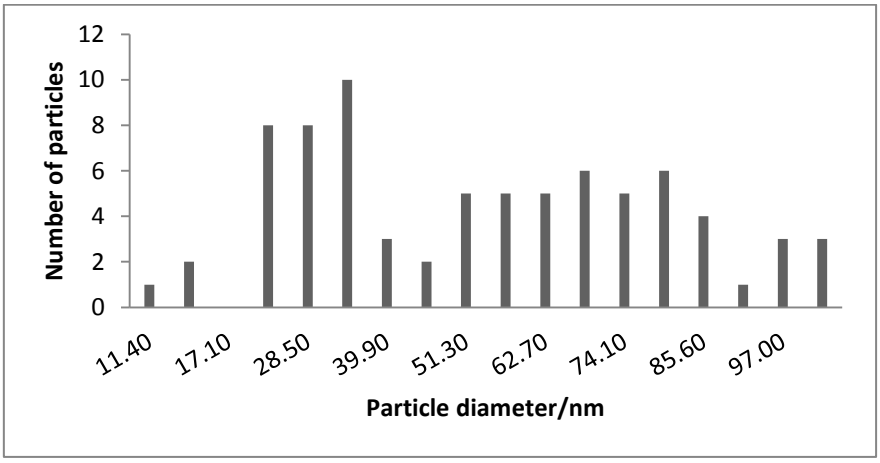

Figure 4.25 Particle size distribution histogram of **AuNP 2**

From **Figure 4.24** and **4.25** it is seen that **AuNP 2** TEM images reveal a mean diameter of 54 nm. The highest number of AuNPs with the same diameter was 10 with a diameter of 34 nm. The AuNPs showed an even distribution on the SiO_2 gel and varied from 2 nm to 5 nm.

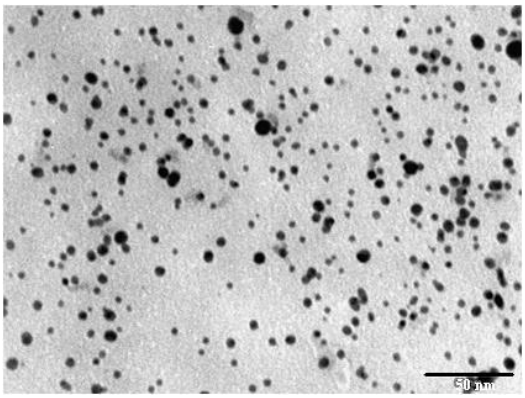

Figure 4.26 TEM image of **AuNP 6**

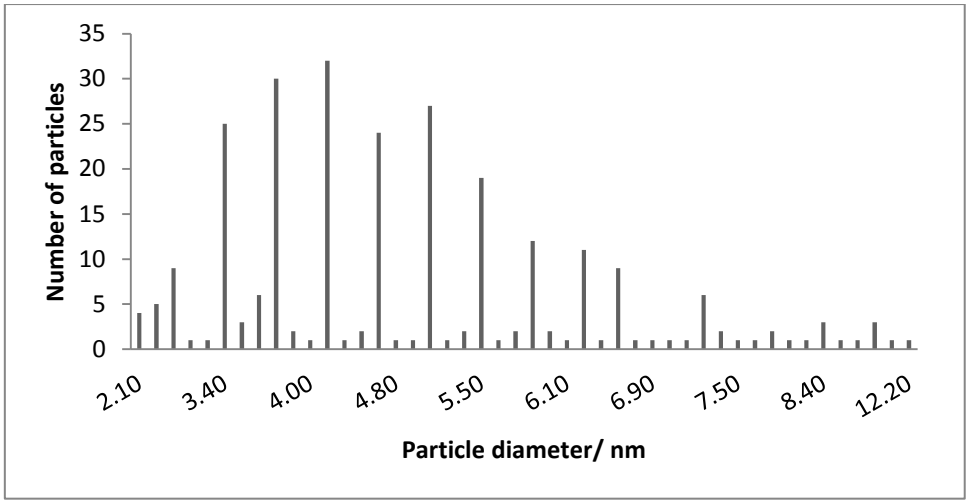

Figure 4.27 Particle size distribution histogram of **AuNP 6**

From **Figure 4.26** and **4.27** it is seen that **AuNP 6** TEM images reveal a mean diameter of 4 nm. The highest number of AuNPs with the same diameter was 32 with a diameter of 4 nm. The AuNPs showed an even distribution on the SiO_2 gel and varied from 1 nm to 11 nm.

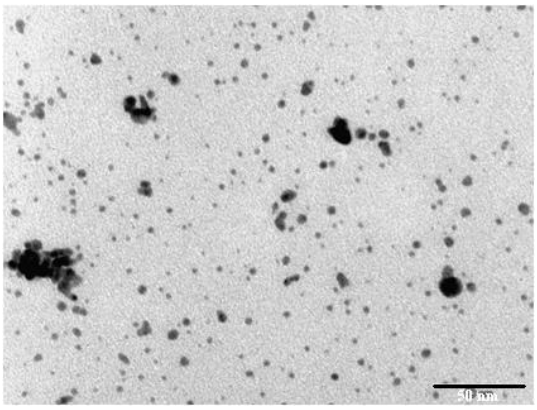

Figure 4.28 TEM image of **AuNP 10**

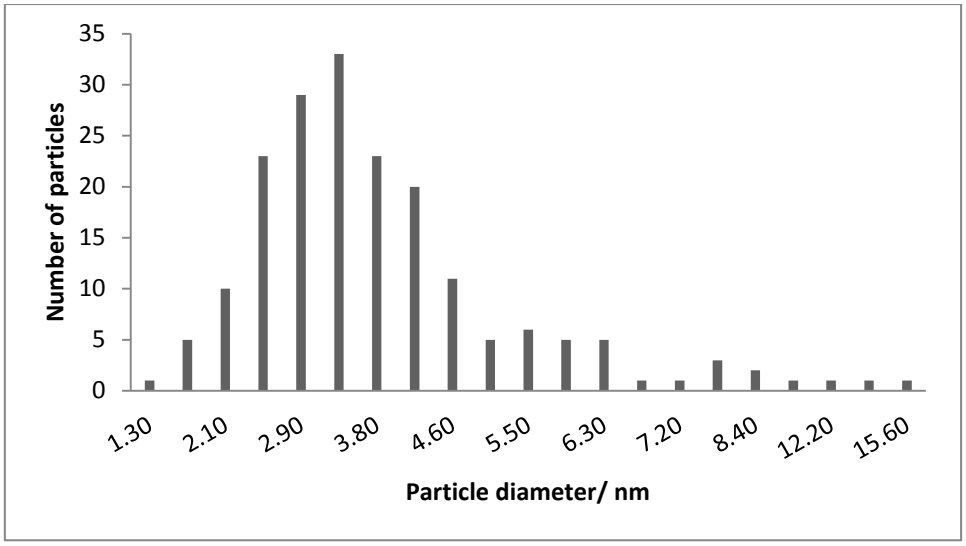

Figure 4.29 Particle size distribution histogram of **AuNP 10**

From **Figure 4.28** and **4.29** it is seen that **AuNP 10** TEM images reveal a mean diameter of 4 nm. The most number of AuNPs with the same diameter was 33 with a diameter of 3 nm. The AuNPs showed an even distribution on the SiO_2 gel and varied from 1 nm to 16 nm.

The results of the 100 °C samples correlate to decrease in particle size with the increase in concentration. The SiO_2 does stabilize the AuNPs however, with regard to the **AuNP 2**, large particles are formed.

AuNP 2 gave a count of 77 nanoparticles and a mean diameter of 54 nm. **AuNP 6** gave a count of 267 nanoparticles and a mean of 5 nm. **AuNP 10** gave a count of 187 nanoparticles and a mean of 4 nm. It should also be noted that there are more nanoparticles in the 0.5 M sample than in the 1.25 M sample, and this is visible for all the above samples and this could be due to the fact that aggregation occurs in the larger concentration.

4.2.2.4 TEM results of AuNP/SiO_2 composites for samples at 50 °C

Figure 4.30 to **Figure 4.35** show results for 50 °C at the various concentrations. The images obtained are as follows:

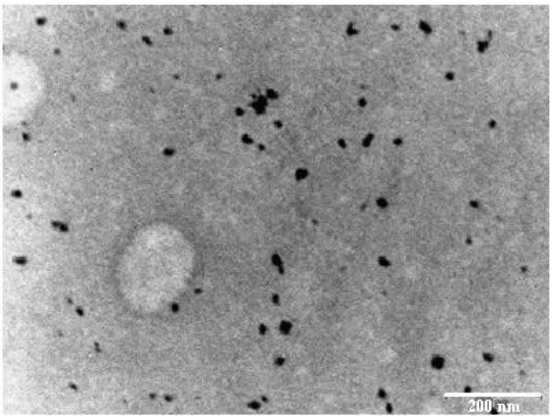

Figure 4.30 TEM image of **AuNP 1**

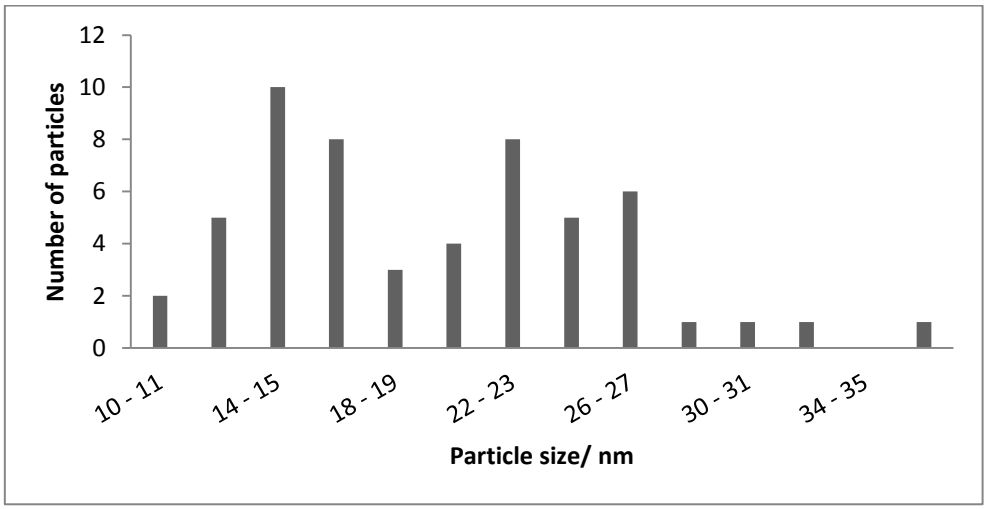

Figure 4.31 Particle size distribution histogram of **AuNP 1**

From **Figure 4.30** and **4.31** it is seen that **AuNP 1** TEM images reveal a mean diameter of 20 nm. The highest number of AuNPs with the same diameter was 10 with a diameter range of 14 – 15 nm. The AuNPs showed an even distribution on the SiO_2 gel and varied from 10 nm to 36 nm.

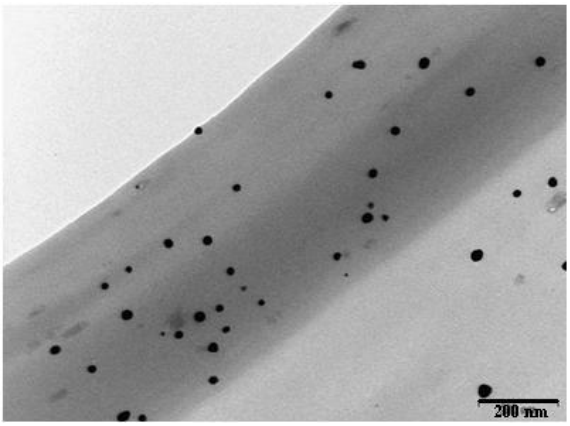

Figure 4.32 TEM image of **AuNP 5**

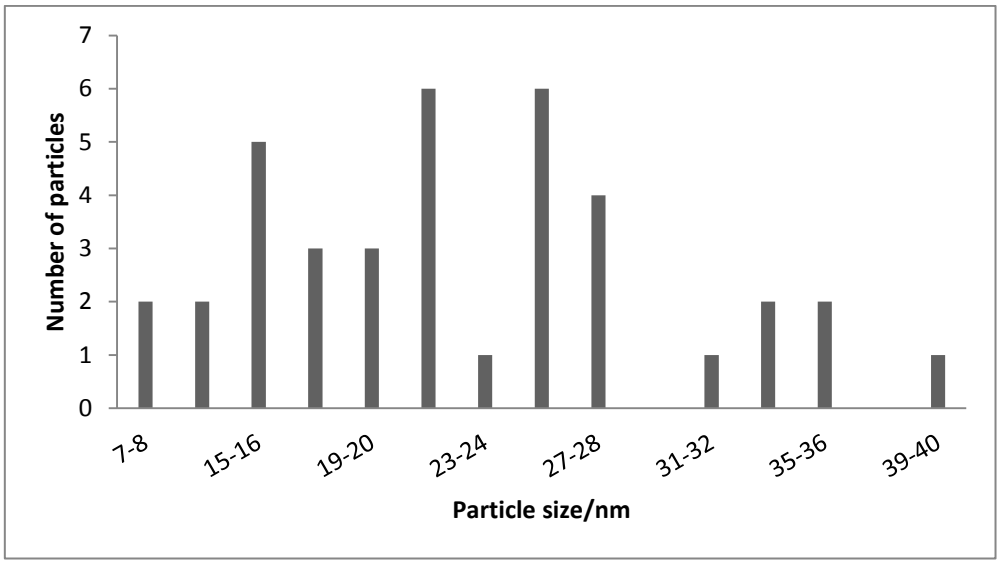

Figure 4.33 Particle size distribution histogram of **AuNP 5**

From **Figure 4.32** and **4.33** it is seen that **AuNP 5** TEM images reveal a mean diameter of 22 nm. The highest number of AuNPs with the same diameter was 6 with a diameter of 21 – 22 nm and 25 – 26 nm. The AuNPs showed an even distribution on the SiO_2 gel and varied from 7 nm to 39 nm.

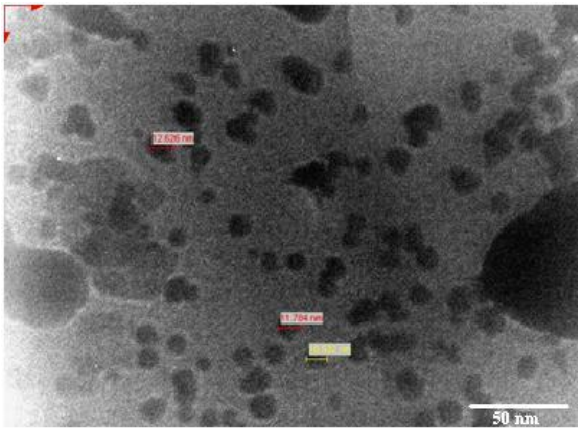

Figure 4.34 TEM image of **AuNP 9**

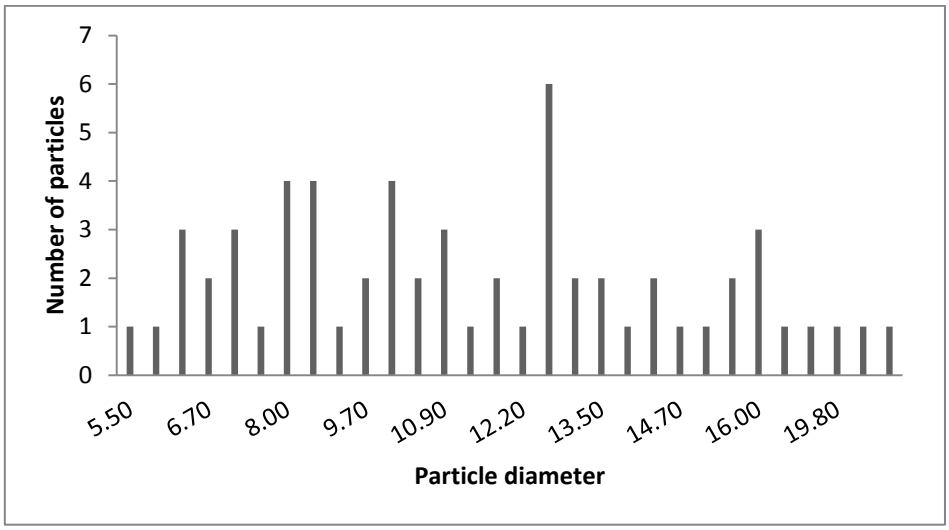

Figure 4.35 Particle size distribution histogram of **AuNP 9**

From **Figure 4.34** and **4.35** it is seen that **AuNP 9** TEM images reveal a mean diameter of 12 nm. The highest number of AuNPs with the same diameter was 6 with a diameter of 13 nm. The AuNPs showed an even distribution on the SiO_2 gel and varied from 6 nm to 26 nm.

The results for the 50 °C samples show similar trends to that of the 200 °C and 300 °C, however the size of the nanoparticles are greater than those of any of the above samples. The rationale behind this could be at the low temperature there could be chlorine in the samples and that the gold solution of tetrachloroauric acid did not reduce fully at the temperature of 50 °C.

AuNP 1 gave a count of 57 nanoparticles and a mean diameter of 20 nm. **AuNP 5** gave a count of 38 nanoparticles and a mean of 22 nm. **AuNP 9** gave a count of 60 nanoparticles and a mean of 12 nm.

4.2.2.5 Analyses of TEM results

Interactions with gold and the silica are relatively strong.[25] Due to the intrinsic properties of gold (gold – gold interaction), aggregation of gold nanoparticles is seen.[24] Aggregation of gold nanoparticles is a function of reaction time and temperature.[26] When the AuNP-SiO_2 interaction ruptures it leads to the movement of particles on the surface thus aggregating and leading to larger particles.[22] Literature has shown that an increase in temperature leads to an increase of particles size, however, from **Table 4.2**, a different trend was established

Table 4.2 Results for mean diameter (*ca*.) of samples at various temperatures and concentrations

	50 °C	**100 °C**	**200 °C**	**300 °C**
	Mean Diameter /nm	**Mean Diameter /nm**	**Mean Diameter /nm**	**Mean Diameter /nm**
0.01 M	**19**	**54**	**3**	**4**
0.5 M	**22**	**5**	**4**	**6**
1.25 M	**11**	**4**	**3**	**4**

From the graphs in **Figures 36** and **37** it is seen that as temperature increases, the particle size decreases (**Figure 4.38**) except for the lowest concentration. As concentration increases (from 0.01 M to 0.5 M) particle size increases and then decreases (From 0.5 M to 1.25 M). These results should be further investigated with individual concentrations between 0.01 M and 0.5 M, and 0.5 and 1.25 M.

The assumption that, as the total number of pores exposed to gold increase (or the total number of pores occupied by gold), the number of smaller gold nanoparticles formed increases and as the concentration increases the total number of nanoparticles formed increases, until a maximum concentration is reached and the pores reach saturation,[27] holds, and this is when aggregation becomes prevalent. Stabilizing agents such as sodium citrate could aid in the stability of the gold nanoparticles, and prevent it from aggregating.

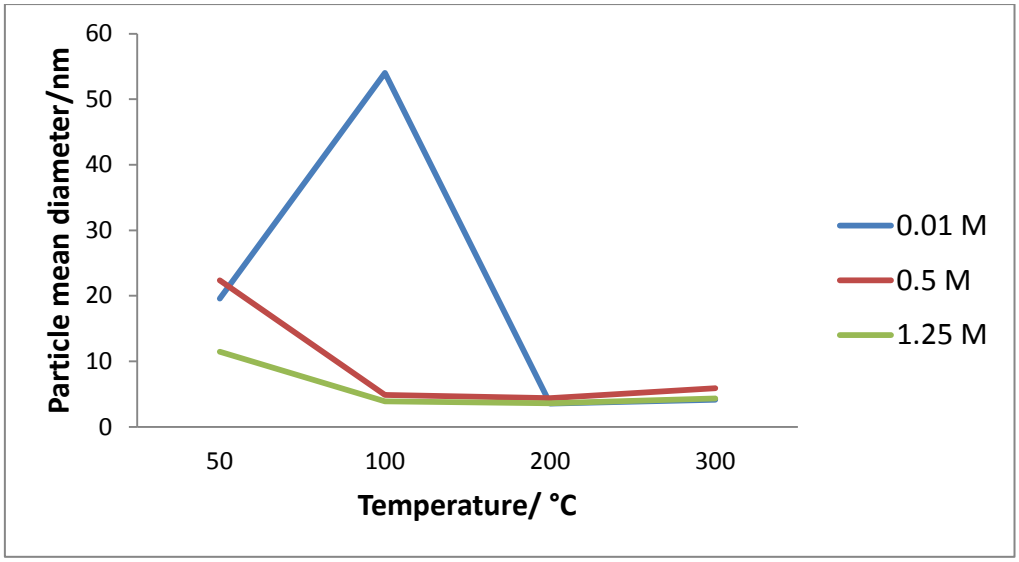

Figure 4.36 Line plot mean particle diameter vs. temperature

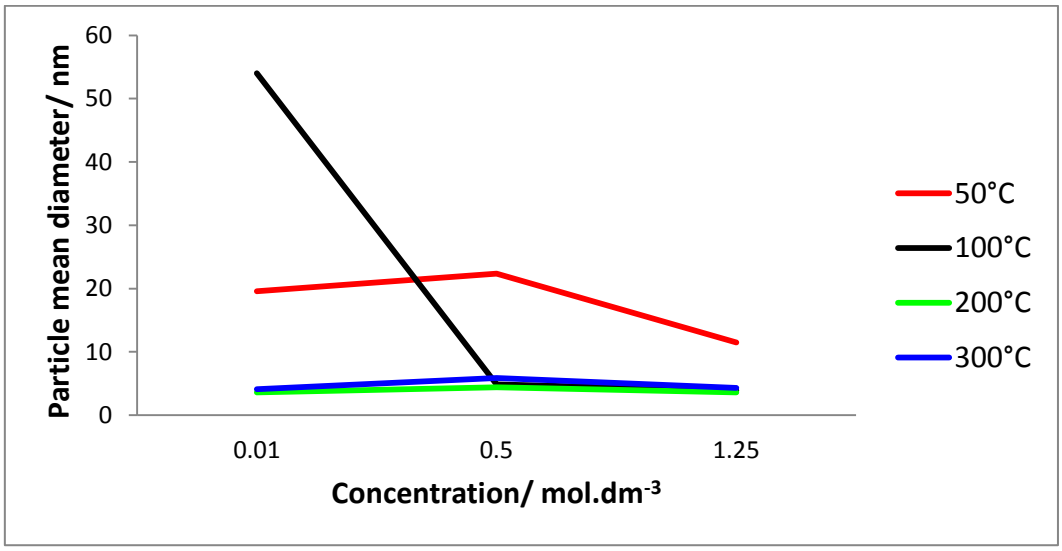

Figure 4.37 Line plot mean particle diameter vs. concentration

4.2.3 Surface area analysis of ($AuNP/SiO_2$) composites

Results for the BET surface area analysis are shown, as well as colour of samples which could give a broad idea of size of gold nanoparticles.

Table 4.3 Results for BET surface area analysis with mean diameter of samples at various temperatures and concentrations

	50 °C		100 °C		200 °C		300 °C	
	Mean Diameter /nm	**BET Surface area/m^2g^{-1}**	**Mean Diameter /nm**	**BET Surface area/m^2g^{-1}**	**Mean Diameter /nm**	**BET Surface area/m^2g^{-1}**	**Mean Diameter /nm**	**BET Surface area/m^2g^{-1}**
Silica gel	**-**	**550**	**-**	**546**	**-**	**543**	**-**	**542**
0.01 M	**19**	**538**	**54**	**526**	**3**	**542**	**4**	**534**
0.5 M	**22**	**461**	**5**	**226**	**4**	**332**	**6**	**495**
1.25 M	**11**	**363**	**4**	**179**	**3**	**166**	**4**	**379**

Table 4.3 shows that BET surface area decreases with increase of concentration at all temperatures. This can be rationalised from the fact that SiO_2 is porous and has a surface area of ≈ 540 – 550 m^2g^{-1} and during the reduction of the gold solution, the gold particles penetrate through the pores occupying them. The specific temperatures at different concentrations in descending order, the following trends are seen. At 50 °C the surface area decreases from 550, 538, 461, to 363 m^2g^{-1}. At 100 °C the surface area decreases from 546, 526, 226, to 179 m^2g^{-1}. At 200 °C the surface area decreases from 543, 542, 332, to 166 m^2g^{-1}. At 300 °C the surface area decreases from 542, 534, 495, to 379 m^2g^{-1}.

These trends are observed for all temperatures; however, when looking at different temperatures in ascending order at same concentrations, a different trend is seen. At 0.01 M concentration surface area varies from 538, 526, 542 to 534 m^2g^{-1}. At 0.5 M concentration surface area varies from 461, 226, 332 to 495 m^2g^{-1}. At 1.25 M concentration surface area varies from 363, 179, 166 to 379 m^2g^{-1}. A trend is seen whereby the surface area decreases from 50 °C to 200 °C, thereafter it increases for the 300 °C set of samples. A motive for this could be the formation of porous gold.[23] In literature the formation of porous gold is seen when etching out of the SiO_2 is done.[23] By the formation of porous gold, the surface area increases.

4.2.4 XRD analysis of (AuNP/SiO_2) composites

The X-Ray Diffraction (XRD) results showed that gold is present in the form of metallic gold (JCPDS card no. 04-0784). The most intense diffraction is corresponding to the **111** plane. The increase in the two theta value resulted in decrease in the intensity of the diffractions. The peak "hump" at low two theta values is characteristic to the amorphous silica that was

used as a support for gold immobilization. The effect of the temperature was studied by analysis of the diffractograms of the samples obtained at different temperatures using the same gold solution concentration (**Figure 4.38** – **Figure 4.40**).

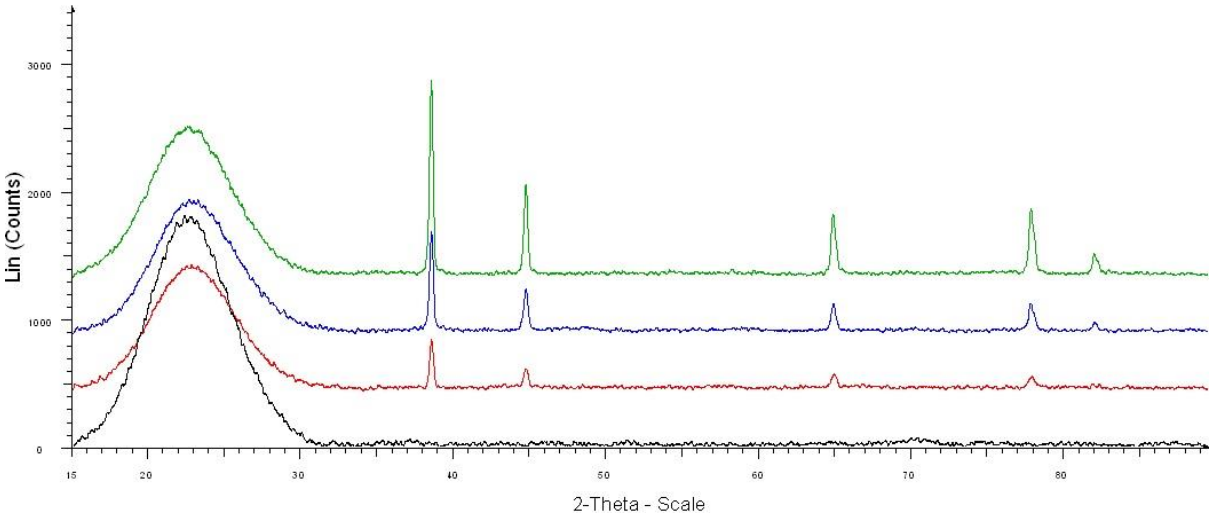

Figure 4.38 Diffractogram of composites **silica** (black), **AuNP 2** (red), **3** (blue) and **4** (green)

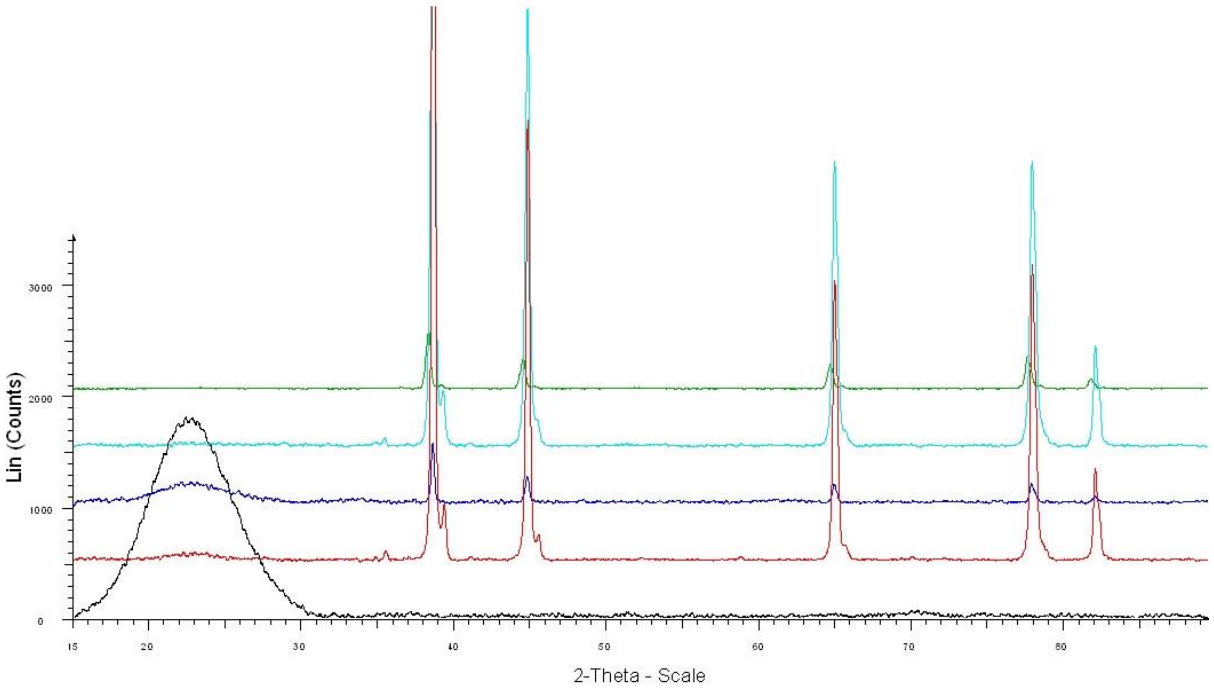

Figure 4.39 Diffractogram of composites **silica** (black), **AuNP 5** (red), **6** (blue), **7** (teal) and **8** (green)

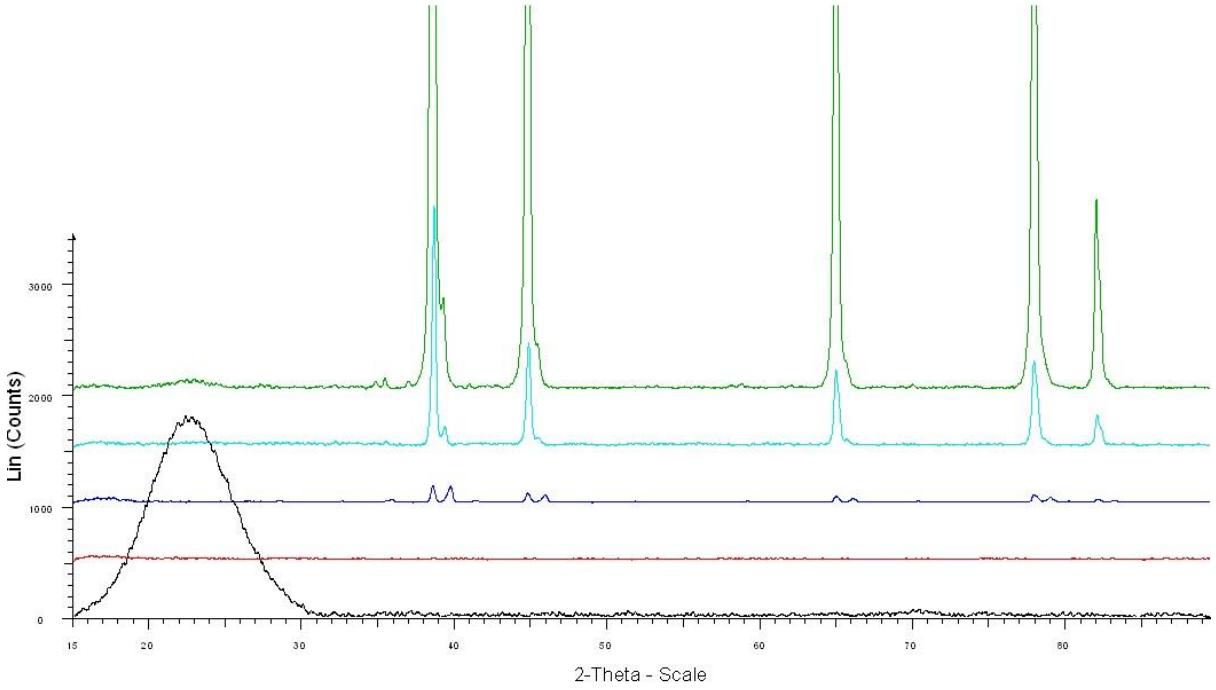

Figure 4.40 Diffractogram of composites **silica** (black), **AuNP 9** (red), **10** (blue), **11** (teal) and **12** (green)

The main observation that was seen is the increase in the intensity of the diffraction line as the synthesis (or calcination) temperature increased. This could be due to gold particles starting to agglomerate with increase in the temperature, leading to the observation that the composites are more crystalline at these higher temperatures and therefore have a higher intensity. This observation emphasizes the results obtained from TEM where larger particles were observed with increase in the preparation temperature (preparation temperature of 200 and 300 °C). Samples prepared with a 0.5 M concentration solution (**Figure 4.39**) showed the silica characteristic "hump", however, higher concentration of gold samples did not show the "hump" at high preparation temperature (**Figures 4.39** and **4.40**). This is due to the combined effect of an increase in the loading of gold on silica and the increase in the temperature of preparation.

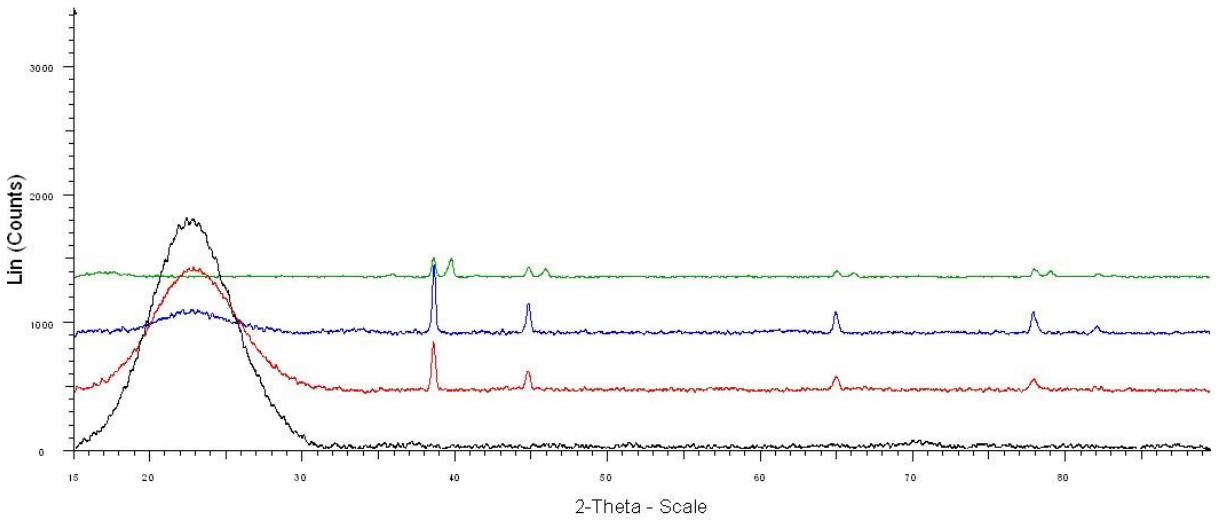

Figure 4.41 Diffractogram of composites **silica** (black), **AuNP 2** (red), **6** (blue) and **10** (green)

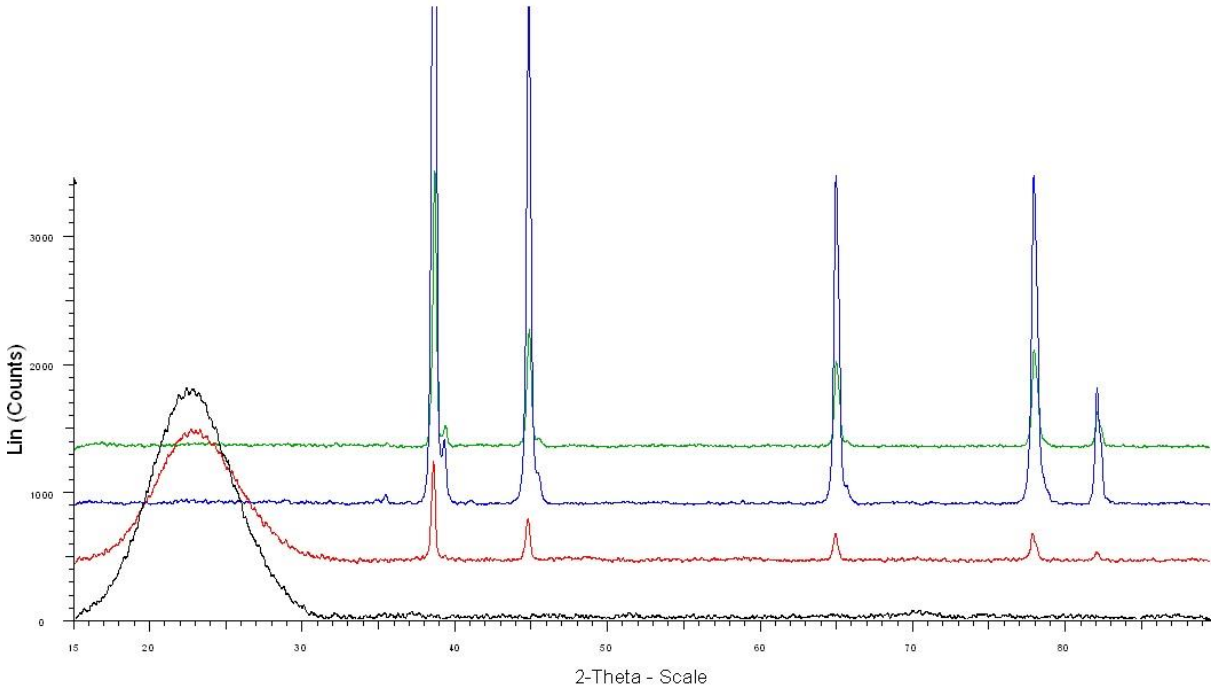

Figure 4.42 Diffractogram of composites **silica** (black), **AuNP 3** (red), **7** (blue) and **11** (green)

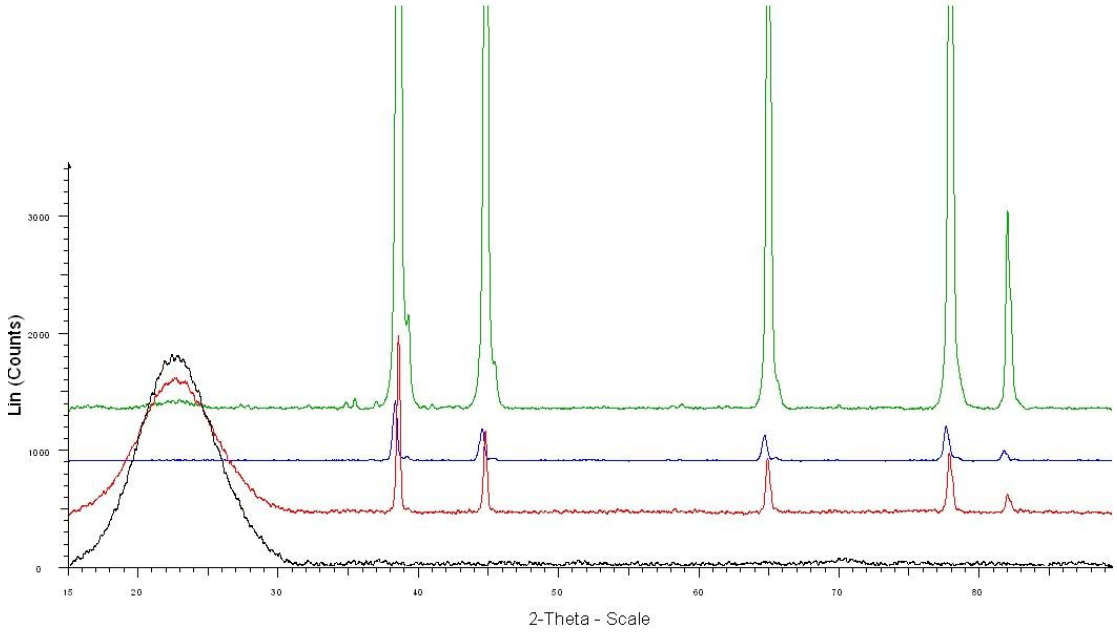

Figure 4.43 Diffractogram of composites **silica** (black), **AuNP 4** (red), **8** (blue) and **12** (green)

The increase in the concentration (**Figure 4.41** – **4.43**) was accompanied by decrease in the intensity of the silica "hump" and this could be due to an increase in the loading of gold on the surface of the amorphous silica and the increase in the crystallite size of the gold particle size. This observation is also supported by the TEM particle size analysis, which show increase in the particle size with increase in temperature and gold loading (concentrations of 0.01 and 0.5 M).

4.2.5 Formation of Self Assembled Monolayers

Previous studies have encapsulated the use of dialkyl dithiophosphinic acid in the preparation of self assembled monolayers.[28] In the present study the use of a dithiophosphonate (dtp) ligand incorporating the cholesteryl moiety was used in an attempt to form SAMs.

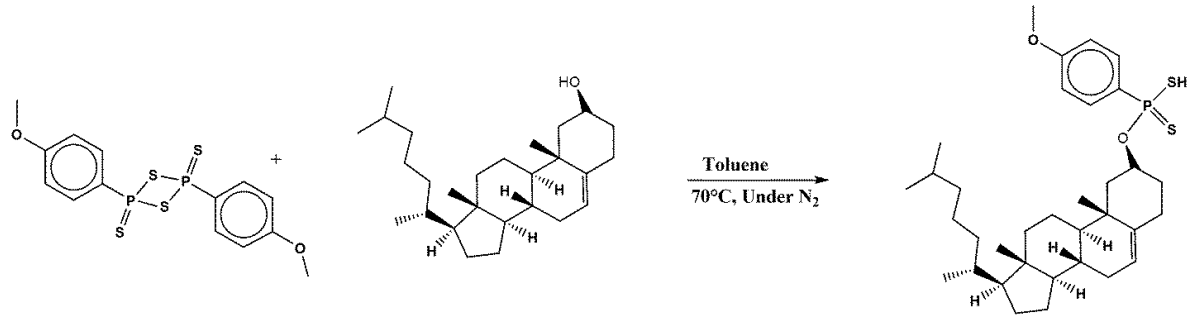

Scheme 4.2 Preparation of dithiophosphonic acid with the cholesterol moiety

Upon preparation of the dtp acid, an attempt to prepare self assembled monolayers was undertaken with the use of nanoparticle composites synthesized from a concentration 0.5 M at a temperature at 100 °C. This batch of nanoparticles was chosen as it showed good results in terms of average nanoparticles size and number of nanoparticles.

The dtp acid was characterized using ^{1}H and ^{31}P NMR as well as IR and elemental analysis. The IR shows a strong peak at 2934 cm^{-1} which agrees with a $\nu(S - H)_{sym}$ stretch.

The preparation involves the dissolution of the dtp acid in toluene and the immersion of the nanoparticles composite into this solution. After 24 hours the composite was removed by filtration and washed three times with toluene.

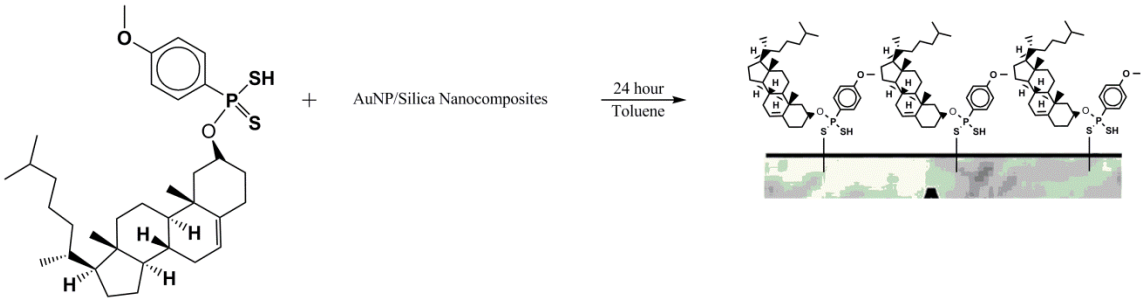

Scheme 4.3 Preparation of SAMs using a solution of dithiophosphonate acid and AuNP/SiO_2 Nanocomposites

4.2.5.1 SEM results of the Self assembled monolayers

SEM results indicate the presence of gold, sulfur, phosphorus, and SiO_2.

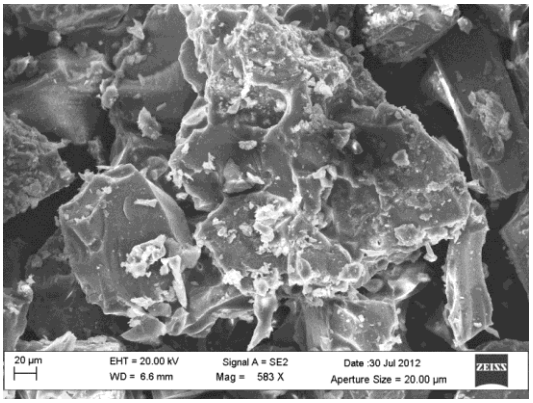

Figure 4.44 SEM image of nanocomposite after emersion in dtp acid

The mapping of **Figure 4.45** was carried out to determine qualitatively, the presence of the above mentioned elements.

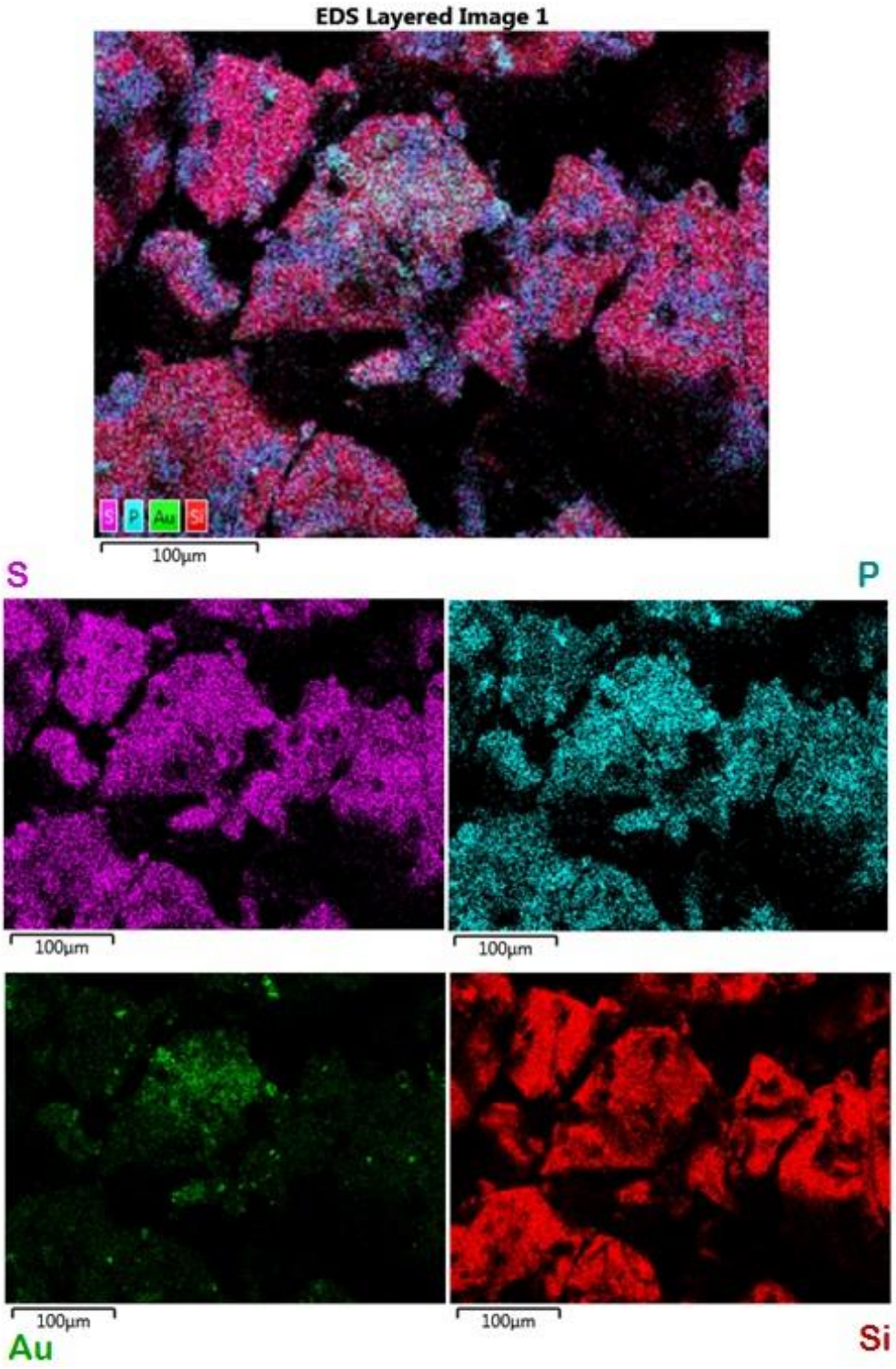

Figure 4.45 SEM mapping image of elements representing nanoparticle composite

Figure 4.45 indicates that after 24 hours of immersion of the nanoparticle composite in the solution of the dtp acid there is interaction between the dtp acid and the nanocomposite. This is not conclusive evidence as to whether there is Au-S bond formation but it leads to the

postulation that the interaction between the dtp acid the nanocomposite is strong enough to infer the formation of self assembled monolayer's on the surface of the nanocomposite.

4.2.5.2 TEM results of the Self assembled monolayers

On analysis of the TEM image of the hybrid composite it is evident that the nanoparticles retain their size and on addition of the dtp solution only partial aggregation is seen.

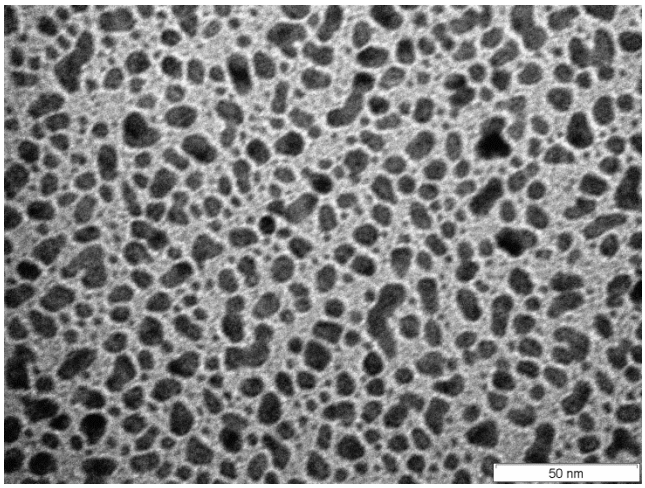

Figure 4.46 TEM image of (Au/SiO_2) composites after emersion into the dtp solution

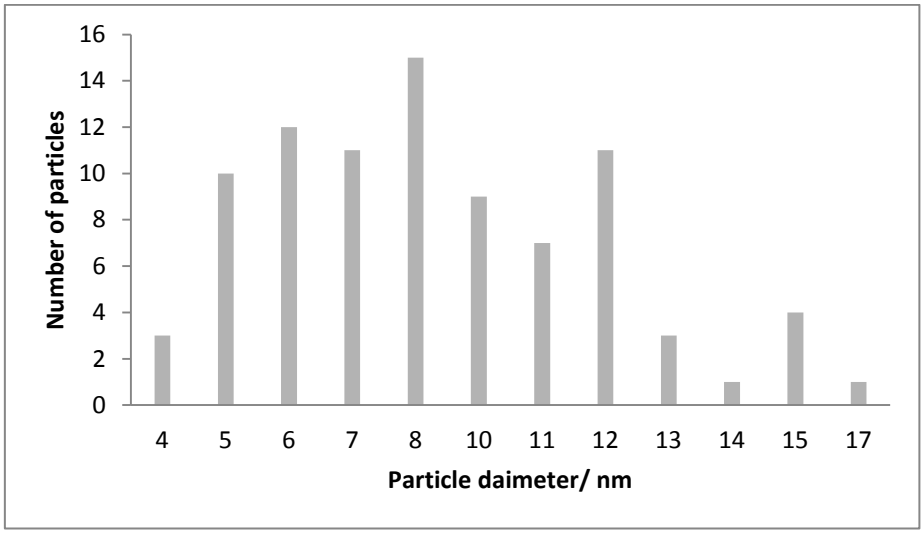

Figure 4.47 Particle size distribution histogram of (Au/SiO_2) nanocomposite after emersion into dtp solution

From **Figure 4.46** and **4.47** it is seen that with the use of **AuNP 5**, the TEM image reveals a mean diameter of 8.76 nm. The highest number of AuNPs with the same diameter was 15

with a diameter of 8.00 nm. The AuNPs showed an even distribution on the Support and varied from 4 nm to 17 nm.

In Summary, this chapter showed that the synthesis of AuNP/SiO_2 composites is possible by the use of an *in situ* thermal approach. The possibility of tailoring size and the number of particles can be done by adjusting the condition parameters. This method provided an easy protocol to form gold nanoparticles as a homogeneous distribution within a SiO_2 matrix. In addition, the possibility of using dithiophosphonates in the formation self assembled monolayers is illustrated but not fully proven.

4.3 Experimental Procedure

4.3.1 General considerations

Tetrachloroauric acid, $H[AuCl_4].3H_2O$ obatained from Rand Refineries was used to make up the solutions and SiO_2 (size = 0.063 – 0.200 mm) was purchased from Sigma-Aldrich. Temperatures of 50 °C, 100 °C, 200 °C and 300 °C and concentrations of 0.01 M, 0.5 M, and 1.25M were used. Time of emersion was kept constant at one hour.

4.3.2 Instrumentation

The furnace used was an electric carbolite furnace, Sheffield, UK. The imaging was done with a JEOL JEM-1010 TEM operating at 100 kV, as well as Megaview III software imaging to quantify the results. Surface area analysis was carried out using a Micromeretics surface area and porosity analyzer under nitrogen and helium flow at 100 kPa. The surface morphology and elemental analysis was characterized using a JEOL JSM – 6100 Scanning Electron Microscope with a Bruker signal processing detector.

Scanning Electron Microscopy (SEM): The surface morphology of the AuNP composites where analyzed using a JEOL JSM – 6100 Scanning Electron Microscope with a Bruker signal processing detector. The samples were placed in a sampled holder and were then carbon-coated and placed into the sample holder. Elemental analysis was also attained.

Transmission Electron Microscopy (TEM): The shape and size of the AuNP composites where determined using a JEOL JEM-1010 Transmission Electron Microscope operating at

100 kV, to capture images and Megaview III software imaging to analyze the images. Samples were prepared by weighing out 0.02 g of sample in a vial, then adding 0.5 ml absolute ethanol. Thereafter the vial was swirled and 10 μL of suspension was drawn with a micro-pipette and place on the copper grid coated with formvar resin and was allowed to dry under a lamp.

Image analysis was carried out digitally by counting particles manually. The particle diameter, standard deviation, and particle count where generated.

Brunauer-Emmet-Teller (BET) Surface area analysis: Surface area measurements where done using the Brunauer-Emmet-Teller method. It was done using the Micromeretics surface area and porosity analyzer. The samples where pre-weighed (0.4 g) and degassed under nitrogen flow at 50, 100, 200 and 300 °C overnight and analyzed.

X-Ray Diffraction diffractograms were obtained using a Bruker D8 Advance with diffracplus XRD commander software and a Bruker VENTEC detector. The radiation source used was *Cu Kα* (wavelength of 0.1540 nm), operating on a focus line with a voltage and amperage of 40 kV and 40 mA.

4.3.3 Synthesis of Gold Nanoparticle/SiO_2 composites

11.5 ml of the $HAuCl_4$ was placed into a pre-weighed beaker (250 mL, 101.147 g), to this a stirrer bar was added (0.776 g). Water (50 mL) was then added to dilute the acid present in the solution. The beaker, equipped with a thermometer, was then placed on a hot-plate and was heated to a temperature of 80 °C. The solution was left to stirring for 6 hours at a constant temperature to evaporate the dilute acid. The evaporation of the solution results in orange microcrystals (9.096 g). The wet crystals were then dissolved in water and the various concentrations where made up (0.01 M, 0.5 M, and 1.25 M).

Once the concentrations were made up, the solutions were then added to the pre-weighed SiO_2 (≈1.2 g) with a size = 0.063-0.200 mm, and allowed to soak for one hour. The mixture was completely wet and forming a slurry, and was then calcined in the furnace at different temperatures (50 °C, 100 °C, 200° C and 300 °C) for one hour. The products were then stored in a desiccator and characterized using the various above mentioned techniques.

4.3.4 Preparation of self assembled monolayers

Approximately 2 cm x 2 cm of the nanocomposite that was previously synthesized was immersed into a 0.2M dtp solution in anhydrous toluene for 24 h. Substrates were then removed from solution, rinsed with anhydrous toluene, and dried under a stream of nitrogen. The products where then stored in a desiccator and characterized using the various above mentioned techniques.

4.3.5 Synthesis of cholesterol derived dithiophosphonate ligand

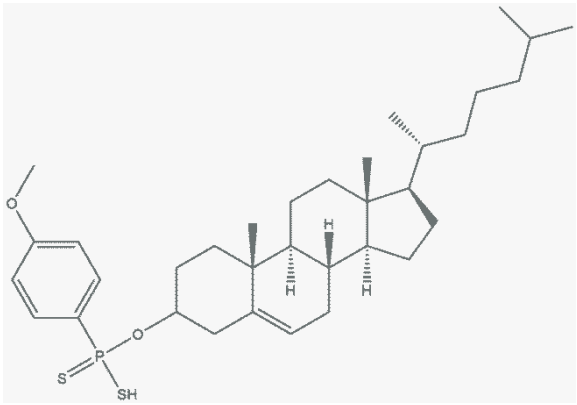

A Schlenk flask was charged with (4-$C_6H_4OMeP(S)S)_2$ (1.280 g, 3.18 mmol) and placed under vacuum for 30 minutes. The solid was heated to 70 °C, cholesterol (2.508 g, 6.49 mmol) and toluene (2 mL) was added. The temperature was maintained at 70 °C for 60 minutes, until dissolution of all the solids had been observed. The clear residue was cooled to room temperature, before being placed in an ice bath for 10 minutes were it solidified in to a white powder. Yield 3.429 g (90%). Melting point: 90.5 – 94.6 °C. ^{1}H-NMR (Methanol-D4) ppm: 0.72 (s, 3H), 0.89 (d, 6H, J = 6.52 Hz), 0.95 (d, 3H, J = 6.52 Hz), 1.01 (s, 3H), 1.15 – 1.18 (m, 11H), 1.41 (t, 5H, J = 8.03 Hz), 1.49 – 1.54 (m, 6H), 1.82 – 1.95 (m, 6H), 2.23 – 2.40 (m, 2H), 4.06 (s, 3H), 6.87 (d, 2H, J = 8.76 Hz), 8.05 (d, 2H, J = 8.68 Hz). ^{31}P NMR (Methanol-D4) ppm: 96 (s). Anal. calc. for $C_{34}H_{53}O_2PS_2$: C 69.34, H 9.07 %. Found: C 69.42, H 9.16 %.

Selected IR data ν/cm-1: 2934 (s), 1115 (m), 1029 (m), 684 (s), 543 (s).

4.4 References

(1) El-Sayed, S. E. a. M. A. *Chem. Soc. Rev.* **2006**, *35*, 209.
(2) Huang, C.-J.; Chiu, P.-H.; Wang, Y.-H.; Meen, T.-H.; Yang, C.-F. *Nanotechnology* **2007**, *18*, 395603.
(3) Faraday, M. *Philos. Trans.* **1857**, 145.
(4) Kimling, J.; Maier, M.; Okenve, B.; Kotaidis, V.; Ballot, H.; Plech, A. *J. Phys. Chem. B* **2006**, *110*, 15700.
(5) Turkevitch, J. S., P. C.; Hillier *J. Discuss.Faraday Soc.* **1951**, *11*, 55.
(6) Brust, M. W., M.; Bethell, D.; Schiffrin, D. J.; Whyman, R. J 801-802 *J.Chem. Soc.* **1994**, 801.
(7) Daniel, M. C.; Astruc, D. *Chem. Rev.* **2004**, *104*, 293.
(8) Chen, S. W. *Langmuir* **1999**, *15*, 7551.
(9) Mokoena, E. M., University of the Witwatersrand, 2005.
(10) Pol, V. G.; Gedanken, A.; Calderon-Moreno, J.; Palchik, V.; Slifkin, M. A.; Weiss, A. M. *Chem. Mater.* **2003**, *15*, 3402.
(11) Zanella, R.; Sandoval, A.; Santiago, P.; Basiuk, V. A.; Saniger, J. M. *J.Phys. Chem. B* **2006**, *110*, 8559.
(12) Ma, Z.; Brown, S.; Howe, J. Y.; Overbury, S. H.; Dai, S. *J.Phys. Chem. C* **2008**, *112*, 9448.
(13) Gajan, D.; Guillois, K.; Delichere, P.; Basset, J. M.; Candy, J. P.; Caps, V.; Coperet, C.; Lesage, A.; Emsley, L. *J.Am. Chem. Soc.* **2009**, *131*, 14667.
(14) Lee, K. Y.; Lee, Y. W.; Kwon, K.; Heo, J.; Kim, J.; Han, S. W. *Chem. Phys.Lett.* **2008**, *453*, 77.
(15) Mishra, Y. K.; Mohapatra, S.; Avasthi, D. K.; Kabiraj, D.; Lalla, N. P.; Pivin, J. C.; Sharma, H.; Kar, R.; Singh, N. *Nanotechnology* **2007**, *18*.
(16) Schaadt, D. M.; Feng, B.; Yu, E. T. *Appl. Phys. Lett.* **2005**, *86*.
(17) Ona Burgos, P.; Fernandez, I.; Iglesias, M. J.; Garcia-Granda, S.; Lopez Ortiz, F. *Org. Lett.* **2008**, *10*, 537.
(18) Ulman, A. *Organic thin films and surfaces: directions for the nineties*; Academic Press, 1995.
(19) Ulman, A. *Chem. Rev.* **1996**, *96*, 1533.
(20) McMurry, J. *Fundamentals of organic chemistry*; Thomson-Brooks/Cole, 2003.
(21) Voet, D.; Pratt, C. W.; Voet, J. G. *Fundamentals of Biochemistry, Binder Ready Version: Life at the Molecular Level*; John Wiley & Sons, 2008.
(22) Chen, M.; Goodman, D. W. *Chem. Soc. Rev.* **2008**, *37*, 1860.
(23) Pol, V. G.; Gedanken, A.; Calderon-Moreno, J.; Palchik, V.; Slifkin, M. A.; Weiss, A. M. *Chem. Mater.* **2003**, *15*, 3402.
(24) Wang, Y.; Liu, Z.; Han, B.; Sun, Z.; Huang, Y.; Yang, G. *Langmuir* **2004**, *21*, 833.
(25) Westcott, S. L.; Oldenburg, S. J.; Lee, T. R.; Halas, N. J. *Langmuir* **1998**, *14*, 5396.
(26) Kumar, A.; Pushparaj, V. L.; Murugesan, S.; Viswanathan, G.; Nalamasu, R.; Linhardt, R. J.; Nalamasu, O.; Ajayan, P. M. *Langmuir* **2006**, *22*, 8631.
(27) Mandal, S.; Roy, D.; Chaudhari, R. V.; Sastry, M. *Chem. Mater.* **2004**, *16*, 3714.
(28) Miller, M. S.; Juan, R. R. S.; Ferrato, M.-A.; Carmichael, T. B. *Langmuir* **2011**, *27*, 10019.

CHAPTER 5

Conclusions

This dissertation comprised three separate studies. Firstly, a dinuclear gold(I) complex with a dithiophosphonate ligand system yielded two new structures exhibiting intramolecular aurophilicity. The reactivity studies of these complexes with dppm led to a novel structure that departed from previous trends for similar reactions.

Secondly, the synthesis of the phosphinamide ligand yielded a remarkable number of structural features which include hydrogen bonding interactions as well as unique packing properties. The phosphinamide was furthered reacted with silver triflate which led to the formation of a novel dinuclear silver complex that adopts two unique geometries around the silver nuclei, namely a trigonal planar and linear.

Finally, the synthesis and characterization of AuNP/SiO_2 composites and the preparation of resulting self assembled monolayers were achieved. The synthesis of these nanocomposites entailed the *in situ* thermal reduction of tetrachloro-auric acid using varying concentrations at different temperatures. The method studied was advantageous over previously explored preparations in that it was found to be fast, efficient, cheap and had a green chemistry component. The particle size, shape and distribution can be tuned by altering the concentration of gold solution and temperature at which it is reduced.

The objectives of the three studies have been achieved. However, further work could be performed in continuing these studies to attain more detailed results and outcomes.

Possible future work

5.2.1 Identification of reaction mechanism

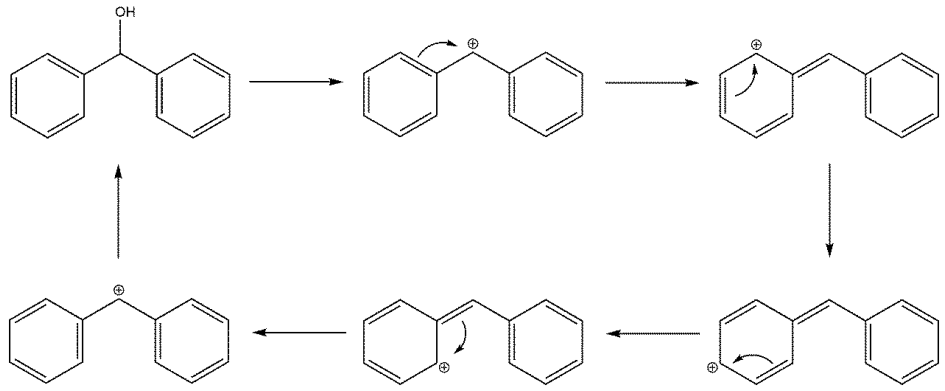

Scheme 5.1 Stable carbo-cation formation of diphenylmethanol

The reactivity of dinuclear gold(I) dithiophosphonate complexes with dppm should be analyzed to acquire the specific conditions which allow for two different isolated structures from similar starting materials. Novel alcohols that involve highly stable carbocations (**Scheme 5.1**) need to be used to help predict the mechanism of formation via different starting materials.

5.2.2 Phosphinamide gold complex

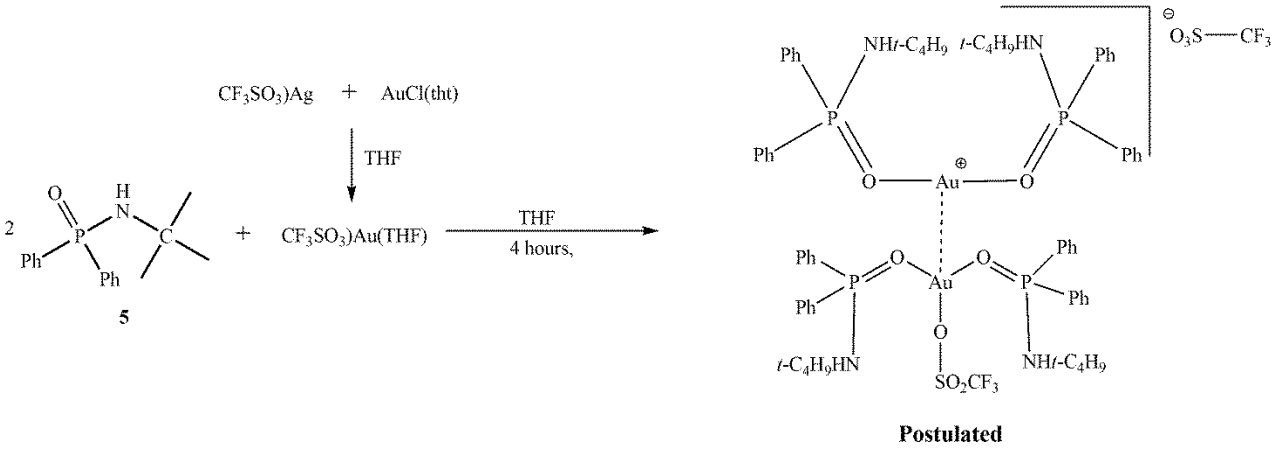

Scheme 5.2 Reaction of compound 5 with a modified gold(I) starting material

Further complexation of compound **5** with gold(I) (**Scheme 5.2**) may lead to prospect of novel structures featuring an elusive Au···O bond as well as an intrinsic study in the aurophilicity of his new complex.

5.2.3 Gold nanoparticles/SiO_2 nanocomposites

Further characterization can be carried out in terms of XRD, Raman spectroscopy, UV – visible spectrometry, and X-ray photoelectron spectroscopy. These characterization techniques had not been undertaken due to the focus of the study being on size and nanoparticles formation. With respect to dithiophosphonate type self assembled monolayers, further characterization techniques into binding modes of the dithiophosphonate moiety and the surface morphology of nanocomposites after formation of monolayers need to be investigated.

APPENDIX

The accompanying CD supports this dissertation as an Appendix and contains X-ray crystallographic data (including *cif* files).